FABRICATION OF MICRO-FEATURES IN INCONEL 718 SUPERALLOY USING HYBRID EDM PROCESSES

Ph.D. Thesis

DEEPAK RAJENDRA UNUNE

(2013RME9051)

DEPARTMENT OF MECHANICAL ENGINEERING

MALAVIYA NATIONAL INSTITUTE OF TECHNOLOGY

JLN MARG, JAIPUR-302017, INDIA

November, 2016

FABRICATION OF MICRO-FEATURES IN INCONEL 718 SUPERALLOY USING HYBRID EDM PROCESSES

A Thesis Submitted

in Partial Fulfilment of the Requirements for the Degree of

DOCTOR OF PHILOSOPHY

in

ENGINEERING

by

DEEPAK RAJENDRA UNUNE

(2013RME9051)

Under the guidance of

Dr. Halal Singh Mali

to the

DEPARTMENT OF MECHANICAL ENGINEERING

MALAVIYA NATIONAL INSTITUTE OF TECHNOLOGY

JLN MARG, JAIPUR-302017, INDIA

Dedication

I dedicate this work to

My Beloved Father

Late. Shri. Rajendra Unune

(1964-2007)

Malaviya National Institute of Technology, Jaipur

CANDIDATE'S DECLARATION

I hereby certify that the thesis entitled "**FABRICATION OF MICRO-FEATURES IN INCONEL 718 SUPERALLOY USING HYBRID EDM PROCESSES**" submitted in partial fulfillment of the requirements for the award of **Doctor of Philosophy** in **Mechanical Engineering** to the **Malaviya National Institute of Technology, Jaipur** is an authentic record of research work carried out by me under supervision and guidance of Dr. Harlal Singh Mali. The work incorporated in this thesis has not been submitted elsewhere for the award of any degree.

<div align="right">

Deepak Rajendra Unune
(2013RME9051)

</div>

This is to certify that the above statement made by the candidate is correct to the best of my knowledge.

<div align="right">

Signature of Supervisor

Dr. Harlal Singh Mali
Assistant Professor
Department of Mechanical Engineering
Malaviya National Institute of Technology Jaipur
Jaipur- 302017, India.

</div>

November-2016

CERTIFICATE

This is to certify that the thesis entitled "**FABRICATION OF MICRO-FEATURES IN INCONEL 718 SUPERALLOY USING HYBRID EDM PROCESSES**", submitted by **Deepak Rajendra Unune (2013RME9051)** to **Malaviya National Institute of Technology, Jaipur**, is a record of bona fide research work under my supervision and I consider it worthy of consideration for the award of the degree of **Doctor of Philosophy** of the Institute.

Signature of Supervisor
Dr. Harlal Singh Mali

The Ph.D. viva voce examination of Mr. Deepak Rajendra Unune has been conducted by the Oral Defense Committee (ODC) constituted by the Dean (Academic Affairs), as per 9.4.3, vide letter No. F.4(P) PhD/Acad/MNIT/2016/1222 dated 19 Oct 2016 on Friday, 25th November, 2016. The ODC declares that the student has successfully defended the thesis in the viva-voce examination.

Dr. Harlal Singh Mali	**Dr. J. Ramkumar**
(Supervisor)	(External Examiner)
Assistant Professor	Professor
Department of Mechanical Engineering	Department of Mechanical Engineering
Malaviya National Institute of Technology Jaipur.	Indian Institute of Technology, Kanpur.

Acknowledgements

First of all, I would like to thank Dr. Harlal Singh Mali, for believing me and providing me an opportunity to work with, for the supervision and guidance, for the motivation, for the freedom and indulgence I had during research, and for everything I learned from throughout my time as a Ph.D. scholar. Working with Advanced Manufacturing and Mechatronics Lab and Materials Research Center, I've had the unique opportunity to access a wide range of the state of the art facilities in advanced manufacturing and materials research technologies. For these reasons, the Ph.D. has been a fantastic experience.

I thank the Malaviya National Institute of Technology (MNIT), Jaipur for supporting my research by providing the research scholarship and to the Advanced Manufacturing and Mechatronics Lab and Materials Research Center for providing the facilities and support, without which the present work would not be possible. I would like to thank Head of the Department of Mechanical Engineering and all faculty, and staff members of the Department of Mechanical Engineering, Materials Research Center, and various other departments in MNIT Jaipur for their help and support in the direct or indirect way throughout my time in MNIT Jaipur.

I would like to deliver my sincere gratitude and indebtedness to Dr. Suhas S. Mohite, my post graduation supervisor, for his valuable guidance, unconditional support, continuous encouragement, and for being the source of inspiration for me into the world of research.

I like to express heartfelt thanks to all my Ph.D. colleagues especially Jaikishan, Bhargav Pathri, Amit Aherwar, Sudarshan Kore, and Manoj Pawar for their constant

Abstract

The emerging miniaturization technologies are evidently driving developments in micro-scale processes, machines, and metrology. The miniaturization of devices appetites the fabrication of mechanical components with micro-features in fields that include optics, electronics, medicine, biotechnology, communications, and avionics, to name a few. For fabrication of miniaturized features and devices, the non-conventional processes play a vital role as compared to conventional machining processes. Among, various non-conventional processes, electro-discharge machining (EDM) is very important and cost-effective process and has undergone significant transformations in last two decades. While fabrication of micro-features, the use of low energy levels becomes vital for the EDM process and the process is termed as micro-EDM. The ability of EDM variant processes to produce highly complex shapes without imparting significant stresses and good repeatability has made them indispensable for the micromachining of miniaturized components especially in hard and difficult-to-cut materials like Inconel 718.

Even though EDM and micro-EDM have the ability to machine conductive materials irrespective of their hardness, they alone cannot meet numerous requirements of the machined component performance owing to some drawbacks like longer machining time, significant tool wear and poor surface integrity. Hybridizing EDM by compounding it with some other machining mechanism or assisting with the aid of some energy in material removal is an effective way to overcome the aforementioned problems. Therefore, the aim of current study is to investigate the performance of several EDM-based hybrid machining processes while fabricating most common

micro-features including micro-surfaces, micro-holes, and micro-channels. These inevitable micro-features are mainly required for micro fuel cells, micro-reactors requiring microscale pumps, valves and mixing devices, microfluidic systems, fiber optics, micro-nozzles for high-temperature jets, micro-molds, and many more devices.

In the first phase, the performance of a new process called abrasive mixed electrode discharge diamond grinding (AMEDDG) has been investigated while machining Inconel 718. High machining rate and low surface roughness are both contradictory objective and to encounter them surface grinding assisted EDM was carryout in the presence of abrasive mixed dielectric fluid. It was observed that the AMEDDG is capable of achieving high machining rate at the same time good surface finish. Both high wheel speed and abrasive mixed dielectric assists in enhanced machining conditions.

In the second phase, an experimental investigation on low-frequency vibration assisted micro electro discharge (μ-ED) drilling while fabricating micro-holes has been performed. The effects of vibrational frequency along with other control factors viz. gap voltage, capacitance, and electrode rotational speed were examined on material removal rate (MRR), electrode wear ratio, overcut and taper angle. A significant improvement in the machining performance, as well as quality and accuracy of micro-holes, was observed when low-frequency workpiece vibration was introduced in the μ-ED drilling of Inconel 718.

At the last, a novel approach for fabrication of microchannels using the μ-ED milling assisted with low-frequency vibration is proposed. Initially, the effects of control factors on machining performance of μ-ED milling were examined. Then, the effects of vibrational frequency on the surface quality and accuracy of the fabricated micro-

channels have been discussed. The proposed approach is compared with previously proposed approaches of µ-ED milling and it is found that proposed approach enhances the machining performance considerably.

The assistance of low-frequency vibration found to be attributing enhanced machining like the effective removal of debris and molten material from the inter-electrode gap, effective flushing conditions, reduced electrode-workpiece adhesion etc. resulting in improved machining performance of both µ-ED drilling and µ-ED milling. To complement these finding, the approach of low-frequency vibration assistance also tested on micro-wire EDM process.

This work was emphasized on achieving improved process performance while fabricating common micro-features in Inconel 718 by hybridized EDM processes to overcome their limitations. The benefits of hybridizing EDM have been successfully demonstrated through experimental investigations. The hybridizing EDM processes facilitate us to improve process capabilities in terms of the surface roughness, material removal rate, tool life and geometrical accuracy. Some of the important contributions of this study include generation of surfaces with a good surface finish at high machining rate using AMEDDG, fabrication of high-aspect-ratio micro-holes using a low-frequency vibration assisted µ-ED drilling and fabrication of complex shaped micro-channels using a low-frequency vibration assisted µ-ED milling.

Overall, it is perceived that hybrid machining processes could be a new future for precision and micro-machining domain for fabrication of complex micro-features on difficult-to-cut materials to obtain higher machining efficiency.

Table of Contents

List of Figures

List of Tables

List of Abbreviations

EDM	:	Electric discharge machining
MRR	:	Material removal rate
3D	:	Three dimensional
ED	:	electro-discharge
HMPs	:	Hybrid machining processes
EDDG	:	Electro discharge diamond grinding
ECDM	:	Electrochemical discharge machining
WEDG	:	Wire electro-discharge grinding
EDG	:	Electro discharge grinding
H-EDM	:	Hybrid electro discharge machining
ECDG	:	Electrochemical discharge grinding
IEG	:	Inter electrode gap
AEDG	:	Abrasive electro-discharge diamond grinding
EDAG	:	Electro-discharge abrasive grinding
POT	:	Pulse-on-time
R_a	:	Average surface roughness
EDDSG	:	Electro discharge diamond surface grinding surface grinding
EDDFG	:	Electro discharge diamond face grinding
EDDCG	:	Electro discharge diamond cut-off grinding
AEDM	:	Additive/abrasive mixed electro discharge machining
AMEDDSG	:	Abrasive mixed electrode discharge diamond surface grinding
RC	:	Resistor–capacitor
W	:	Tungsten
EWR	:	Electrode wear rate
ERS	:	Electrode rotational speed
PMDC	:	Permanent magnet direct current
FEW	:	Frontal electrode wear
RSM	:	Response surface methodology
CCD	:	Central composite design
ANOVA	:	Analysis of variance
C.V.	:	Coefficient of variation

ERS   : Electrode rotation speed

VF   : Vibrational frequency

DE   : Discharge energy

List of Notations

O_c	:	Overcut
D_a	:	Average hole diameter
θ	:	Taper angle
r_t	:	Radius of hole at top
r_b	:	Radius at bottom
d	:	Hole depth
t	:	Machining time
∇M_{wp}	:	Workpiece weight difference before and after the experiment
W_s	:	Wheel speed
AC	:	Abrasive concentration
C	:	Current
T_{on}	:	Pulse-on-time
V_g	:	Gap voltage
Cp	:	Capacitance
R	:	Electrode rotation speed
F	:	Vibrational frequency
$MRR_{\mu EEd}$	:	MRR in μ-ED drilling process
$MRR_{\mu EEm}$	:	MRR in μ-ED milling process
$\emptyset$	:	Vibrational frequency
FR	:	Feed rate

1 Introduction

1.1 Importance of machining difficult-to-cut materials

To encounter demands of materials competent for extreme applications, various superalloys have been developed in last few decades. Superalloys are also known as heat-resistant superalloys or high-temperature alloys and generally classified into four groups such as nickel-base, cobalt-base, and iron-nickel-base alloys, titanium based alloys. Superalloys exhibits high-temperature corrosion resistance, oxidation resistance, and creep resistance and ability to maintain these properties at elevated temperatures severely deters the machinability of these superalloys, therefore, they are usually referred to as difficult-to-cut materials [1, 2]. Owing to excellent mechanical properties, difficult-to-cut materials have been widely used in diverse applications in numerous engineering areas including aerospace, automobile, medical, chemical, etc. [1, 3]. Therefore, the machining of difficult-to-cut materials is an important issue in the field of manufacturing and machining of them can stimulate opportunities for exploiting them comprehensively.

1.2 Challenges in machining of Inconel 718

Among Nickel-based superalloys, Inconel 718 owing to excellent high-temperature resistant characteristics is used in the field of gas turbine components, cryogenic storage tanks, jet engines, pump bodies and parts, rocket motors and thrust reversers, nuclear fuel element spacers, hot extrusion tooling, high strength bolting, and down hole shafting [4]. However, the characteristics such as lower thermal conductivity, work hardening, presence of abrasive carbide particles, hardness, affinity to react with tool

material, etc. make it a difficult-to-cut material. The several challenges in machining of Inconel 718 include [3, 5, 6]:

- Owing to the low-thermal-conductivity, heat produced during machining is neither transferred to the chip nor the workpiece, but concentrates on cutting edges resulting in crater wear and severe plastic deformation of the cutting tool edge.

- Excessive crater wear leads to catastrophic failure of the tool and plastic deformation leads to high cutting forces.

- These alloys chemical react with cutting tools forming built-up edges and coating delamination leading to poor tool life

- The hard, abrasive intermetallic compounds in the microstructure cause severe abrasive wear to the tool tip.

- The high heat generation during machining can cause changes in alloy microstructure and induced residual stresses lead to reduced fatigue life of the component.

Over the past few decades, there has been an increased interest in the machining of Inconel 718 that has captured the imagination of manufacturing industry. Substantial work has been conceded to machine Inconel 718 with conventional machining processes revealing different failure modes and tool wear mechanisms. Dudzinski et al. [7] presented the extensive review on high-speed machinability of Inconel 718. They classified the difficulty in machining of Inconel 718 into two basic problems as short tool life and severe surface integrity of machined workpiece. Critical control over machining variables like tool and coating materials, tool geometry, machining method, cutting speed, feed rate, depth of cut, lubrication are required to attain satisfactory tool life and surface integrity of the machined surface [3, 5, 6].

To overcome problems and high costs associated with the conventional machining processes, non-conventional machining is increasingly attempted for the machining of Inconel 718, particularly for applications where high accuracies, good surface finish and complex geometries, parts machined without burrs or residual stresses are of critical importance. Non-traditional machining processes involve material removal by several methods involving electrical, thermal, chemical and mechanical energy and have unique abilities to process materials which otherwise difficult to machine [8]. Some of the commonly used processes are ultrasonic machining, abrasive jet machining, abrasive water jet machining, abrasive flow machining, electric discharge machining (EDM), electrochemical machining, laser beam machining, electrochemical machining, electron beam machining, etc. Although these processes use different energy sources for material removal, they used the common approach of non-contact type machining. The non-contact machining approach eliminates the prerequisite of cutting tools and rigid work holding devices making them cost effective, power saving, and allowing reduced manpower activity [9]. However, owing to low material removal rate (MRR) these processes are not considered as a substitute to conventional machining processes unless conventional processes cannot be applied.

In recent years, the emerging miniaturization technologies are clearly driving developments in micro-scale processes, machines, metrology to meet needs related to part size, feature definition, accuracy, and precision, and materials development [10]. The miniaturization of devices appetites the fabrication of mechanical components with features in the range of a few to a few hundred microns in fields that include optics, electronics, medicine, biotechnology, communications, and avionics, to name a few. Specific applications include micro fuel cells, micro-reactors requiring microscale pumps, valves and mixing devices, microfluidic systems, micro-holes for fiber optics,

micro-nozzles for high-temperature jets, micro-molds, and much more [11-15]. Figure 1.1 reviews some of the micro-feature based micro-devices and their application areas.
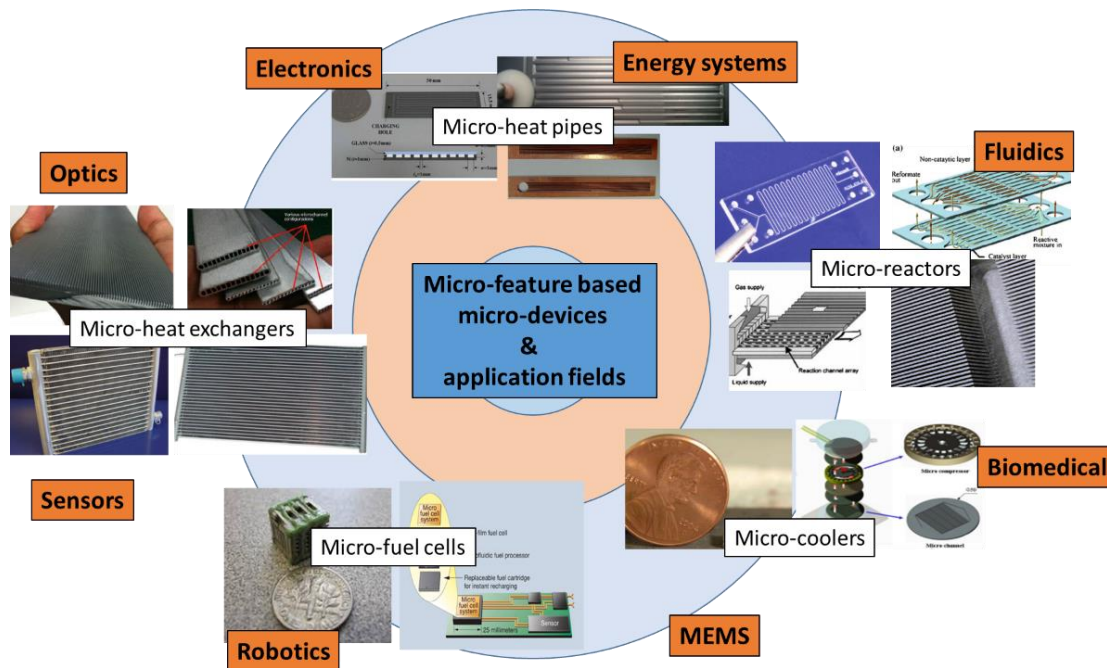
Figure 1.1 Micro-feature based micro-devices and their applications

For fabrication of miniaturized features and devices, the non-conventional processes play a vital role as compared to conventional machining processes. Here owing to sizing effect [16], the specific energy of machining increases immensely instigating larger concern for conventional processes. Contrarily, non-conventional processes can be efficiently used for fabrication by integrating required modifications for micro-scale. For example, reducing the energy, minimizing sparking time or etching duration, reducing beam diameter, enhancing axes precision, etc. [10, 17]. Incorporation of a number of sophisticated modification and investigations given non-conventional processes a new dimension of research and a wide range of application.

Among, various non-conventional processes, electro-discharge machining (EDM) one of the important and cost-effective non-conventional methods and has undergone significant transformations in last two decades [18-20]. In EDM or spark machining,

the material removal of electrically conductive materials takes place due to the rapid and repetitive spark discharges provided by the electric pulse generator in the presence of dielectric fluid supply between tool and workpiece [21, 22]. EDM is non-contact type process, and there is no physical cutting forces exist between the workpiece and tool. EDM has been continuously evolving from a mere tools and dies manufacture process to a micro-scale application machining. While fabrication of micro-features, the use if low energy levels become vital for the EDM process and the process is termed as micro-EDM. Micro-EDM has similar characteristics as EDM except that the size of the tool, discharge energy, and axis movement resolutions are in micron level [19, 23]. Currently, micro-EDM is extensively used for high-precision machining of conductive materials such as metals, metallic alloys, ceramics, etc., regardless of their hardness. Both EDM and micro-EDM processes find widespread applications in the field of mold making, production of dies, cavities and complex three-dimensional (3D) structures using difficult-to-cut materials [19]. The key benefit offered by EDM over the conventional machining process is that it is an electro-thermal process of removing metal regardless of hardness where the force between the workpiece and tool is trivial. Therefore, the error produced owing to the tool deformation is nearly zero [24]. In addition, there is no chatter, mechanical stress or vibration problem during the machining as there is no direct contact between the electrode and the workpiece [25]. The ability of EDM to produce highly complex shapes with high aspect ratios, without imparting significant stresses on the component, has made it indispensable for the micromachining of miniaturized components. Therefore, EDM and micro-EDM has been favored as one of the most effective techniques of machining Inconel 718.

1.3 Significance of the research

Even though EDM has numerous benefits over other machining processes and several studies have been reported on EDM and micro-EDM of Inconel 718 in last decade, few issues remain to be solved before the EDM process can become a reliable, efficient and economical process for fabrication of micro-features in Inconel 718.

Various applications of Inconel 718 frequently include demands at the surface; therefore, the quality and integrity of the surface finish resulting from the EDM process may attribute a substantial influence on the product performance. The poor surface finish and the cavities produced on dies and molds by EDM replicated on final products. Therefore, the surface quality is of principal importance in the EDM of Inconel 718. One of the main downside the EDM is that the discharge energy considerably influences the Surface finish and integrity of workpiece. Microcracks induce residual stresses and change the microhardness of the subsurface, which occurs due to thermal action in EDM [18]. Secondly, the EDM processes are relatively slower that the conventional machining processes [26]. The difficulties become more evident while fabricating the micro-features such as deep micro-holes, micro-channels, using micro-EDM variants such as micro-electro-discharge drilling (μ-ED drilling), micro-electro-discharge milling (μ-ED milling).

Inconel 718 extensively used in aerospace industries for elevated temperature application like turbine blades, guide vanes, afterburners, etc. and these parts requires high-aspect-ratio miniaturized holes for enhanced cooling that results in excellent operating efficiency [27]. While fabrication of high-aspect-ratio micro-holes using μ-ED drilling, the passage of dielectric and removal of debris become very problematic and results in higher machining time and low-aspect-ratio of the hole [28, 29]. Also, the electrode wear leads to degeneration of quality of micro-holes. The μ-ED milling

has prodigious prospects in the fabrication of micro-features owing to its easiness to apply, relatively lower setup cost and ability to fabricate micro-features with complex 3D geometries. Fabrication of micro-channels has broad applications in the miniaturized products like micro-fluidic devices, lab on a chip, micro-heat-sinks, or heat exchangers, etc. [30] and μ-ED milling a competent process for fabrication of micro-channels in difficult-to-cut materials. However, while fabrication of micro-channels using μ-ED milling, the process suffers from longer machining times [31]. Also, significant electrode wear during generation of micro-channels results in degeneration of shape of micro-channel and requires multiple machining passes to achieve the desired shape of micro-channel [32]. Overall, longer machining and significant electrode wear rate limit the applications of μ-ED milling.

In response to challenges in machining difficult-to-cut materials and limitations of individual machining processes, researchers have been attracted toward developing hybrid machining processes (HMPs), which employs simultaneous or ensuing action of two or more machining processes or takes aid of some energy assistance in material removal to enhance the advantages of constituent processes, while at the same time minimizing their adverse effects when they are applied individually [33]. The performance characteristics of a hybrid process are considerably different from those of the single-phase processes in terms of productivity, accuracy, and surface quality [33, 34]. The hybridization of EDM resulted in enhanced machining performance and therefore, various hybrid EDM processes have been developed in last two decades. The hybrid EDM processes can be either assisted processes or compound processes. The processes which take the aid of different energy sources to enhance process performance are known as assisted processes e.g. laser-assisted EDM, cryogenic assisted EDM, vibration assisted EDM and magnetic assisted EDM. Whereas,

processes which involve simultaneous or ensuing action of two or more material removal mechanisms are known as compound processes e.g. electro discharge diamond grinding (EDDG), electrochemical discharge machining (ECDM), etc [23, 33, 34].

It has been found that requirements for micro-features in difficult-to-cut materials have made EDM a cost-effective manufacturing process. However, the process suffers from longer machining time, significant electrode wear, and poor surface quality, and there is a need to investigate the feasibility of hybridizing EDM to enhance the process performance and overcome the challenges of macro and micro-EDM. The hybridization of EDM can deliver micro-features with good surface quality and better dimensional accuracy at high machining efficiency. In this regard, this study considered hybridization of EDM had been performed in view to achieve enhanced the performance while fabricating micro-surface finish, micro-holes, and micro-channels in Inconel-718 superalloy.

First of all, the EDM is hybridized with diamond grinding which is called as electro-discharge diamond surface grinding (EDDG) for initial understanding of the process performance on machining of Inconel 718. Then EDDG is carried out in abrasive mixed dielectric and process is called as abrasive mixed electro discharge diamond surface grinding (AMEDDSG). The AMEDDSG is investigated for fabrication of surfaces with low surface roughness and good surface integrity. Secondly, μ-ED drilling and μ-ED milling are hybridized with low-frequency workpiece vibration assistant in a view enhance the performance of the micro-EDM based micro-feature fabrication and to make micro-EDM a more feasible process. The main implication of this research is hybridized EDM processes should have a considerable contribution in the machining of Inconel 718, and the processes should be more competent for fabrication of micro-features in Inconel 718.

8

1.4   Organization of the Thesis

This chapter introduces the importance of and challenges in machining difficult-to-cut Inconel 718 and the significance of the research of this study.

Chapter 2 presents a review of the current status of research related to the current study in addition to a brief overview on the EDM, micro-EDM, and micro-EDM based multi-processes and hybridized EDM processes. Chapter two ends with identifying research gaps and defining objectives of current work.

Chapter 3 describes the experimentation and methodology including the machine tools used for conducting the experimentation, experimental set-up along with experimental procedures followed while performing different hybrid EDM processes.

Chapter 4 presents an experimental investigation on the performance of abrasive mixed electrode discharge diamond surface grinding of Inconel 718. The effect of various control factors on the performance measures during machining of Inconel 718 has been presented. A multi-response optimization performed to determine the optimal machining conditions. At last, the surface morphology of machined surface is examined by FESEM images.

Chapter 5 presents an experimental investigation on low-frequency vibration assisted μ-ED drilling of Inconel 718 based on the MRR, EWR, overcut and the taper angle of the micro-holes. The surface morphology of fabricated micro-holes at different machining conditions has been assessed at last.

Chapter 6 present an experimental investigation on low-frequency vibration assisted μ-ED milling of Inconel 718 based on the MRR, FEW. The effects of vibrational frequency and discharge energy on surface quality and dimensions of fabricated micro-

channels have been discussed. At last, the proposed approach is compared with previous studies and utilized to fabricating complex shapes of micro-channels.

The conclusions and summary of the contributions are presented in chapter 7. Also, some directions for future work related to this study are also presented.

2 Literature review

The current chapter presents an overview and background EDM, and variants of EDM process highlighting the state-of-the-art on the EDM based processing of difficult-to-cut materials.

2.1 Background

Electro Discharge Machining (EDM) is one of earliest developed non-conventional machining processes, originated more than 65 years ago in a simple die-sinking application. Presently, EDM has been a well-established machining alternative in manufacturing industries all over the world and substituted drilling, milling, grinding and other conventional machining processes in different aspects. Micro-EDM is a later development of EDM when Kurafuji and Masuzawa [35] revealed drilling of a minute hole in carbide plate and has established as a cost-effective technique in the manufacture of micro-tools, micro-components, and micro-features with good dimensional accuracy and repeatability. Ever since the substantial extent of exploration has been concentrated on the growth of micro-machining processes. In this section, the fundamental working principle of the EDM process, the way of removing materials, and its machining properties are briefly discussed.

2.2 Overview of EDM processes

2.2.1 Principle of EDM

Anybody who has ever seen what ensues after hitting off a bolt of lightning on the ground has seen the working dynamism of the EDM process in its most basic form. EDM is the process of machining electrically conductive materials in which material

removal takes place in the form of craters due to the rapid and repetitive spark discharges provided by the electric pulse generator in the presence of dielectric fluid supply between tool and workpiece (Figure 2.1) [36, 37].
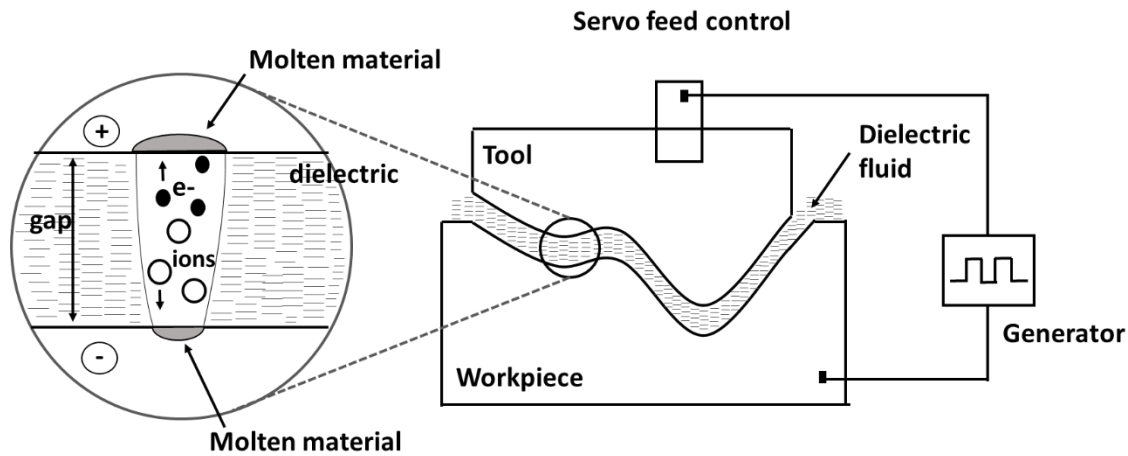
Figure 2.1 Schematics of the electro discharge machining process [35]

The working phenomena of macro and micro-EDM processes are fundamentally similar with the main contrasting features like size of the tool used, the power supply of discharge energy, and the resolution of the X-, Y-, and Z-axes movement [38]. The controlled action of voltage, sparking gap, energy, and frequency of discharge drives the metal removal. In micro-EDM, high accuracy and good surface qualities are obtained at high frequencies (200 Hz) and small energies (10^{-6}–10^{-7} J) for every discharge (40–100 V) [39]. A pulse generator used to deliver the discharge energy. A servo control is used for controlling the tool movements so that precise spark gap between tool and workpiece can be maintained. Flushing of debris from the inter-electrode gap is ensured with the provision of fresh dielectric which is maintained through a dielectric circulation unit with pump, filter, and tank. The working principle of EDM (Figure 2.1) can be explained through sparking phenomena which happen in three stages as ignition formation stage, discharge stage, and interval stage between discharges [40].

12
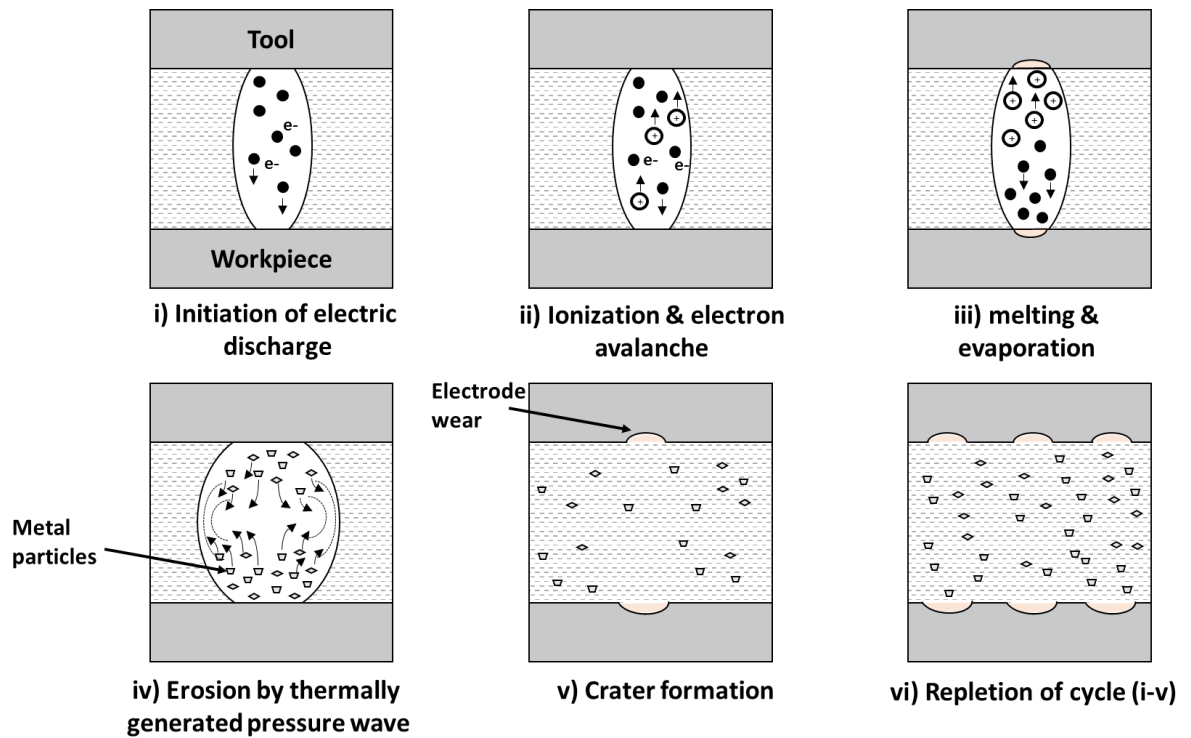
Figure 2.2 Working principle of electric discharge machining (adapted from [38])

- An energy column is formed upon application of the gap voltage, which attains maximum strength when the electrode and surface are closest.

- The electrical field finally breakdowns the dielectric insulation. When the resistivity of the fluid reaches to the lowest, a single spark is capable of streaming through the ionized flux tube and striking the workpiece.

- The spark results in melting and vaporizing of the area in contact, forming in a single crater.

- The resistivity of dielectric increase is quickly showing to spark heat and contaminates produced from a workpiece which disturbs the ionized particles in the dielectric.

- For the duration of the pulse of time, as a heat source is removed, the sheath of vapor that was around the spark collapses. Its collapse produces a void or vacuum and pulls in fresh dielectric to remove debris and molten metal.

13

Moreover, the re-ionization occurs providing a positive condition for the next spark.

2.2.2   Macro- vs. micro-EDM

The working principles of the EDM process are basically the same between the macro-scale and micro-scale processes. However, their major differences are in terms of the size of the tool used, the power supply of discharge energy, and plasma channel diameter, all of which are interrelated [41, 42]. Some dissimilarities between the macro- and micro-EDMs are listed below:

- The most imperative modification of micro-EDM is the plasma channel diameter formed during the sparking. In macro-EDM, the plasma channel is considerably smaller than the electrode, but the size is analogous to micro-EDM [36].

- Micro-EDM uses considerably smaller electrodes which allow narrow heat conduction and low spark heat dissipation.

- Micro-EDM utilizes significantly reduced of discharge energy by decreasing discharge voltage, current, and pulse on-times [43, 44]. Therefore, there is a considerable difference in generated crater size for micro-EDM.

- The debris removal is more difficult in micro-EDM because the gap is smaller, the dielectric viscosity is higher, and the pressure drop in micro-volumes is higher [43, 45].

- In micro-EDM, it is very difficult to expel debris from machining gap as the gap is very narrow, the high viscosity of dielectric, and high-pressure drop in micro-volumes [45].

- Micro-EDM based fabrication attributes the high precision and accuracy. However, for macro-EDM for achieving higher precision critical control on electrode wear and vibrations is essential.

- Comparatively, higher electrode wear occurs for each discharge for micro-EDM as compared to macro-EDM.

The dissimilarities between macro- and micro-EDM are summarized in Table 2.1 [17, 46].

Table 2.1 Dissimilarities between macro-EDM and micro-EDM

Sr.No.	Description	Macro EDM	Micro EDM
1	Size / dimension	Greater than or equal to 1mm	Less than 1 mm
2	Volumetric wear	Less	More
3	Sparking gap	100 microns	10 microns
4	Supply energy	Larger than 1000 μJ	Smaller than 1000 μJ
5	Pulse duration	50 μs	150 ns
6	Power circuit	Transistor circuit	Resistance-capacitor circuit

2.2.3 Variants of EDM

EDM has been evolved for variety of specific application and classified into four main variants [47] as:

i) Die-sinking EDM, where an electrode with micro-features is employed to produce its mirror image in the workpiece.

ii) Wire EDM, where a wire is used to cut through a conductive workpiece.

iii) EDM drilling, where microelectrodes are used to 'drill' micro-holes in the workpiece.

iv)   EDM milling, where microelectrodes are used to fabricate 3D shape by implementing the axes movements similar to that in conventional milling.
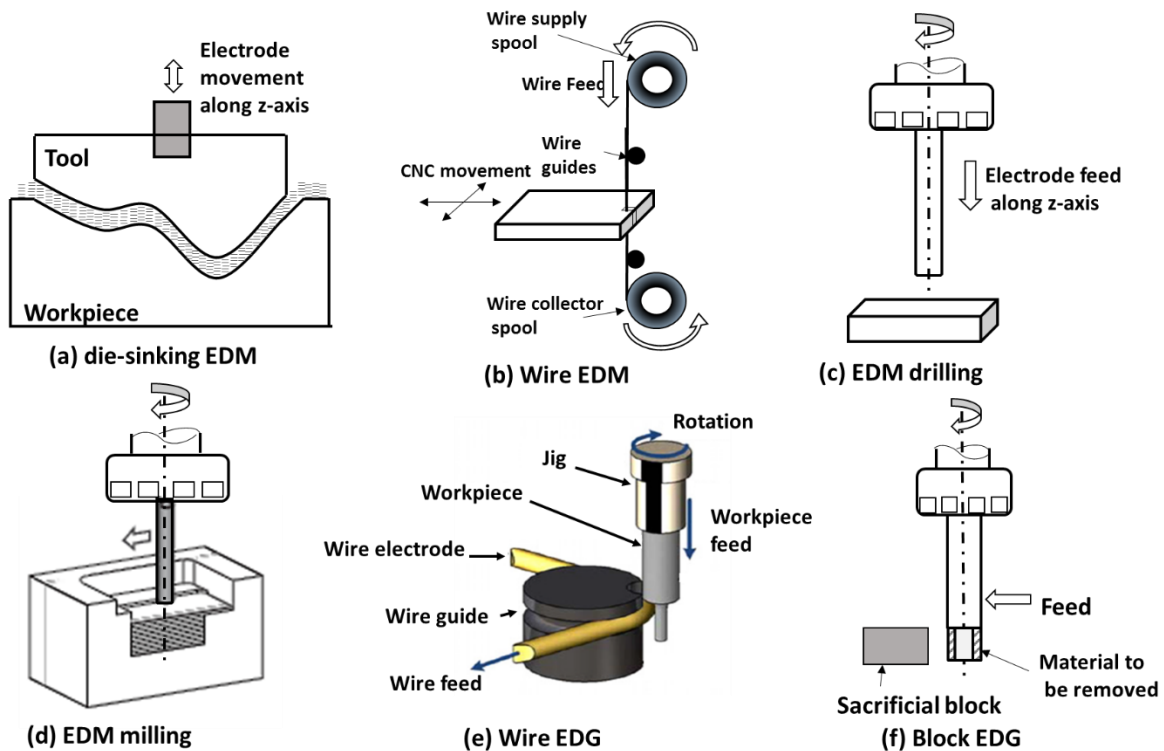
Figure 2.3 Variants of EDM

In recent years, two additional variants of EDM evolved. One is wire electro-discharge grinding (WEDG) in which grinding is done using EDM. This process is mainly used fabricate axis-symmetrical parts like micro-tool electrodes, micro-shafts, etc. Second, is block electro discharge grinding (EDG), which is used to fabricate micro-electrode on-machine from an electrode thicker than the required one. Figure 2.3 shows schematic diagrams of variants of EDM.

2.2.4   Compatibility and benefits of EDM over other machining processes

EDM is capable of machining any conductive material irrespective of its hardness including metals, metallic alloys, graphite, and ceramics. Table 2.2 displays the compatibility of EDM with different micromachining technologies.

Table 2.2 Compatibility of EDM with other machining processes

Machining Process	Feasible materials
LIGA	metals, polymers, ceramic materials
Etching	metals, semiconductors
Excimer-LASER	metals, polymers, ceramic materials
Micro-milling	metals, polymers, ceramic materials
Diamond	cutting Non-Ferro metals,
Stereolithography	Polymers Polymers
EDM	metals, semiconductors, ceramics

EDM offers following benefits as compared to other machining processes [48]:

- A low setup cost compared to lithographic techniques.

- Suitable for batch production due to the flexibility offered.

- Involves little job overhead (such as designing masks, etc.).

- Competent to fabricate complex 3D micro-features.

- Shapes that prove difficult for etching are relatively easy for EDM.

2.3 Hybrid EDM processes

Each nontraditional machining process has its unique and inherent limitations; for example, (i) processes using abrasives (i.e. ultrasonic machining, abrasive jet machining, abrasive water jet machining, abrasive flow machining) necessitate hardness of abrasives more than the workpiece material at the actual temperature of machining; (ii) electrochemical machining can only be used for electrically conducting materials, while chemical machining can only be used for chemically reactive materials; and (iii) thermal processes like EDM, laser machining, etc. may impart thermal damage (i.e. heat affected zone, recrystallization, recast layer and splattered particles). Moreover, costs for equipment, operation, and maintenance of thermal

nontraditional machining are high. A lot of effort has been put to overcome the possible limitation of individual machining techniques through the development of HMP's.

As discusses in section 1.3, HMPs are playing a vital role to meet the challenges imposed by miniaturization and advanced materials. Much work has been reported in hybridization of EDM reporting enhanced machining performance in last two decades. The performance characteristics of a hybrid electro discharge machining (H-EDM) are reported to be considerably enhanced regarding productivity, accuracy, and surface quality [34]. In EDM, discharge pulse energy significantly affects surface integrity. With the increase in discharge energy, the surface roughness of the material increases. The thermal action in EDM also induces micro-cracks, induce residual stresses, and change the micro-hardness of the subsurface and surface layer. To overcome these issues, several studies have been reported in the field of H-EDM since last few years. In compound HMPs, EDM can be hybridized with other processes such as EDG, electro-discharge diamond grinding (EDDG), electrochemical discharge machining (ECDM), and electrochemical discharge grinding (ECDG). Table 2.3 summarizes some H-EDM compound-type HMPs with the mechanism of MR, process parameters and capabilities, and work materials reported in past studies.

Further, some assisted EDM processes have also been developed to enhance machining performance of EDM e.g. laser-assisted EDM, cryogenic assisted EDM; vibration assisted EDM and magnetic assisted EDM. In EDM and micro-EDM, the debris gets trapped in the interelectrode gap (IEG) and results in reduced machining efficiency. A number of studies reported for enhancing debris removal and flushing methods to expel debris from IEG efficiently and developments like vibration assisted EDM, magnetic assisted EDM have arisen. In vibration assisted EDM, tool or workpiece vibrations are induced which continuously changes the spark gap generating a pressure variation in

the sparking gap. The continually changes in pressure promotes in the improved ejection of the debris through enhanced flushing conditions.

Table 2.3 Compound-type hybrid EDM processes [33]

HMP	MR mechanism	Purpose of hybridizing	Advantages of hybridizing	Workpiece materials	Remarks
EDG	Rotary electrode with rapid sparks causing MR due to erosion phase	Enhancement of flushing efficiency of EDM	Improved MRR, surface finish	Tool steel AISI D2 [49]	Thin and fragile materials can be machined with Ease [50] as compared to EDM
EDDG	Electro-discharge erosion and mechanical abrasion phase	EDM productivity improvement	Issues such as re-solidified layer, large tool wear rate and thermal cracks are overcome	Bearing steel (LH15)[51], high-speed steel (HSS)[52], titanium (Ti6Al4V) [53]	MRR eight times better than EDM and two times better than EDG
ECDM	Electrochemical dissolution of the material and thermal erosion by electrical discharges	Micro-machining and scribing hard and brittle non-conductive materials	Non-conductive materials can be machined, MRR 5 times than ECM [54], times than EDM	Glass (mainly pyrex, plexi, and optical), ceramic, refractory bricks, quartz, and composite materials[54]	ECDM reported for hole drilling [55, 56], 3D microsurface Machining [57], and so on
ECDG	Electro-discharge erosion, electrochemical dissolution, and mechanical abrasion	Enhancement of achievable surface finish in ECDM	Improved MRR and surface finish	MMCs [58]	Only conductive materials surface roughness (R_a) 10 times less than ECDM, while MRR 3 times higher [58]

AISI: American Iron and Steel Institute; HMMP: hybrid micromachining processes; AEDG: abrasive electro-discharge grinding; EDG: electro-discharge grinding; MR: material removal; EDM: electro-discharge machining; MRR: material removal rate; 3D: three-dimensional; ECM: electrochemical machining; ECDM: electrochemical discharge machining; MMCs: metal matrix composites.

A stable flow of debris helps the stability of the machining in EDM due to the use of cylindrical workpiece or tool electrode. However, in the manufacturing of rectangular holes or rectangular shafts, where a rotating spindle cannot be used, the indecorous flow of debris causes adhesion of the workpiece and tool electrode [59]. A fair amount of research has focused on Ultrasonically assisted EDM to investigate the effects of high-frequency vibration of the tool or workpiece, on MRR, machining efficiency, surface quality, subsurface damages, and so on [28]. The employment of vibration is mainly

attributed to enhanced dielectric circulation and pumping action, resulting in the effective removal of molten metal from craters, evacuation of debris, and thus improving discharge characteristics [60, 61], resulting in minimum micro-cracks and microstructure modifications on the workpiece at higher MRR and fatigue life [62].

The application of magnetic fields for gap cleaning in EDM was first suggested by De Bruijn et al. [63] introduction of the magnetic field causes improved debris circulation in EDM. Applying magnetic force perpendicular to the electrode's rotational force produces a resultant force that pulls debris out of the hole during machining. Lin and Lee [64, 65] concluded increased MRR as a result of enhanced debris removal from the gap in assistance of magnetic fields. Magnetic field–assisted micro-EDM can produce high-aspect-ratio holes compared with the conventional micro-EDM process under similar working conditions.

Overall, it is perceived that HMPs facilitate to enhance process competencies while fabricating macro and micro 3-D features. To produce micro-features on difficult-to-cut advanced materials, HMPs can deliver higher machining efficiency with high accuracy and surface quality. HMPs are just starting to be developed in many features, leaving ample opportunity for future investigation. The following section is focused on presenting a review of studies aimed to fabricate micro-features like micro-surfaces, micro-holes, and micro-channels using EDM based processes.

2.4 Literature survey

2.4.1 Electro discharge diamond grinding

As discussed previously, EDM has emerged as one of the major non-conventional machining processes, though, discharge energy considerably influences the surface integrity of workpiece and process involves longer machining time. Microcracks induce

residual stresses and change the microhardness of the subsurface, which may occur due to thermal action in EDM. To overcome these issue, different research studies have been presented. The use of rotary electrodes to enhance the performance of EDM has been proposed in some studies to improve machining performance of EDM [49, 66]. Mohan et al. [67] experimentally demonstrated that the rotating tool electrode improved the flushing efficiency as that of the stationary electrode in EDM. Further, to overcome issues related to surface integrity in EDM, Koshy et al. [68] suggested the use of metal fused abrasive grinding wheel. The use of diamond particle abrasives on grinding wheel then termed this process as electro-discharge diamond grinding (EDDG) [69]. EDDG is a process in which synergistic interactive effect of the combination of EDM and grinding process is employed to increase machining productivity. The electro-discharge erosion by EDM and the mechanical abrasion action by grinding responsible for material removal in EDDG as shown in Figure 2.4. EDDG is also referred as abrasive electro-discharge diamond grinding (AEDG) and electro-discharge abrasive grinding (EDAG) in some research articles. The EDDG process becomes evident when machining super hard materials, engineering ceramics, sintered carbides, and metal composites [70, 71].

The use of metal bonded diamond grinding wheel resulting two times higher material removal rate than rotary electrode was reported by Kozak [70]. It is also reported that grinding wheel gets self-dressed continuously without need of interrupting the process. Yadav et al. [52] used copper bonded diamond wheel and experimentally evaluated the effects of wheel speed, pulse-current and pulse-on-time (POT) on MRR in EDDG of High Speed Steel. Singh et al. [72-74] in their studies reported bronze bonded diamond wheel in EDDG of HSS and Tungsten Carbide-Cobalt composite. They studied the effects of machining parameters on MRR, average surface roughness (R_a) and wheel

wear rate of EDDG process. They observed that wheel glazing at low current and high wheel speed slumps the MRR capability of diamond wheel.
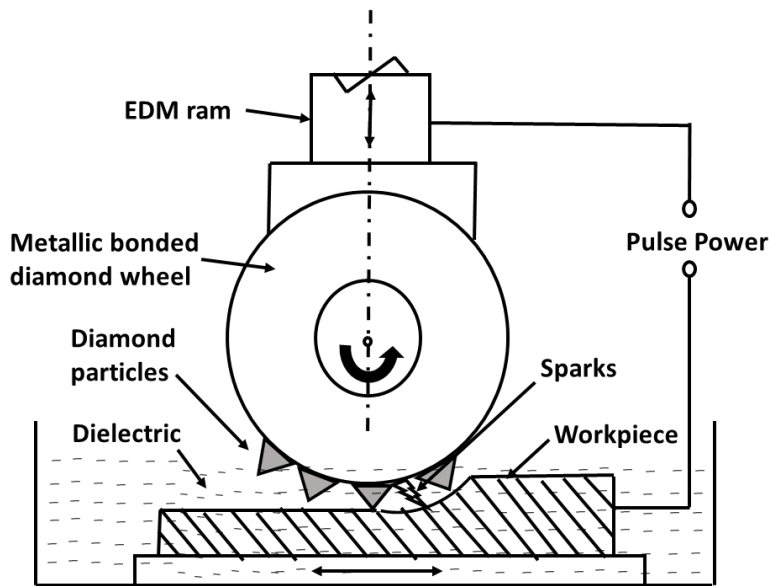
Figure 2.4 Mechanism of material removal in EDDG process

Electro discharge diamond grinding can be operated in three different setups known as i) electro discharge diamond surface grinding surface grinding (EDDSG), ii) electro discharge diamond face grinding (EDDFG), and iii) electro discharge diamond cut-off grinding (EDDCG). Agrawal and Yadava [75] reported the effectiveness of EDDSG in machining of Al-10wt%SiC and Al-10wt%Al_2O_3 composite MMC materials. It has been reported that that MRR improves with pulse current, wheel speed, workpiece speed, depth of cut. The R_a also rises due to higher current, duty factor, depth of cut, and reduced due to high wheel speeds. Kumar et al. [76] claimed that the abrasive particles substantially improves the MRR after removing the solidified layer from the machined surface of 6061 Al/Al_2O_3p 10% Composite during EDDSG process. They also reported that tool polarity, current, and wheel speed are the most significant parameters that affect MRR in EDDSG process.

The use of abrasive powders in dielectric fluid of EDM to overcome issues like micro-crack, recast layers has also been proposed in the literature to fulfill requirements of minimum surface damage and the process is known as additive/abrasive mixed electro discharge machining (AEDM) [77-79]. It has been reported that in AEDM, a different machining mechanism observed than that of EDM. The suspension of abrasive powder in dielectric fluid enhance the machining conditions by facilitating ignition process and increase in gap size, thereby improving process stability [78]. Kumar et al. [80] studied effects different machining parameters on MRR, surface roughness, and wear ratio in AEDM of Inconel 718. They reported that aluminum powder concentration of 6g/l results in higher MRR during AEDM. In other research [79], they reported improvement of 26.85% in MRR with 12g/l concentration of graphite powder in AEDM of Inconel 718. Kumar and Batra [81] reported the surface modifications in die steels by material transfer mechanism due to the presence of tungsten powder in a dielectric fluid.

From above discussions, it was inferred that both AEDM and EDDSG which are hybrid EDM processes offers distinct assets during machining of difficult-to-cut materials. Therefore, it is proposed to combine AEDM with EDDSG to form a new hybrid machining process called abrasive mixed electrode discharge diamond surface grinding (AMEDDSG) to take combined advantage of formed hybrid version of EDM.

2.4.2 Micro-ED drilling

Inconel 718 extensively used in aerospace industries for elevated temperature application like turbine blades, guide vanes, afterburners, etc. and these parts requires high-aspect-ratio miniaturized holes for enhanced cooling that results in excellent operating efficiency [27]. However, fabrication of micro-holes in Inconel 718 using conventional drilling is very challenging as the elevated temperature at tool tip during

drilling results in built-up edge formation [82]. The untimely drill breakage owing to the fragile nature of the micro-drill is one of the major limitation of mechanical micro-drilling [83]. While drilling micro-holes, the drill tip is exposed to huge lateral force at tool-workpiece interface which tends to diverge of drill tip. This huge lateral force leads to bending and ultimately in micro-drill breakage. Moreover, burr formation in mechanical micro-drilling deteriorates the accuracy and quality of fabricated micro-holes [84]. The formation of large recast layers and heat affected zone is a major concern in laser micro-drilling [85]. Further, while fabricating micro-holes in hollow parts such as airfoil blades and fuel injector nozzles, the laser often damages the back wall. The μ-ED drilling is one of the most efficient and competent non-conventional machining technology that can produce high-aspect-ratio high quality and burr free micro-holes; and being a contact-less process, no distortion or breakage occur which is inevitable in physical-force based processes [86]. The μ-ED drilling is capable of fabricating micro-holes as small as 5 μm in diameter [87]. This is unlike mechanical drilling, which can produce holes just up to 70 μm, or the micro-fabrication process such as laser machining, which can only create holes of 40 μm [38].

The studies based on the fabrication of micro-holes in aerospace alloys like Inconel 718 are very vital from aircraft and aerospace industries perspective. There numerous studies on μ-ED drilling available in the literature investigating properties of fabricated micro-holes related the effects of type of generators (i.e. transistor circuit and resistor–capacitor (RC) circuit type), effects of input process parameter like pulse current, gap voltage, POT, duty factor, electrode rotation speed, capacitance, feed rate etc., effects of electrode materials, effects of dielectric fluid properties, and so on. Kuppan et al. [88] experimentally investigated the deep hole drilling capability of Inconel 718 using the tubular copper electrodes of Ø3mm in EDM. They developed empirical models for

MRR and depth-averaged surface roughness revealing that the peak current, duty factor, and electrode rotation are significant for MRR while surface roughness influenced by peak current and POT. Yilmaz and Okka [89] claimed that single channel brass, as well as copper electrodes, attributes in higher MRR and low electrode wear rate (EWR) as compared to multichannel electrodes, however, multichannel electrodes yields superior surfaces of drilled micro-holes in Inconel 718 and Ti–6Al–4V. Recently, Bassoli et al. [90] presented effects of electrode shape and geometry on micro-ED drilling process performance. They claimed that electrode shape and geometry significantly affect the gap flushing efficiency. Ay et al. [91] suggested optimum µ-ED drilling parameters for better taper ratio and hole dilation for Inconel 718 using grey relational optimization. They suggested that low values of discharge current and pulse duration attributed to reduced crack and damage characteristics of micro-holes. The performance of different electrode materials in the µ-ED drilling of Inconel 718 and stainless steel was investigated by Unune et al. [92] and D'Urso et al. [93-95] respectively. They suggested that electrodes with high electrical conductivity are suitable for higher MRR while electrodes with low thermal conductivity are suitable for lower EWR. The tungsten electrodes best suitable for high-quality surfaces of micro-holes since the thermal and electrical conductivity of the electrode materials significantly affects surface finish of micro-holes.

To enhance the process capabilities of micro-EDM based process, hybridization of µEDM has been presented in several studies e.g. Sequential laser, and EDM micro-drilling [96, 97], ultrasonic and low-frequency vibration assisted µEDM [29, 98, 99], magnetically assisted µEDM [100], etc. Gao and Liu [28] reported that ultrasonic vibration assisted µEDM yields eight times higher MRR as compared to normal µEDM. However, generations of ultrasonic vibrations are very complex and costlier. Therefore,

the investigations on low-frequency workpiece vibration in µ-ED drilling performed by [29, 99, 101] to improve flushing conditions and unstable machining in deep hole drilling. Jahan et al. [29, 99] evaluated low workpiece vibration assisted µ-ED drilling of tungsten carbide and claimed that low-frequency vibrations have a considerable effect on both the machining characteristics and micro-hole accuracy parameters. Recently, Lee et al. [101] concluded that low-frequency vibration (10-70Hz) were reduced machining time by 70% compared to that of non-vibration machining at non-rotating electrode condition.

The above discussion shows that hybridizing µ-ED drilling offers the better efficiency of the process. Some studies reported on ultrasonic vibration assisted µ-ED drilling, however, rare studies are available on the application of low-frequency vibration while µ-ED drilling for deep micro-holes fabrication. No study is existing of vibration-assisted µ-ED drilling of Inconel 718.

2.4.3   Micro-EDM milling

The die-sinking µ-EDM is the original and common form of µ-EDM in which an electrode analogous to mirror images of required shape is used to produce the required 3D shape on workpiece [20]. However, in the µ-ED milling, a cylindrical electrode travels in predefined motion and evaporates the workpiece material at defined manner to produce 3D shape [60]. The advantages offered by µ-ED milling such as the use of simpler cylindrical electrode unlike die-sinking µ-EDM, high-aspect-ratio profile generation, machinability of any conductive material irrespective of its hardness, etc., makes it a competent micro-machining technique. The µ-ED milling can produce high-aspect-ratio micro-features with good surfaces finish at the low MRR and significant electrode wear limits its applications as compared to other micro-fabrication processes [32]. The discharge energy noticeably influences the workpiece surface integrity related

issues like micro cracks, microvoids, the formation of white layers, changes in microhardness, etc., in the EDM processes [102]. However, the advantages offered by μ-ED milling are more important and fewer research studies available on this process open ups avenues for new research.

The physical behavior of the μ-EDM has been addressed in detail in studies by [103-105]. However, the studies addressing the issues of large machining time and significant electrode wear in the μ-ED milling are limited. The investigation of effects of μ-ED milling process parameter like feed rate, capacitance, and the voltage on MRR, R_a, and tool wear ratio was discussed in [106]. Bayramoglu and Duffill (29-31) studies the effects of control factors using cylindrical electrode for fabrication of curved surfaces. The experimental investigation on effects process parameters viz. discharge energy, electrode rotations, feed rate, was performed by [107] and reported that electrode rotation is critical in deciding the thickness of recast layer in the μ-ED milling process. Further, they explained physics of μ-ED milling process by shape, form and surface quality of produced micro-channels [108]. Recently, Kuriachen and Mathew [109] investigated the performance of the μ-ED milling on non-ferrous Ti–6Al–4V biocompatible alloy and claimed that capacitance is the most influencing process parameters.

The μ-ED milling can be performed using either the layer-by-layer or the bulk machining approach. In layer-by-layer method, the prerequisite depth is achieved in multiple passes and the electrode wear compensation based on uniform wear method is provided in each successive layer. Yu et al. [110] proposed a uniform wear method for micro-ED milling with the simple cylindrical electrode. They further [111] presented an analysis of machining parameters such as tool path and a number of cutting step on precision machined surface. Rajurkar and Yu [87] adopted this method integrating

27

CAD/CAM in EDM for generating the tool path for 3D micro-features. They successfully showed machining of complex cavities through this method. The uniform wear method is described in detail by Yu et al. [112] using a theoretical approach for compensating for tool wear. Zhao et al. [113] introduced CAD/CAM system to generate contour, tool path and NC codes for fabrication of free-form cavities. The tool path was obtained using the sliced contour data of solid mode. They demonstrated the fabrication of some complex 3D features with this approach.

In the bulk-machining method, the entire prerequisite depth is machined in a single cut and hence, the compensation required is not feasible as tool wear from both bottom and side of the tool. Karthikeyan et al. [32] claimed that bulk machining method is more suitable for producing the straight micro-channels. Shukla et al. [114] extended this work and determined the number of compensation pass require in bulk machining approach while fabricating the complex micro-channels. They determined the optimum machining conditions for straight and curved micro-channels.

Jafferson et al. [115] compared individual and combined effects ultrasonic and magnetic assisted μ-ED milling and recommended both techniques effective when applied individually. Kunieda et al. [116] proposed ED-milling in presence gas as a working fluid. The approach high-pressure gas flow assistance for effective removal of the molten metal and debris enhanced machining efficiency. Su et al. [117] used gas in ultrasonic assisted ED milling with lamination machining approach.

The above discussion shows that μ-ED milling has been reported while fabricating 3D micro-feature using various approached. The hybridization of μ-ED milling is newer trend to enhance the performance of this process and very few studies report hybridized μ-ED milling.

2.5 Research gaps

- Though significant research work is reported in macro machining of Inconel-718, rare studies have been reported in micro-machining of Inconel-718 intending to fabricating common micro-features like micro-surfaces, micro-holes, and micro-channels.

- Although EDM has been established as one of important machining processes for machining of difficult-to-cut materials, still it alone cannot meet numerous requirements of the micro-machining domain owing to some drawbacks like longer machining time, significant tool wear and poor surface integrity. There is a need to develop EDM based processes which can overcome aforesaid problems.

- At higher material removal rate, the EDM results in an inferior surface integrity of the machined materials which lead to mechanical degradation of these materials. There is a need to investigate a process which can machine material at a high cutting rate without degrading the surface finish.

- Rare studies are reported on utilizing a hybrid machining approach of a low-frequency vibration assisted μ-ED drilling in focus to produce deep micro-holes with dimensional accuracy. No study has been conducted on low-frequency vibration-assisted μ-ED drilling of Inconel 718. Hence there in need to study machining performance of a low-frequency vibration assisted micro-hole drilling in Inconel-718.

- Although the μ-ED milling is a competent process for fabrication of complex 3D micro-features, it suffers from long machining time and significant electrode wear rate. There is a need to improve the machining rate of this process. To the best of author's knowledge, no work has been reported on utilizing a hybrid

machining approach of a low-frequency vibration assisted µ-ED milling for fabrication of micro-channels. No investigation has been reported on analyzing the effects of vibrational frequency on surface quality and dimension accuracy of fabricated micro-channel.

2.6 Research objectives

The primary aim of this work is to investigate the performance of hybrid EDM processes with a view to improve and enhance the performance of EDM while fabricating micro-features in Inconel 718 superalloy. It is decided to investigate the performance of hybrid EDM processes while fabricating common micro-features like micro-surfaces, micro-holes, and micro-channels. In this context, a number of objectives have been set to accomplish the main aim are as follows:

- Experimental investigation on the feasibility of achieving high machining rate without affecting the surface quality using AMEDDG of Inconel 718.

- Experimental investigation of low-frequency workpiece vibration assisted µ-ED drilling of Inconel 718 in deep-hole drilling based on the MRR and EWR.

- Examination of effects of low-frequency workpiece vibration assistance, discharge energy, and electrode rotational speed on the surface quality and the dimensional accuracy of the fabricated micro-holes by µ-ED drilling.

- Experimental investigation of low-frequency workpiece vibration assisted µ-ED milling of Inconel 718 while micro-channel fabrication based on the MRR and EWR.

- Examination of effects of low-frequency workpiece vibration assistance on the surface quality and the dimensional accuracy of the fabricated micro-channels by µ-ED milling.

3 Experimentation and methodology

This chapter explains the experimental set-ups and experimental procedures adopted for fabrication of micro-features in Inconel 718 superalloy with hybrid EDM processes used throughout the thesis. The overview of the setups including a brief description of the machine tool, workpiece, electrode and dielectric materials. Numerous measurement techniques and equipment are also described in the final section.

3.1 Machine tools

3.1.1 Electro discharge machine: ENC-35

The EDM machine (ENC-35: Electronica Machine Tools Ltd.) modified with diamond surface grinding attachment was used to perform EDDG experiments. The photograph of the machine is shown in Figure 3.1. The specifications of ENC-35 are given in Table 3.1 below:

Table 3.1 Specifications of ENC-35 EDM

Description	Specification
Design	Fixed column, moving table
Supply	415V, 3 phase, 50 Hz
Machining current max (amps)	35 A
Open gap output voltage	200 V dc +/- 5%
Machine travels	Maximum travel: X – 300mm, Y – 200mm, Z – 250mm
Dielectric capacity	400 Litres

Figure 3.1 Electronica EDM ENC-35

3.1.2 Micro-machining tool DT-110

Mikrotools DT110 high precision integrated multi-process micromachining tool working on the RC-pulse generator was used to for fabrication of micro-hole and micro-channels. The photograph of the machine is shown in Figure 3.2. The machine can perform wide varieties of operations such as μ-EDM, μ-ED drilling, μED milling, μ-WEDM, block-EDG, μ-WEDG, μ-turning, and μ-milling. It has a resolution of 0.1 μm on all axis with an accuracy of ±1 μm upon 100 mm and repeatability of 1 μm for all axes. The specification of DT100 is listed in Table 3.2. The other details of the machine are available at [118].

Table 3.2 Specification of DT-110

Description	Specification
EDM Power supply	Voltage: 80V~150V RC discharge circuit: R:1KOhm fixed, C: 6 selectable
Machine travels	Maximum travel: X – 200mm, Y – 100mm, Z – 100mm
Position accuracy	± 1 micron/100mm
Axes resolution	0.1 µm
Spindle speed	0-2000 rpm
Linear drive systems	Digital AC servo motor system with full-closed feed back control

Figure 3.2 Photograph of DT-110 machine

3.1.2.1 Vibration device

The low-frequency vibration was employed using a vibration device provided along with machine tool. The vibration device works on the electromagnetic actuation principle and is capable of generating low-frequency vibration ranging from 0 to 120 Hz with an amplitude ranging from 1-15 microns. A power transistor switch supplies the periodic power supply to the electromagnet, and the control of the on-off sequence of the power transistor is maintained using a frequency controlled pulse generator. The on-off sequence of electricity flowing through the circuit energize or de-energize the electromagnet producing the vibration. The photograph of vibration device is shown in Figure 3.3. An accelerometer along with data acquisition system (National Instruments) was used for frequency and amplitude measurement purpose.
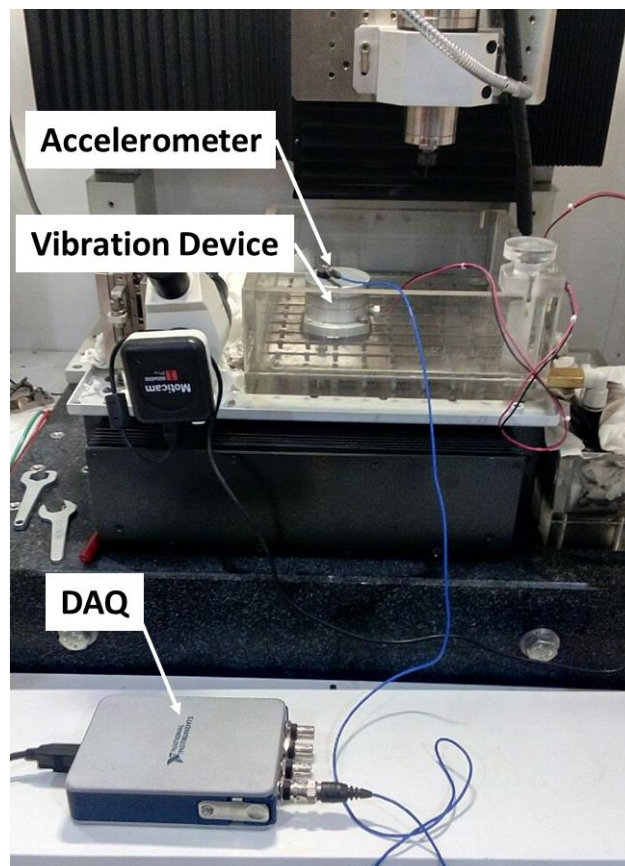
Figure 3.3 Vibration device

3.1.3   Workpiece material

Commercially available Inconel 718 superalloy was used as the workpiece material in this study. The composition of Inconel 718 specimen was determined using an optical spectrometer (LECO GDS500A) and shown in Table 3.3.

Table 3.3 Chemical composition of Inconel 718

Component	Ni	C	Si	Mn	P	Cr	Fe	Mo
Weight %	54.4	0.04	0.084	0.06	0.001	18.8	8.84	13.3
Component	V	Nb	W	Co	Ti	Al	Zr	
Weight %	0.085	2.78	0.259	0.259	0.814	0.194	0.078	

3.1.4   Dielectric

The commercially available dielectric 'Total Diel 7500 IN' was used as a dielectric fluid which is having superior electrical resistivity. This dielectric is a blend of refined hydrocarbon and selected additives. The properties of the dielectric fluid are shown in Table 3.4.

Table 3.4 Properties of dielectric

Name	Density at 29.5°C	Flashpoint, COC, °C	Viscosity @ 40 c, cSt	Aromatics, % by weight
Total Diel 7500 IN	0.776	110	2.0	0.1

3.2   Experimental procedures

3.2.1   Machining of Inconel 718 using AMEDDSG

For performing electro discharge diamond grinding operation, the ENC-35 EDM machine was modified with diamond surface grinding attachment [119]. Figure 3.4 shows actual photograph and schematics of in-house fabricated EDDG setup. This setup consists of bronze–diamond abrasive grinding wheel, direct current motor (Horse

Power: 2, Speed: 4600 rpm max), horizontal shaft (diameter, 32mm), V-pulley (diameter, 32mm) and bearing, and alternating current reversible synchronous motor (speed: 60 rpm, 50 Hz).

The relative motion between grinding wheel and material to be machined has been attained by reciprocating the machine bed with the help of an automatic feed arrangement consisting of a synchronous motor control circuit, a relay switch, two limit switches, and regulated power supply. The workpiece can be fixed on machine bed using the fixture and then dipped in the dielectric fluid. The bronze–diamond wheel attached to the ram of the machine through special attachment, and the servo system of the Z-axis numeric controlled EDM machine was used to uphold the predetermined gap between the two electrodes, that is, the diamond wheel and the flat workpiece. The details of the metal-bonded diamond wheel are given in Table 3.5.

The surface grinding on workpiece was achieved by rotating the grinding wheel about the horizontal axis perpendicular to the downward motion of servo system of EDM machine with the help of variable speed permanent magnet direct current (PMDC) motor through a V-belt and pulley arrangement. The speed of the PMDC motor has been controlled with the help of a DC drive. For performing abrasive mixed EDDG experiments, an acrylic flask of 36 liters capacity was fitted in the main tank of the EDM machine. The Silicon Carbide abrasives with average grain size of 1.5 to 1.9 μm were selected as abrasives to be mixed in the dielectric fluid. A small pump and stirrer were put in the container that ensures continues the supply of abrasives in the IEG and properly mixes abrasives in dielectric without allowing settling in container respectively.
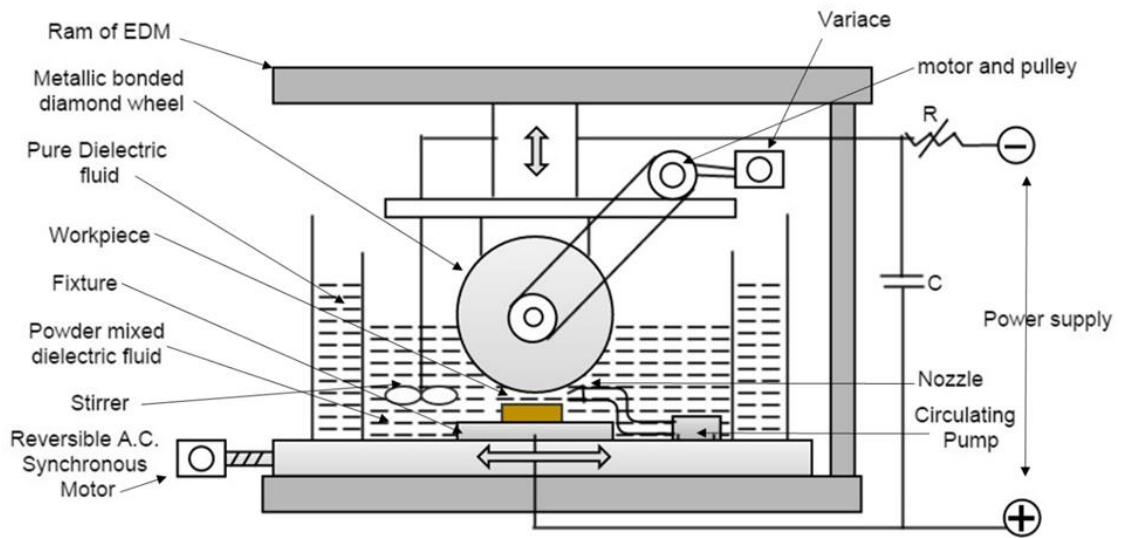
(a)
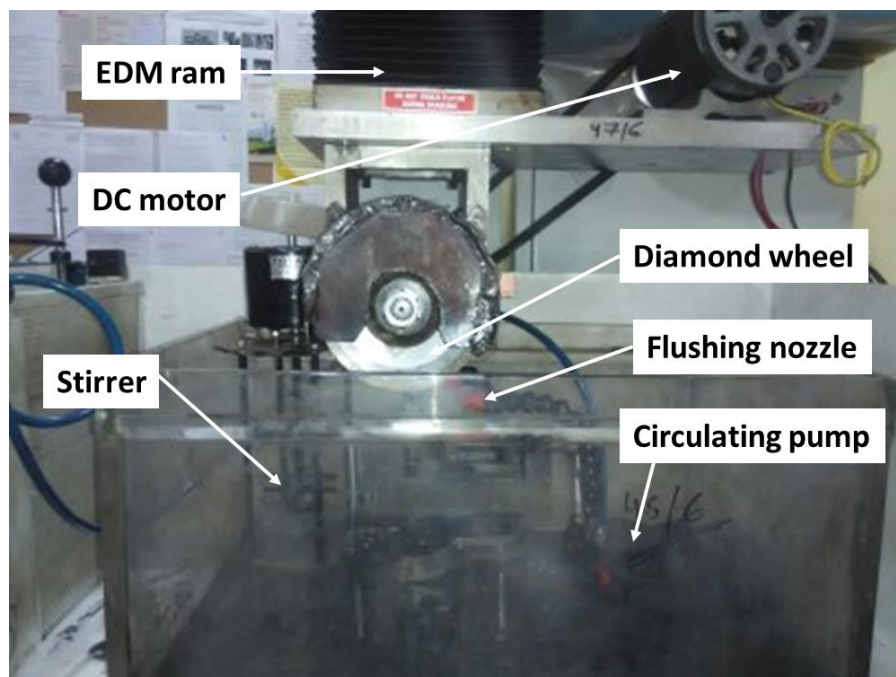
(b)

Figure 3.4 (a) Schematics and (b) Photograph of EDDSG setup

The high MRR is essential for high productivity while low R_a values assure better surface quality. The weight loss by workpiece before and after machining was determined with the help of electronic digital balance. The average surface roughness (R_a) of machined surfaces was measured perpendicular to feed direction of grinding

37

wheel by the Taylor Hobson Surtronic-25 profilometer. The MRR was calculated by the following equation:

$$MRR \; (mm^3/min)$$

$$= \frac{Weight \; loss \; by \; workpiece \; (g)/density \; (g/mm^3)}{Machining \; time \; (min)} \quad (3.1)$$

$$\times \; 100$$

3.2.2   Fabrication of micro-holes with μ-ED drilling

The high-speed diamond cutter (Isomet 4000 Buehler) was used to prepare the workpiece specimens of size 30 mm X 10 mm X 2.2 mm. The workpiece specimens after polishing and grounding using the semiautomatic polishing machine (MetaServ® 250 Buehler) used to perform experiments. The prepared specimen of Inconel 718 was fastened on the fixture such a that the surface (30 mm X 10 mm) become perpendicular to Tungsten (W) electrode of Ø300 μm so that electrode can drill holes 2.2 mm deep. The trail experiments (Appendix-B) were performed using copper, copper-tungsten, and tungsten electrodes and based on results the tungsten electrodes were found suitable for achieving accurate micro-holes.

Table 3.5 Details of metal-bonded grinding wheel

Description	Specification
Diamond wheel diameter	100mm
Thickness	10mm
Abrasive used	Diamond
Bore diameter	32mm
Bonding material	Bronze
Concentration	75%
Grit size	80/100

Initially, a study has been performed to investigate the performance of different electrode materials in the μ-ED drilling of Inconel 718 which is provided in Appendix-B. Owing to the low wear rate; tungsten electrodes produce accurate holes with smaller overcut and taper angle as compared to copper or brass electrodes due to less EWR [92, 94, 95]. Therefore, tungsten electrodes are chosen for micro-EDM operations. The electrode negative polarity was chosen while performing μ-ED drilling as its leads to more MRR from the workpiece. After performing each experiment, the electrode tip was dressed using the block-EDG to make electrode tip flat and circular before doing next experiment. The block-EDG has carried out at electrode positive polarity so that more material can be removed from Tungsten electrode. The schematic diagram and photograph of the experimental setup used while fabricating micro-holes i.e. vibration assisted μ-ED drilling is shown in Figure 3.5. The workpiece fixture was mounted on vibration device, and vibration device was clamped inside the main EDM tank.

The MRR$_{\mu EDD}$, EWR, surface quality and accuracy of micro-holes were investigated to analyze the performance of Inconel 718 in the μ-ED drilling. The accuracy of micro-holes was determined using the overcut and taper angle. The average volume of material removed (MR) divided by machining time to calculate MRR in mm^3/min. The volume of the MR from electrode divided by the volume of MR from the workpiece to determine EWR. The MRR$_{\mu EDD}$, EWR, overcut and taper angle was computed using following equations [120].

$$MRR_{\mu EDD} = \left[\frac{\pi}{3}\ (r_t^2 + r_t r_b + r_b^2) \times d\right] \div t \qquad (3.2)$$

Where, r_t is radius of hole at top, r_b is radius at bottom, d is hole depth, and t is machining time.

$$EWR = \frac{TW}{MRR} \tag{3.3}$$

Where TW is volumetric tool wear rate computed as $TW = \frac{\pi D^2 F}{4t}$, FEW is frontal electrode wear, D is electrode diameter. The method to measure FEW to explained later in section 3.2.3. The method to measure FEW is explained at the end of next section.

The overcut (O_c) was calculated as:

$$O_c = \frac{D_a - D}{2} \tag{3.4}$$

Where D_a is average hole diameter measured as,

$$D_a = (r_t + r_b) \tag{3.5}$$

The taper angle (θ) was calculated as:

$$\theta = tan^{-1}\left(\frac{r_t - r_b}{h}\right) \tag{3.6}$$

3.2.3 Fabrication of micro-channels with the μ-ED milling

The fabrication of micro-channels was achieved with the μ-ED milling setup on the DT-110 machine. The bulk machining method was employed for producing micro-channels since it takes less machining time as compared to a layer-by-layer machining method for same dimensions [32]. In bulk machining method, the electrode is fed along the length of the micro-channel in multiple passes until the desired shape of the channel is produced as shown in Figure 3.6. The electrode is worn out considerably from the side as well as bottom after each pass and therefore, electrode dressing is required to provide a renewed tool accessible before next successive pass. Figure 3.7 elaborates the electrode dressing process which was performed by passing the worn out portion of the electrode on a sacrificial plate. The electrode positive polarity setting with voltage and capacitance values of 95 V and 0.1 μF, respectively, was chosen while performing the electrode dressing.
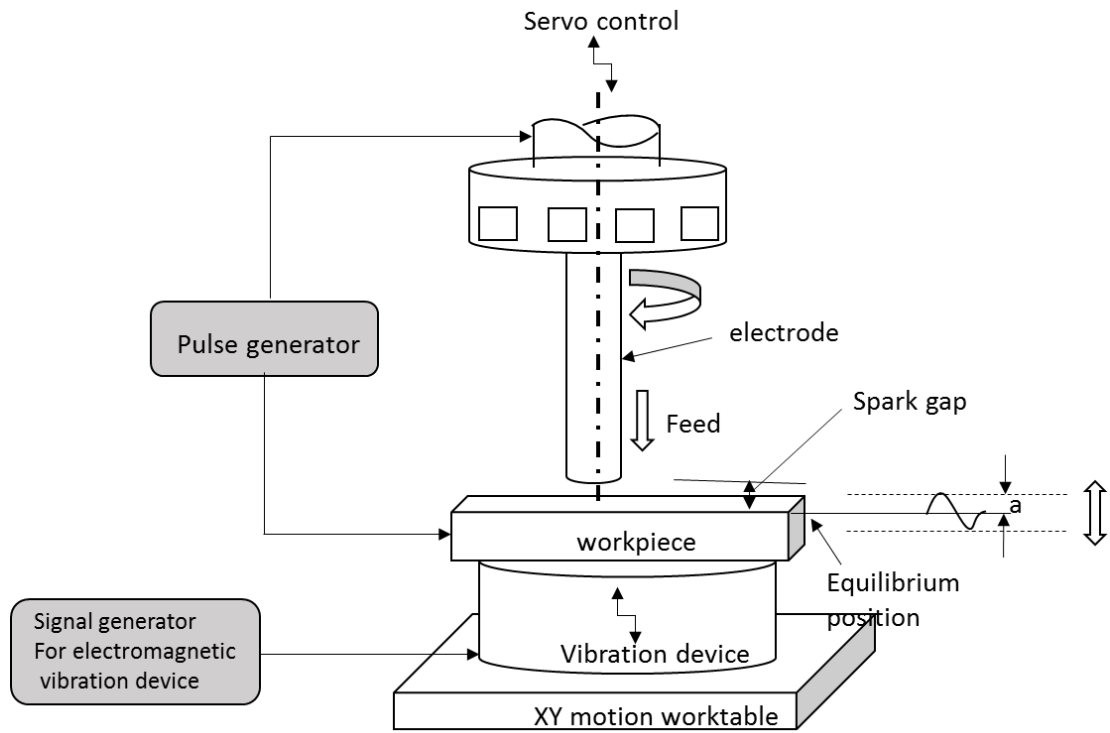
(a)
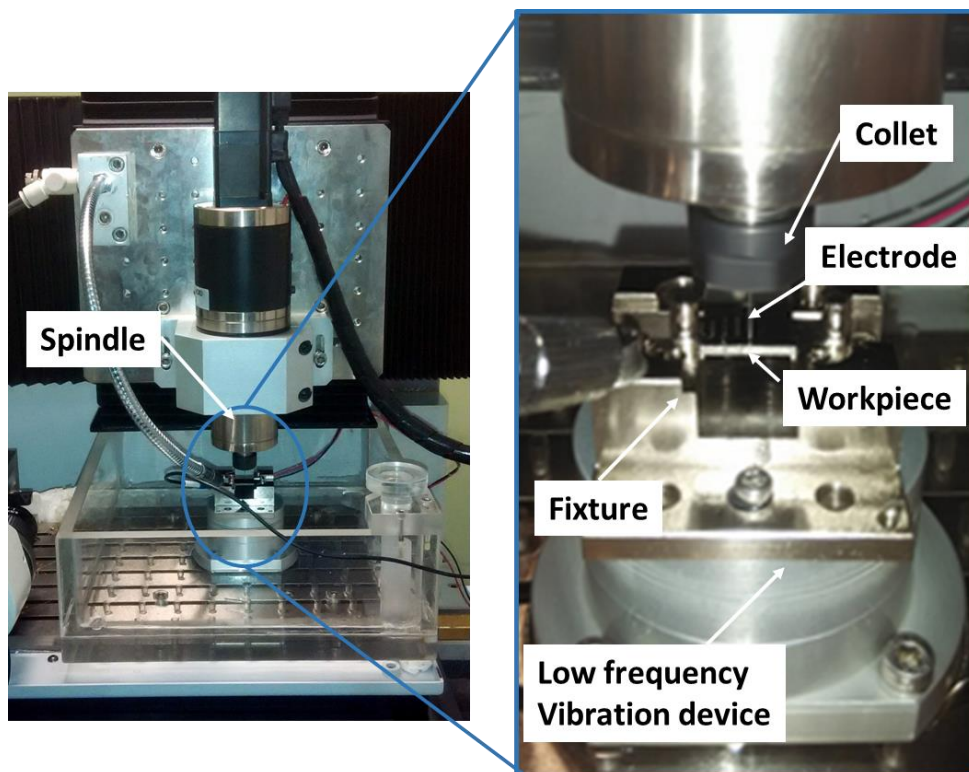
(b)

Figure 3.5 (a)Schematics and (b) Photograph of low-frequency vibration assisted μ-ED drilling setup

41

The workpiece of Inconel 718 with dimensions of 27 mm X 2.2 mm X 10 mm was prepared using a high-speed diamond cutter (Isomet 4000 Buehler) and then polished by a semiautomatic polishing machine (MetaServ® 250 Buehler) before performing μ-ED milling experiments. The workpiece was clamped to the fixture such a that the surface (27 mm X 2.2 mm) become perpendicular to the electrode. The tungsten electrodes of Ø0.3mm diameter were used to produce micro-channels of 0.5 mm depth and 2.2 mm in length. The negative polarity of the electrode was selected during the μ-ED milling operation as electrode intended to wear less as compared to workpiece [109].

In each experiment, the bulk machining method with three passes was used to attain the straight line shape of micro-channel. The number of passes required to produce the straight micro-channel was determined based on preliminary experiments. The schematic diagram and photograph of the low-frequency vibration assisted μ-ED milling setup are shown in Figure 3.8.
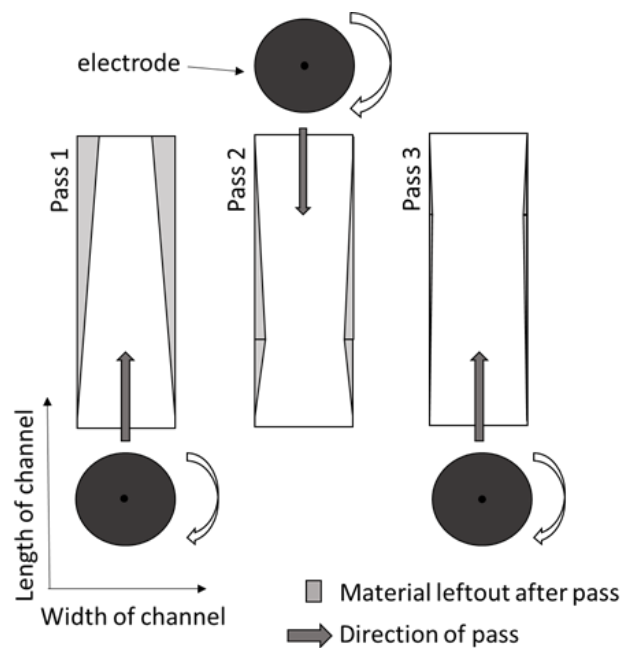
Figure 3.6 Bulk machining method
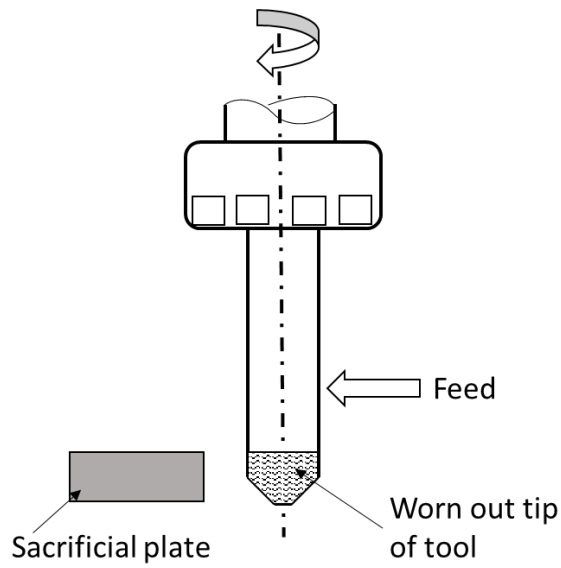
Figure 3.7 Dressing of electrode tip
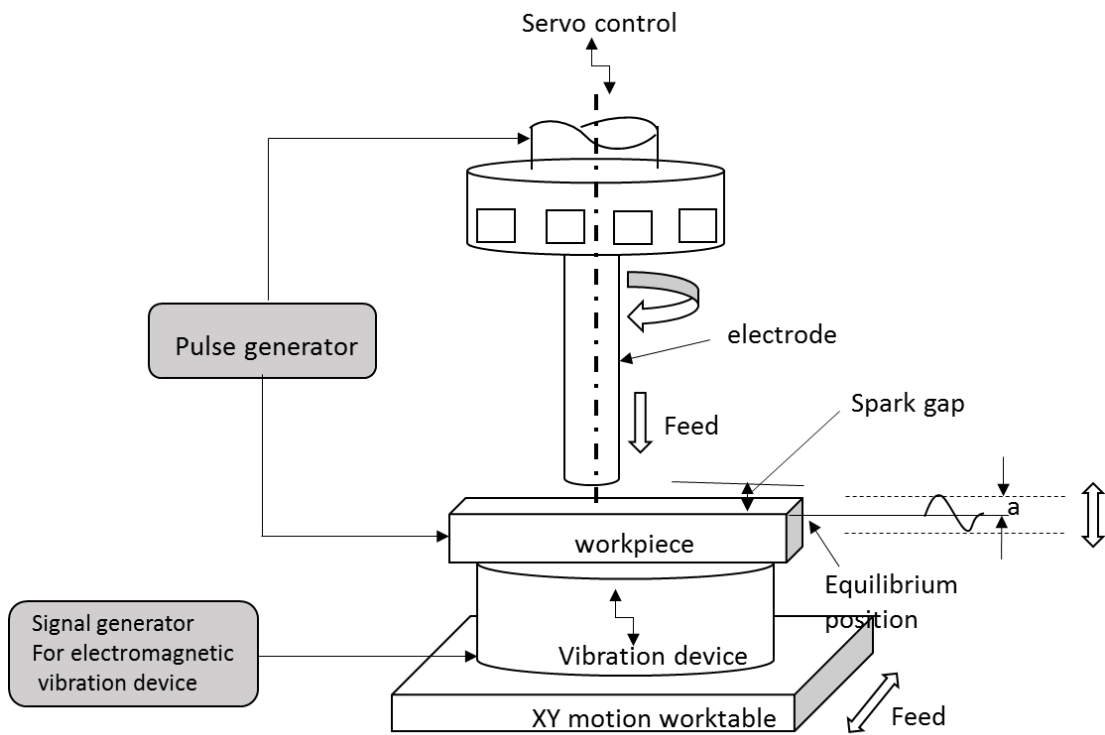
(a)
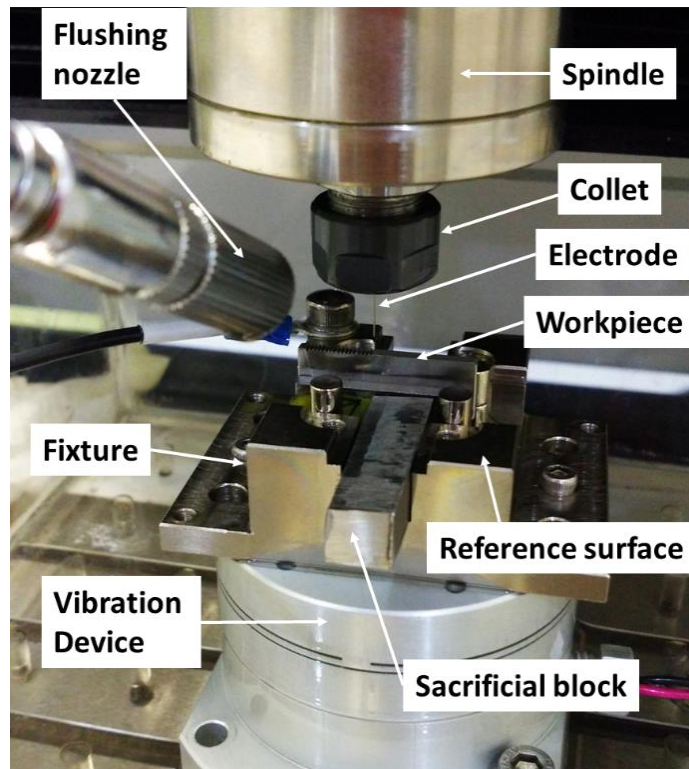
(b)

Figure 3.8 (a) Schematics and (b) photograph of low-frequency vibration assisted µ-ED milling

The performance of Inconel 718 in the µ-ED milling was examined by $MRR_{\mu EDm}$, frontal electrode wear (FEW), and the surface quality of produced micro-channel. On the machine, measurements were performed to measure the FEW after each machining pass and then overall FEW was determined by adding three FEW after respective three machining passes. The method to measure the FEW is schematically elaborated in Figure 3.9. In step-1, the electrode tip was touched to the reference surface of referencing block at contact probe settings of spindle and work table. After feeding the electrode in vertical z-direction towards to reference surface, the servo mechanism stops motion of z-axis as soon as the electrode touches the reference surface. At this point, the initial Z_1 position prior to machining was measured. Then after performing the machining pass, the Z_2 position was measured again by touching the electrode on the reference surface. The difference Z_2-Z_1 gives the frontal electrode wear for a

44

machining pass. Finally, the total FEW for producing a micro-channel was calculated by adding the three differences in electrode height (Z_2-Z_1) in three respective machining passes. The resolution of Z-axis of the machine tool is 0.1 micron. Therefore, the accurate FEW measurements can be performed by on-machine measurement method on DT110 machine tool. Various methods to calculate MRR in the µ-ED milling are available in the literature. However, weight difference before and after machining divided by machining time was adopted to calculate MRR in this study [121]. The Citizon CY104 Analytical Balance (make: GMI Inc, USA) with ±0.1mg readability and repeatability was used to measure the weight difference. The MRR was computed using following equation:

$$MRR_{\mu EDm} = \frac{\nabla M_{wp}}{t} \qquad \left(\frac{mg}{min}\right) \qquad (3.7)$$

where, ∇M_{wp} is the weight difference before and after the experiment.
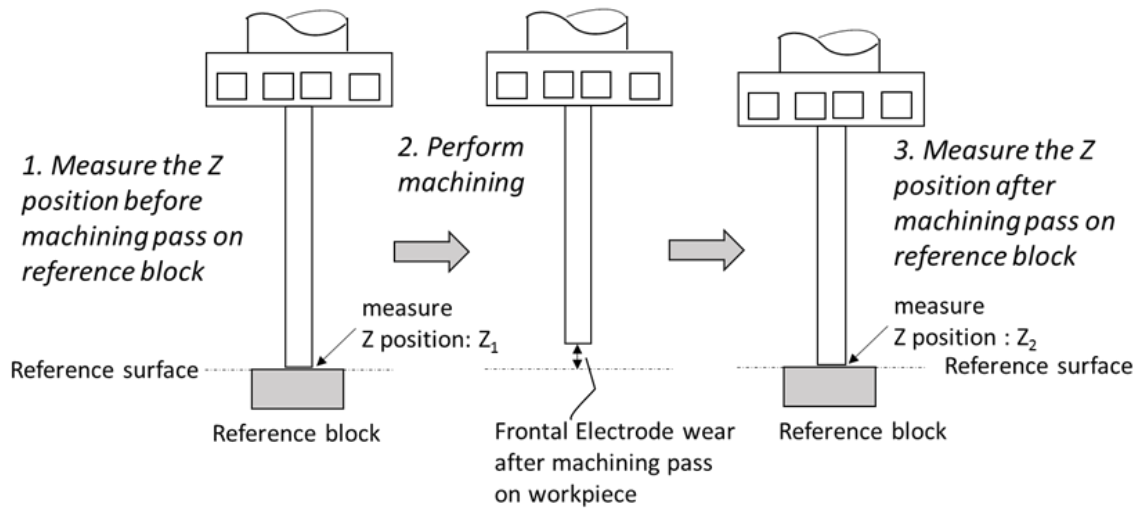
Figure 3.9 Measurement of frontal electrode wear

3.3 Equipment used for measurement and analysis

The field emission scanning electron microscopy (Nova NanoSEM 450) was used to capture the surface quality of fabricated micro-holes, micro-channels, and micro-surfaces. The fabricated micro-holes and micro-channels were observed under the

digital microscope (AxioCam AX10; Zeiss). To measure the radius of the micro-holes and dimensions of micro-channels, the AxioCam Software was used. The Citizon CY104 Analytical Balance (make: GMI Inc, USA) with ±0.1mg readability and repeatability was used to measure the weight differences in workpiece specimen before and after the experiment. The microhardness was measured using Vickers Microhardness Testing Machine (make: Walter UHL, GmbH & Co. KG).

4 Experimental investigation on abrasive mixed electro discharge diamond surface grinding of Inconel 718

Fabrication of surfaces with the good surface finish is an inevitable requirement for miniaturized devices as well as many other applications. The EDM processes involve longer machining time and also deteriorates the surface integrity of the machined component. The hybridization of EDM with diamond grinding has been proposed by Koshy et al. [68, 122] to form electro discharge diamond grinding (EDDG) and this process found to be competent for achieving good surfaces at high machining rate. Therefore, initial experiments were performed to understand the feasibility of electro discharge diamond surface grinding (EDDSG) on machining of Inconel 718 for such fabrication and results are presented in Appendix-A.

As discusses in section 2.4.1, it has been inferred that both AEDM and EDDSG which are hybrid EDM processes offers distinct assets during machining of difficult-to-cut materials. Therefore, it is decided to combine AEDM with EDDSG to form a new hybrid machining process called abrasive mixed electrode discharge diamond surface grinding (AMEDDSG) to offer distinct benefits. The experimental procedure of machining Inconel 718 by AMEDDSG is elaborated in section 3.2.1. In AMEDDSG, the collegial action of mechanical abrasion due to surface diamond grinding and spark erosion due to electro-discharge machining results in material removal. The abrasive

addition in dielectric fluid and application of a voltage of 75-325 V between wheel and workpiece results in an electric field intensity of 10^5 to 10^7 V/m. A small pump circulates the abrasive powder particles in spark gap and then these powder particles get energized moving in zigzag direction behaving as conductors which result in reduced breakdown stability of dielectric fluid. Thus, gap contamination promotes the ignition causing stability of process due to growth in gap size. Further, the chain of discharges takes place underneath the electrode region. A widened and large plasma channel attributed due to abrasives increases the discharge frequency and thus rapid erosion of workpiece [79, 80]. Finally improved MRR could be achieved as the decreased electric density cause uniform distribution of sparks.

4.1 Control factors and their range

The wheel speed (W_s), abrasive concentration (AC), current (C), and POT (T_{on}) were selected as control factors while MRR and R_a were chosen as performance measures. These control factors and their range were decided based on the literature, pilot experimentation, manufacturer's manual, and machine competence. The independent control factors and their levels in coded and actual values are shown in Table 4.1.

Table 4.1 Experimental control factors and their levels.

Control factors (symbol)		Notation	Level				
	Unit		-2	-1	0	+1	+2
Wheel speed	rpm	*WS*	450	800	1150	1500	1850
Abrasive concentration	g/L	*AC*	0	2	4	6	8
Current	A	*C*	2	4	6	8	10
Pulse-on-time	μs	*T_{on}*	17	20	23	26	29

4.2 Experimental design

A well-known technique to model and optimize the response variables integrating quantifiable independent variables is response surface methodology (RSM) and RSM is based on a synergistic combination of mathematics and statistics. The performance of the process is described by the second order polynomial regression model known as a quadratic model. In this study, 'Design Expert 8.1' software was used to evaluate the coefficients of regression based on the experimental results.

RSM fits polynomial models for the existing data into following equation:

$$y = \beta_0 + \sum_{i=1}^{k} \beta_i x_i + \sum_{i=1}^{k} \beta_{ii} x_i^2 + \sum_{i} \sum_{j} \beta_{ij} x_i x_j \qquad (4.1)$$

where y is the predicted response; β_0 is a constant; β_i is the linear coefficient; β_{ii} is the squared coefficient; β_{ij} is the cross product coefficient, and k is the number of factors [123].

In this study, the experiments were based on the central composite design (CCD) method. The factorial portion of CCD is a full factorial design with all groupings of the factors at two levels (high, +1, and low, −1) and consisting of the eight-star points and the six central points (coded level 0) which are the midpoints between the high and low levels. The star points are at the face of the cube portion of the design that corresponds to an α = ±2, and this type of design is commonly called the "face-centered CCD." The ''face-centered CCD'' includes 30 experimental runs at four independent control factors" [124]. The experimental design matrix with a combination of control factors and corresponding performance measure values obtained from experimentation are listed in Table 4.2.

4.3 Reproducibility

The reproducibility of the procedure is confirmed by execution of six experiments at the center point of the control factors using CCD technique. The results of experimental runs (2,18,19,21,26,28) shown in Table 4.2 are presented individually in Table 4.3. The percentage error mentioned in Table 4.3 shows the variability of the performance measures with reference to its average value (sum of all terms divided by the number of terms).

Table 4.2 Experimental design matrix and observed performance measures in AMEDDSG of Inconel 718

Std	Run	Control Factors				Performance Measures	
		Wheel Speed	Abrasive Concentration	Current	Pulse-on-Time	Material removal rate	Average Surface Roughness
		W_s (rpm)	AC (g/L)	C (A)	T_{on} (µs)	MRR (mm³/min)	R_a (µm)
24	1	1250	4	6	29	13.67	3.988
23	2	1250	4	6	17	9.52	2.765
11	3	1000	6	4	26	6.91	4.029
25	4	1250	4	6	23	14.11	2.688
13	5	1000	2	8	26	13.54	4.543
19	6	1250	0	6	23	9.91	3.495
7	7	1000	6	8	20	6.03	3.087
27	8	1250	4	6	23	14.06	2.719
6	9	1500	2	8	20	9.60	2.390
3	10	1000	6	4	20	6.54	3.627
30	11	1250	4	6	23	13.85	2.449
21	12	1250	4	2	23	7.15	3.489

2	13	1500	2	4	20	9.93	2.582
17	14	750	4	6	23	6.74	3.892
16	15	1500	6	8	26	13.47	3.735
4	16	1500	6	4	20	12.76	3.523
20	17	1250	8	6	23	12.11	3.186
29	18	1250	4	6	23	12.85	2.459
26	19	1250	4	6	23	12.98	2.479
18	20	1750	4	6	23	10.72	2.967
10	21	1500	2	4	26	10.08	2.809
1	22	1000	2	4	20	5.95	3.399
9	23	1000	2	4	26	8.52	3.975
14	24	1500	2	8	26	11.81	4.000
15	25	1000	6	8	26	13.12	4.049
22	26	1250	4	10	23	10.92	4.002
8	27	1500	6	8	20	10.83	2.622
5	28	1000	2	8	20	7.81	3.666
28	29	1250	4	6	23	14.35	2.729
12	30	1500	6	4	26	10.29	3.538

The percentage error is calculated by using the equation (4.2):

$$Percentage\ error = \left(\frac{Average\ value - Experimental\ value}{Average\ value}\right) \times 100 \quad (4.2)$$

The results presented in Table 4.3 point out that the MRR and R_a were reproduced within the tolerable range of ±5% [125]. Further, the values of experimental standard deviation and standard uncertainty were evaluated for performance measures to

illustrate their variability over a repeated set of experiments [124]. The results of standard uncertainty calculated using equation (4.4) for MRR and R_a were determined to be 3.83% and 0.75%, respectively, which are well within the tolerable range.

$$\text{Experimental standard deviation (s)} = \sqrt{\frac{\sum_{i=1}^{5}(x_i - \bar{x})^2}{(N-1)}} \qquad (4.3)$$

$$\text{Standard uncertainity} = \frac{s}{\sqrt{N}} \qquad (4.4)$$

Where, x_i is each value of data set, $\bar{x}$ is mean value of data, and N is number of data set considered.

4.4 Empirical models for performance measures

Finding the analytical model for AMEDDG built on process physics is very problematic due to complicated and stochastic nature of the process. Hence, to evaluate the mathematical relationship among the control factors and performance measures, a multi-variable regression model using response surface methodology was developed for each performance measure.

Table 4.3 Reproducibility and percentage (%) error for material removal rate and average surface roughness

Expt. No.	Ws (rpm)	AC (g/L)	C (A)	T_{on} (μs)	MRR (mm³/min)		R_a (μm)	
					Expt. value	% Error	Expt. value	% Error
2	1250	4	6	23	14.11	-2.99	2.688	-3.90
18	1250	4	6	23	14.06	-2.63	2.719	-5.09
19	1250	4	6	23	13.85	-1.09	2.449	5.34
21	1250	4	6	23	12.85	6.21	2.459	4.96
26	1250	4	6	23	12.98	5.26	2.479	4.18
28	1250	4	6	23	14.35	-4.76	2.729	-5.48

Analysis of variance (ANOVA) was executed to statistically investigate the results of the selected model. Significant control factors were recognized and interaction effects of these control factors on performance measures were studied using response surface graphs.

4.4.1 ANOVA for material removal rate

The experimental results for MRR shown in Table 4.2 were examined using Design-Expert software. The sequential model sum of squares, lack-of-fit test, and model summary statistics tests were executed, and fit summary of these tests suggest the adequacy of the quadratic model and thus quadratic model was used for analysis of MRR as it is statistically significant. The backward elimination procedure was executed to eliminate the unimportant terms from model thereby improving the model. The results of ANOVA after backward elimination are summarized in Table 4.4.

Table 4.4 The ANOVA Table for MRR

Source	Sum of squares	df	Mean square	F value	p-Value Prob. > F	
Model	208.09	12	17.34	38.32	< 0.0001	significant
W_S-Wheel Speed (RPM)	33.39	1	33.39	73.78	< 0.0001	
AC-Abrasive Concentration (g/L)	2.11	1	2.11	4.65	0.0456	
C-Current (A)	21.66	1	21.66	47.86	< 0.0001	
T_{on}-Pulse-on-time (µs)	29.49	1	29.49	65.17	< 0.0001	
$W_S \times AC$	5.22	1	5.22	11.53	0.0034	
$W_S \times C$	6.14	1	6.14	13.56	0.0018	
$W_S \times T_{on}$	10.95	1	10.95	24.20	0.0001	
$C \times T_{on}$	18.14	1	18.14	40.08	< 0.0001	
$W_S{}^2$	45.47	1	45.47	100.49	< 0.0001	
AC^2	14.13	1	14.13	31.22	< 0.0001	
C^2	40.22	1	40.22	88.88	< 0.0001	
$T_{on}{}^2$	8.94	1	8.94	19.76	0.0004	

Residual	7.69	17	0.45			
Lack of Fit	5.71	12	0.48	1.20	0.4508	not significant
Pure Error	1.99	5	0.40			
Cor Total	215.8	29				
Std. Dev.		**0.67**		**R-Squared**		**0.9643**
Mean		**10.67**		**Adj R-Squared**		**0.9392**
C.V. %		**6.30**		**Pred R-Squared**		**0.8848**
PRESS		**24.86**		**Adeq Precision**		**17.348**

W_s: wheel speed (RPM), AC: Abrasive concentration (g/L), C: current (A), T_{on}: Pulse-on-time (µs)

The normal probability plot of the residuals (Figure 4.1 (a)) indicates that residuals fall on a straight line indicating that errors are normally distributed [125]. Also, from Figure 4.1 (b), it can be seen that the actual values are in good agreement with predicted values from the model. Thus, it can be inferred that ANOVA results given in Table 4.4 are reliable as the both the plots (Figure 4.1) fulfills the error normality and prediction capability criteria.
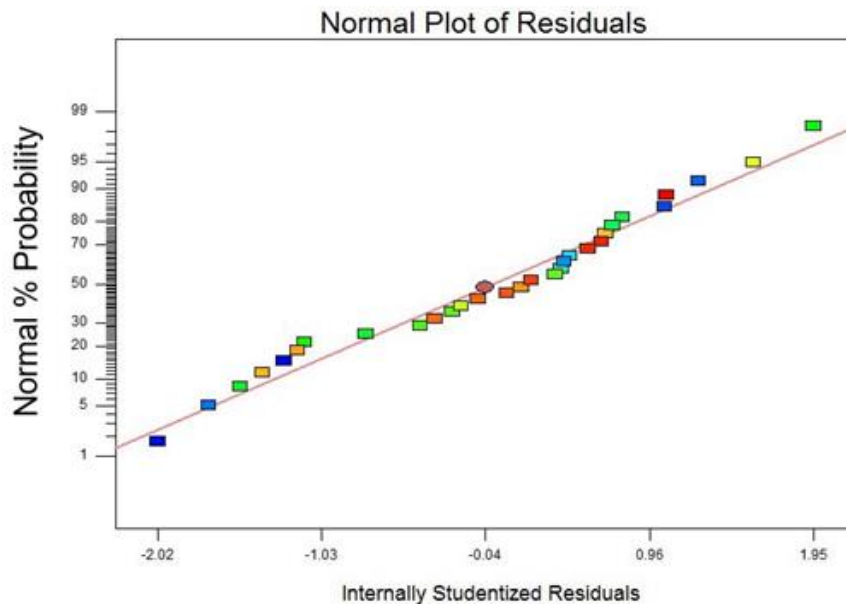
(a)
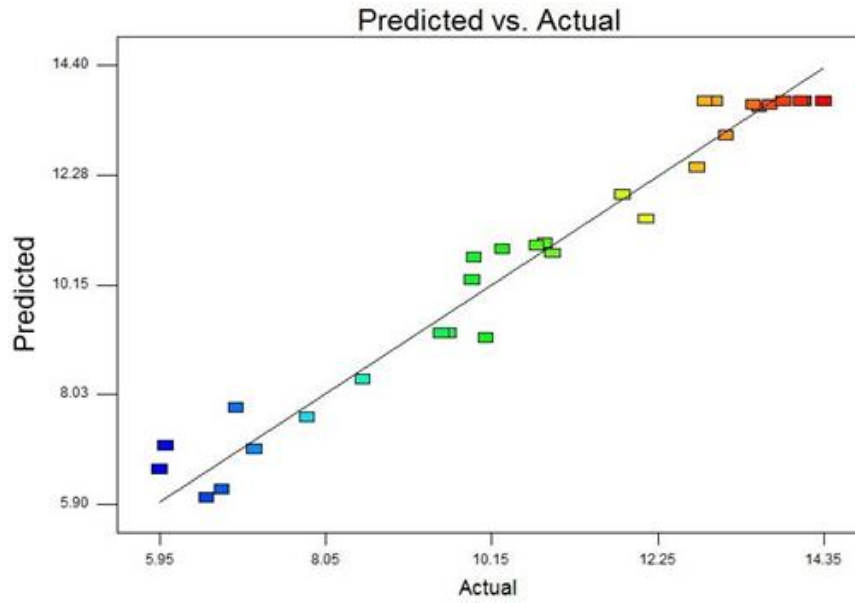
(b)

Figure 4.1 Normal probability plot of residuals for MRR, (b) Plot of predicted vs. actual response for MRR

The model F-value of 38.32 with its Prob>F value less than 0.0001 as shown in Table 4.4 directs that the model is significant for MRR as it validates that the terms in the model have a significant effect on the response. There is only a 0.01 % chance that such a large model F value could occur due to noise. The values of Prob>F less than 0.05 indicate the significance of model terms, The W_s, AC, C, T_{on}, $W_s \times AC$, $AC \times C$, $W_s \times T_{on}$, $C \times T_{on}$, W_s^2, AC^2, C^2, T_{on}^2 are significant model terms for MRR with their percentage contribution of 16.05, 1.01, 10.41, 14.17, 2.51, 2.95, 5.26, 8.72, 21.85, 6.79, 19.33, and 4.30 % respectively. The "individual (model) term" sum of squares was divided by "model" sum of squares to compute the percentage contribution.

The determination coefficient (R^2) was computed to check the adequacy of the fitted model to describe the experimental data. The determination coefficient shows the extent of the degree of fit and is the ratio of the explained deviation to the total deviation. The R^2 values near to one correspond to the superior fit of the model to real data and direct towards match among the predicted and actual data. In this case, the determination

coefficient for MRR is found to be 0.9643 (Table 4.4) which suggest that the established model is accomplished of explaining the variation on MRR up to 96.43 %, and model is adequate in demonstrating the process. The other R^2 statistics, the Pred R^2 (0. 8848), is in good agreement with the Adj R^2 (0.9392). The coefficient of variation (CV) of the model is known as the ratio of the standard deviation to the mean. The smaller value (6.30) of CV % given in Table 4.4 shows enhanced accuracy and consistency of the performed experiments [41]. Further, the Adeq Precision measures the signal-to-noise ratio. Generally, a ratio greater than 4 is desirable. The Adeq Precision found for the model is 17.348, which is well more than desired value of 4 and thus specifies a sufficient signal for the model. Hence, this model may be used to navigate the design space and forecast the values of the MRR within the limits of the factors studied.

4.4.1.1   *Regression equation for MRR*

The empirical relation between the MRR and control factors (actual terms) can be expressed by the following second-order polynomial equation (4.5):

$$
\begin{aligned}
MRR = &-62.04911 + (0.04771 \times W_s) + (0.64524 \times AC) \\
&+ (1.04389 \times C) + (3.12916 \times T_{on}) \\
&+ (0.000815 \times W_s \times AC) - (0.000884 \times WS \times C) \\
&- (0.000787 \times W_s \times T_{on}) + (0.17745 \times C \times T_{on}) \\
&- (0.00001 \times W_s{}^2) - (0.17943 \times AC^2) - (0.30274 \\
&\times C^2) - (0.06344 \times T_{on}{}^2)
\end{aligned}
\tag{4.5}
$$

4.4.2   **ANOVA for surface roughness**

The experimental results listed in Table 4.2 were analyzed for ANOVA of average surface roughness. The adequacy of the quadratic model has been suggested by Design-

Expert software on the account of the fit summary. The results of ANOVA after backward elimination are summarized in Table 4.5.

Table 4.5 The ANOVA Table for R_a

Source	Sum of squares	df	Mean square	F value	p-Value Prob. > F	
Model	10.62	11.00	0.97	31.81	< 0.0001	significant
W_s-Wheel Speed (RPM)	2.06	1.00	2.06	67.73	< 0.0001	
AC-Abrasive Concentration (g/L)	0.00	1.00	0.00	0.07	0.7937	
C-Current (A)	0.11	1.00	0.11	3.67	0.0714	
T_{on}-Pulse-on-time (μs)	2.82	1.00	2.82	92.97	< 0.0001	
$W_s{\times}AC$	0.37	1.00	0.37	12.15	0.0026	
$AC{\times}C$	0.58	1.00	0.58	19.26	0.0004	
$C{\times}T_{on}$	0.70	1.00	0.70	23.00	0.0001	
W_s^2	1.22	1.00	1.22	40.12	< 0.0001	
AC^2	0.97	1.00	0.97	32.09	< 0.0001	
C^2	2.30	1.00	2.30	75.83	< 0.0001	
T_{on}^2	1.07	1.00	1.07	35.25	< 0.0001	
Residual	0.55	18.00	0.03			
Lack of Fit	0.45	13.00	0.03	1.83	0.2618	not significant
Pure Error	0.09	5.00				
Cor. Total	11.16	29.00				
Std. Dev.		0.17		R-Squared		0.9511
Mean		3.30		Adj R-Squared		0.9212
C.V. %		5.29		Pred R-Squared		0.8417
PRESS		1.77		Adeq Precision		19.353

W_S: wheel speed, AC: Abrasive concentration, C: current, T_{on}: Pulse-on-time

The normal probability plot of the residuals for the average surface roughness is shown in Figure 4.2 (a). It can be seen in Fig. 3b that the actual data resembles the predicted data calculated from the model, therefore confirming the reliability of ANOVA results (Table 4.5). A model F value of 44.20 as shown in Table 4.5 indicates that the model is

significant. There is only a 0.01 % chance that a model F value this large could occur due to noise. Values of Prob>F less than 0.0500 indicate that the model terms are significant. In the present case, the model terms W_s, T_{on}, $W_s{\times}AC$, $AC{\times}C$, $C{\times}T_{on}$, $W_s{}^2$, AC^2, C^2, $T_{on}{}^2$ are significant for average surface roughness with their percentage contribution of 19.36, 0.02, 1.05, 26.57, 3.47, 5.51, 6.57, 11.47, 9.17, 21.67, and 10.08 % respectively.

The value of determination coefficient (R^2) is 0.9511. It illustrates that the quadratic model can explain up to 95.10 % variation in the average surface roughness. The Pred R^2 value of 0.8417 is in reasonable agreement with the Adj R^2 of 0.9212. The smaller value (5.29) of the coefficient of variation discloses enhanced precision and reliability of the executed experiments. A value of 19.353 for Adeq Precision states an adequate signal for the model as a ratio greater than 4 is desirable. Therefore, this quadratic model can be used to navigate the design space and considered substantial for fitting and predicting the experimental results.

4.4.2.1 *Regression equation for average surface roughness*

The empirical relation between the surface roughness and control factors (actual terms) can be expressed by the following equation (4.6):

$$R_a = 22.59339 + (0.00565 \times W_s) - (0.33474 \times AC)$$
$$- (1.44439 \times C) - (1.10390 \times T_{on})$$
$$+ (0.000216 \times W_s \times AC) - (0.034812 \times C \times T_{on}) \quad (4.6)$$
$$+ \left(0.0000017 \times W_s{}^2\right) + (0.047103 \times AC^2)$$
$$+ (0.07240 \times C^2) + \left(0.021942 \times T_{on}{}^2\right)$$
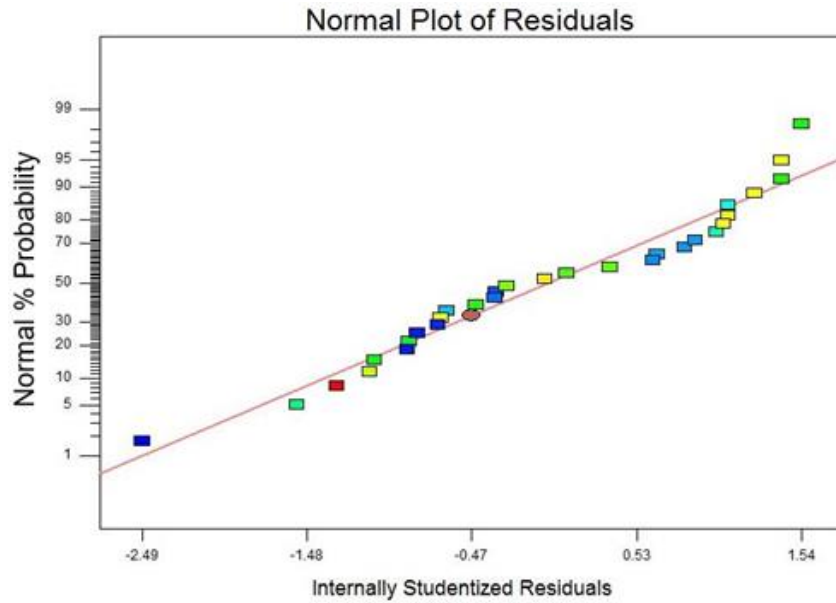
(a)
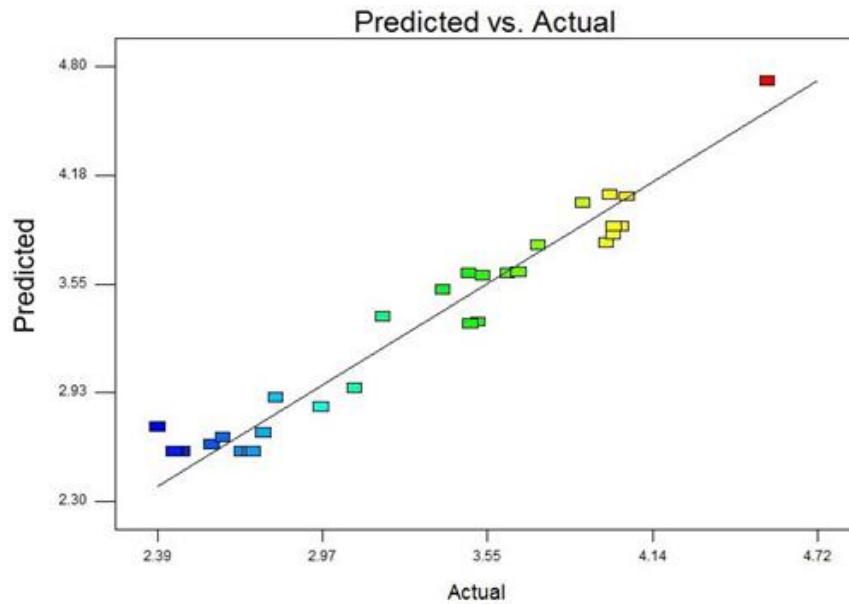
(b)

Figure 4.2 (a). Normal probability plot of residuals for average surface roughness
(b). Plot of predicted vs. actual response for average surface roughness

4.5   Validation of models

The five additional experiments were performed using different control factors settings within the range of selected factors. The different control factors settings were used than one used for forming the regression models. Table 4.6 shows the results of validation experiments. The prediction error (%) calculated using the equation (4.7).

The results experiments performed for the validation of model were found to be in good agreement with the predicted results obtained from the regression equations and prediction errors were less that ±5 %. Consequently, the established models can be treated as a reliable demonstrative of the experimental results.

$Prediction\ error$

$$= \left(\frac{Experimental\ results - Predicted\ results}{Experimental\ results} \right) \quad (4.7)$$

$$\times 100$$

Table 4.6 Results of validation experiments for material removal rate and average surface roughness

Expt. No.	Ws (RPM)	AC (g/L)	C (A)	Ton (µs)	MRR (mm³/min)			Ra (µm)		
					Experimental value	Predicted value	Prediction error %	Experimental value	Predicted value	Prediction error %
1	1500	3	2	23	7.12	7.41	-4.06	3.226	3.368	-4.38
2	800	5	5	25	10.86	10.64	2.02	3.296	3.463	-5.05
3	1000	3	5	23	12.65	12.04	4.79	3.021	2.913	3.59
4	1400	4	5	20	12.25	12.80	-4.50	2.641	2.534	4.04
5	1400	5	4	23	12.21	12.39	-1.49	2.852	2.953	-3.54

4.6 Results and discussion

Perturbation plot and 3D response curves have been used to discuss the effects of individual control factors as well as their interactions on the performance measures.

4.6.1 Influence of control factors on material removal rate

The comparative effects of significant control factors on MRR of Inconel 718 by AMSEDDG were shown in Perturbation plot (Figure 4.3). By default, Design-Expert software keeps the reference point at the midpoint (coded value 0) of all factors. A sharp

slope for wheel speed (W_s), current (C), and POT (T_{on}) directs that the MRR is very subtle to them whereas a less sharp slope for abrasive concentration (AC) directs towards comparatively low sensitivity of MRR towards it. The reasons for above results have been discussed in successive paragraphs while explaining the interaction effects.
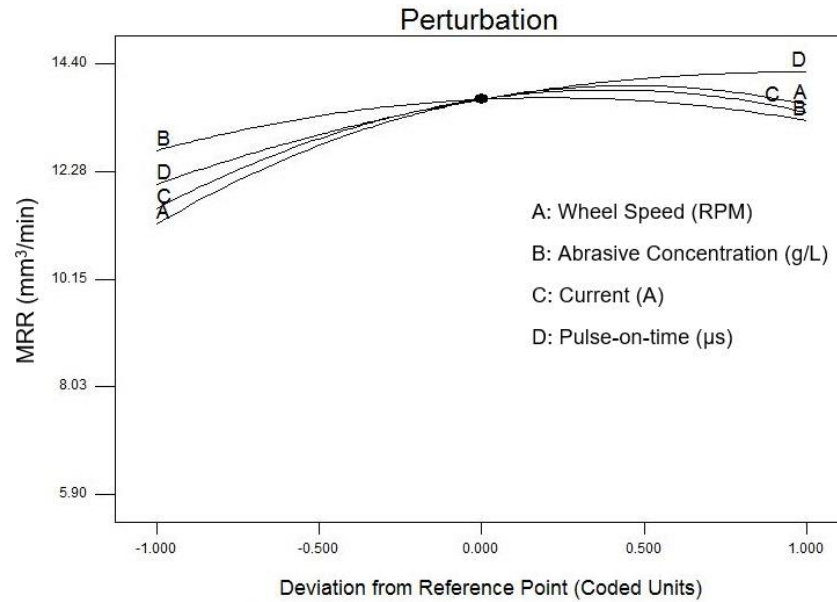
Figure 4.3 Perturbation plots for MRR

4.6.1.1   Interactive effects of control factors on material removal rate

It is observed from the Table 4.4 that the interactions which significantly contributes to the model are those between the wheel speed and abrasive concentration '$W_s \times AC$', wheel speed and current '$W_s \times C$', wheel speed and POT '$W_s \times T_{on}$', and current and POT '$C \times T_{on}$' and the interaction plots corresponding to these interaction terms are shown in Figure 4.4 (a), (b), (c) and (d) respectively.

The interaction effect of wheel speed and abrasive concentration at other control factors at middle values in shown in Figure 4.4 (a). It can also be observed from Figure 4.4 (a) is that the MRR increases with an increase in wheel speed up to an optimum wheel speed and then starts decreasing for further increase in wheel speed. The increase in MRR with an increase in wheel speed is due to the fact that at higher wheel speed more

number of abrasives on the surface of grinding wheel will come in contact with workpiece abrading more volume of the workpiece. Also, at greater speed enhanced flushing conditions expels the molten material from the workpiece surface avoiding debris gathering in IEG. Consequently, better MRR can be attained. The results observed about wheel speed is consistent with that reported by [75, 126]. However, after an optimum wheel speed value, the further increase in wheel speed slows down the material removal by not allowing the plasma to constitute. Similarly, it can also be seen from Figure 4.4 (a) that the MRR increases with an increase in abrasive concentration up to an optimum point and then starts decreasing with further increase in the abrasive concentration. The addition of abrasives in dielectric promotes the bridging of IEG, and thus multiple discharges occurs within single spark resulting in an increase of discharge energy and thereby quicker erosion of workpiece. However, after an optimum level, the higher abrasive concentration leads to discharge interference and results into slowing down the MRR.
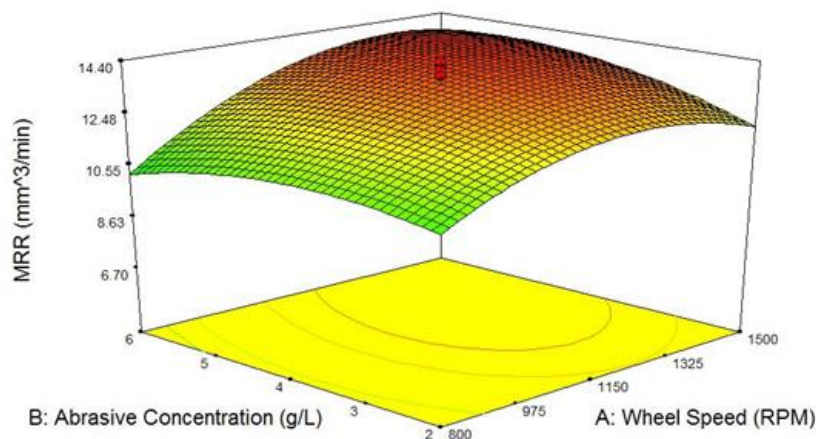
(a)
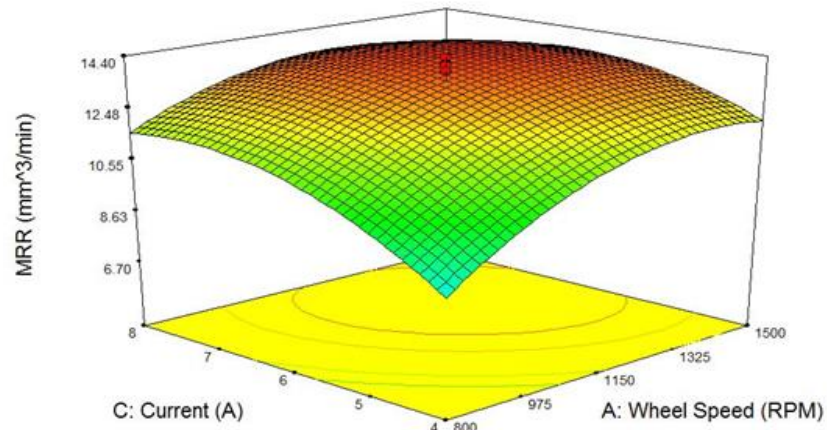
(b)
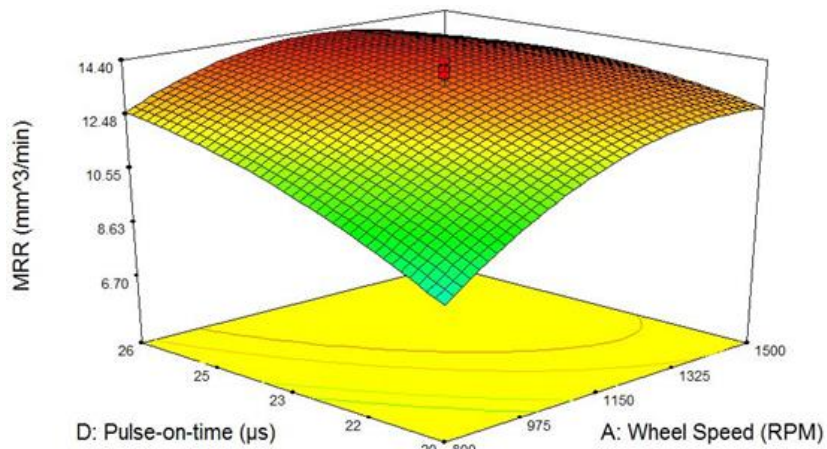
(c)
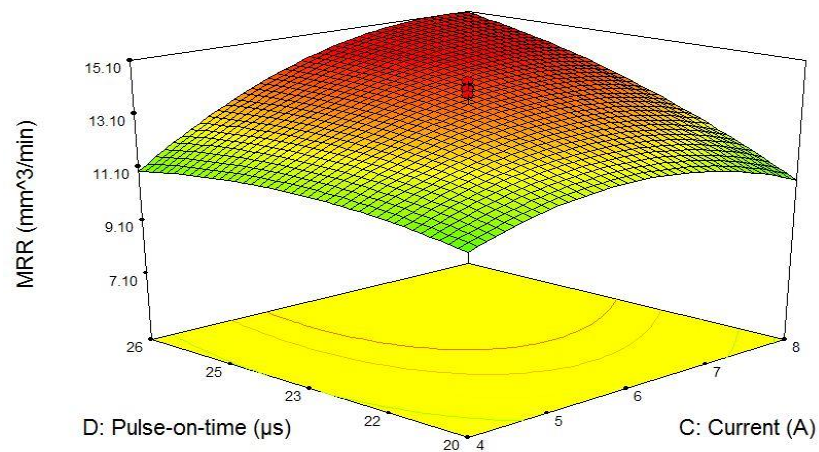
(d)

Figure 4.4 (a), and (b),(c), and (d) shows the response graph of MRR

It is demonstrated through Figure 4.4 (b, c, and d) that with an increase in current and

POT there is an increase in MRR. At higher current and POT more discharge energy

will go onto the workpiece melting and evaporating more volume of the workpiece.

The discharge energy is the product of POT and current. It can be recommended that

for higher MRR, high values of the current, pulse-on-time and wheel speed are more suitable. The similar observation also reported by [124].

Therefore, overall it can be perceived that abrasive mixed dielectric does play a vital role in improving the MRR in AMSEDDG process.

4.6.2 Influence of control factors on average surface roughness

The Perturbation plot for average surface roughness is shown in Figure 4.5. A sharp slope for wheel speed (*A*) and POT (*D*) indicates towards high sensitivity of surface roughness to them however comparatively less steep lines for wheel speed (*B*), and current (*C*) directs relatively low sensitivity to surface roughness.
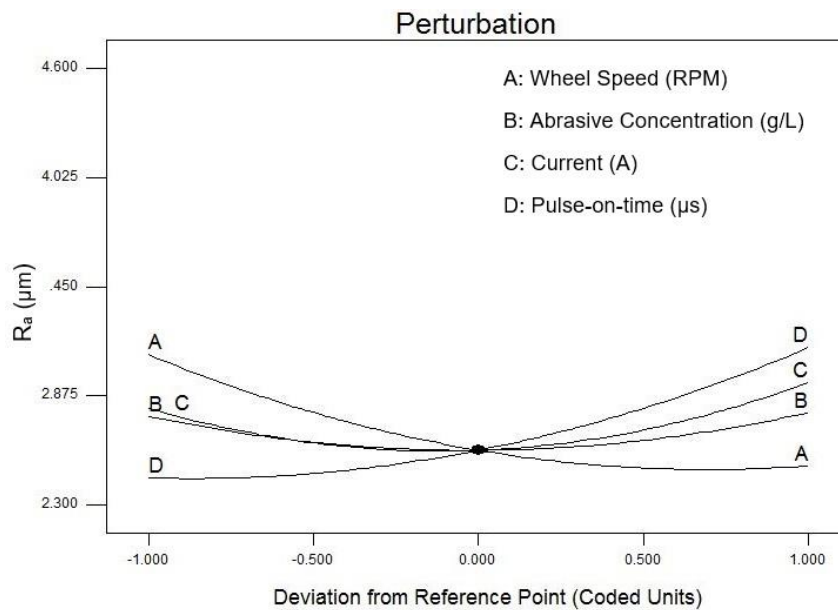
Figure 4.5 Perturbation plots for R_a

4.6.2.1 *Interactive Effects of Control Factors on Average Surface Roughness*

The ANOVA results (Table 4.5) shows that the interactions contributing significantly to the model are those between wheel speed and abrasive concentration '$W_s \times AC$', abrasive concentration and current POT '$AC \times C$', and current and POT '$C \times T_{on}$'. It is observed from Figure 4.6 (a) and (b), that the R_a value of machined surface decreases

with increase in wheel speed. At higher speed the flushing efficiency improved and also the molten material is effectively ejected from the workpiece surface not allowing any debris accumulation in inter electrode gap [71]. Thus, more uniform surface can be achieved. Further, enhanced flushing conditions imposed by high wheel speed results in effective ejection of molten material and thereby leaving behind trivial recast layers. Owing to high wheel speed, the possibility of resolidification of the molten metal on the workpiece is reduced, and as a result surface roughness decreases. In addition, as the wheel RPM increases, a small amount of the material will be removed by each diamond abrasive particle.

It is also observed from Figure 4.5 that the surface roughness decreases initially with an increase in abrasive concentration up to an optimal point and then starts to increase with further increase in abrasive concentration. It can be inferred that the addition of the abrasives plays a noteworthy part in the modification of the plasma channel by enlarging and widening it [78]. The addition of abrasives in the dielectric increases the gap distance and occurrence of multiple discharges in single pulse results in a reduction in both the discharge impact force over the crater and the energy density [127]. The discharge energy primarily results in the metal melting all over the crater area reducing the volatilization which generally affects the crater center. The widened plasma channel do not strappingly push the molten metal. These conditions result in uniform crater formation and therefore, the surface tends to be smooth, less concave and more homogeneous. Overall, the addition of powder in dielectric leads to uniform distribution of the sparks resulting in a uniform surface generation, and lower values of R_a will be achieved [79]. The high wheel speed and low abrasive concentrations are suggested for better surfaces. It can also be noted that the surface roughness value starts to increase again after powder concentration of 6 g/l. With the increase in powder concentration,

the dielectric conductivity also increases. This results in more concentrated spark energy acting on the workpiece and thus increasing the surface roughness.

It can also be observed that the higher values of current and pulse on time are not suitable for better surface finish. At high values of current and POT, the discharge energy acting on the workpiece is higher. As higher discharge energy is going on to the material bigger craters will be formed. These bigger craters cannot be entirely machined in grinding process owed to the ineffectiveness of protrusion height of abrasives. Thus, larger current and POT values decrease the surface quality and result in high R_a values.

(a)

(b)

(c)
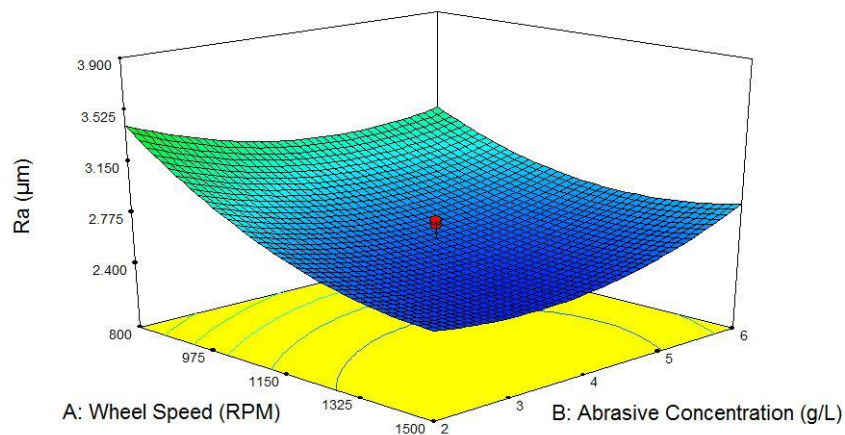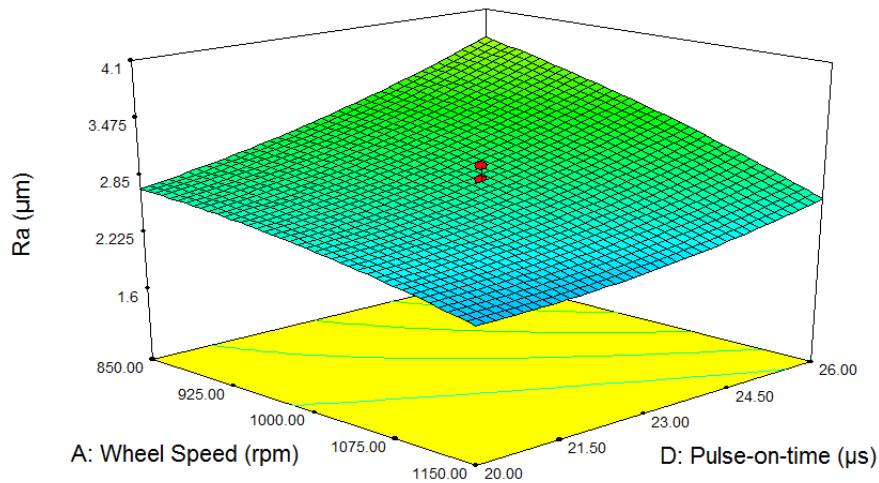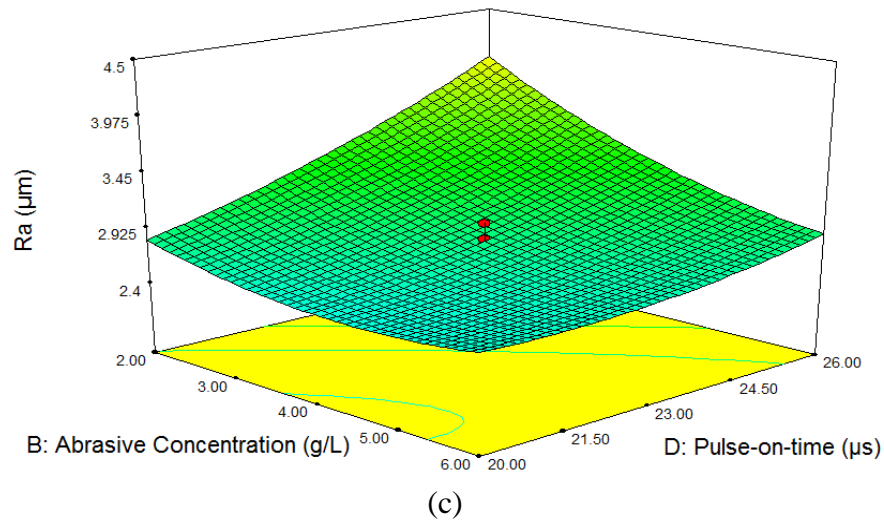
Figure 4.6 (a), (b), and (c) shows the response graph of R_a

4.7 Desirability based multi-response optimization

Desirability function approach is one of the common approaches used for optimization of single and multiple performance variable problems [124]. The control factor sets with maximum desirability are supposed to be the optimal factor conditions. The design expert optimization module was used to determine the combination of control factors, i.e., wheel speed, abrasive concentration, current, and POT, which fulfills the constraint imposed on control factors and performance measures.

A set 30 optimal solution were resultant for the particular design space constraints for MRR and R_a. The combinations owning uppermost desirability value was designated as an optimum state for the preferred responses [124, 128, 129]. The optimal combinations with high desirability function are listed in Table 4.7. After selection of the optimal set of the control factors, prediction, and verification of enhancement in performance measures using the optimal set of the control factors was carried out. A trial was executed to the machine and confirm the AMSEDDG at the optimal control factor combinations for MRR and R_a and related with optimum response value. Table

67

4.9 expresses the percentage of error for trial confirmation of the established models for the responses with optimal control factors combinations in AMSEDDG. A minor error is observed from examination confirming excellent reproducibility of the experiment deductions.

Table 4.7 Range of control factors and responses for desirability.

Control Factor	Goal	Lower limit	Upper limit	Lower weight	Upper weight	Importance
W_s	Is in range	800	1500	1	1	3
AC	Is in range	2	6	1	1	3
C	Is in range	4	8	1	1	3
T_{on}	Is in range	20	26	1	1	3
MRR	Maximize	5.95	14.35	1	1	3
R_a	Minimize	2.390	4.543	1	1	3

Table 4.8 Control factors and optimum values of Inconel 718

Factor	Goal	Optimum value
W_s	In range	1355
AC	In range	4
C	In range	6
T_{on}	In range	22

Table 4.9 Predicted and observed values of responses of Inconel 718

Response	Goal	Predicted	Observed	Error
MRR	Maximize	13.90	14.45	3.81%
R_a	Minimize	2.484	2.621	5.23%
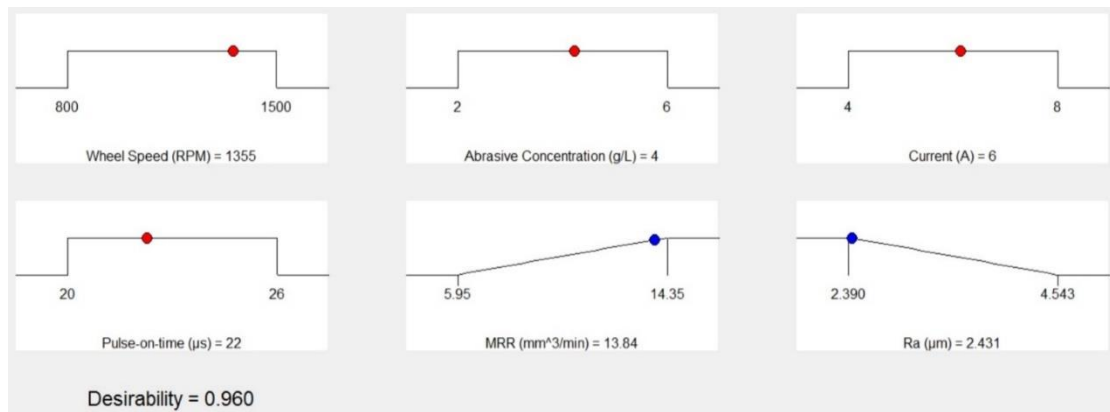
Figure 4.7 Ramp function graph of Desirability for Inconel 718
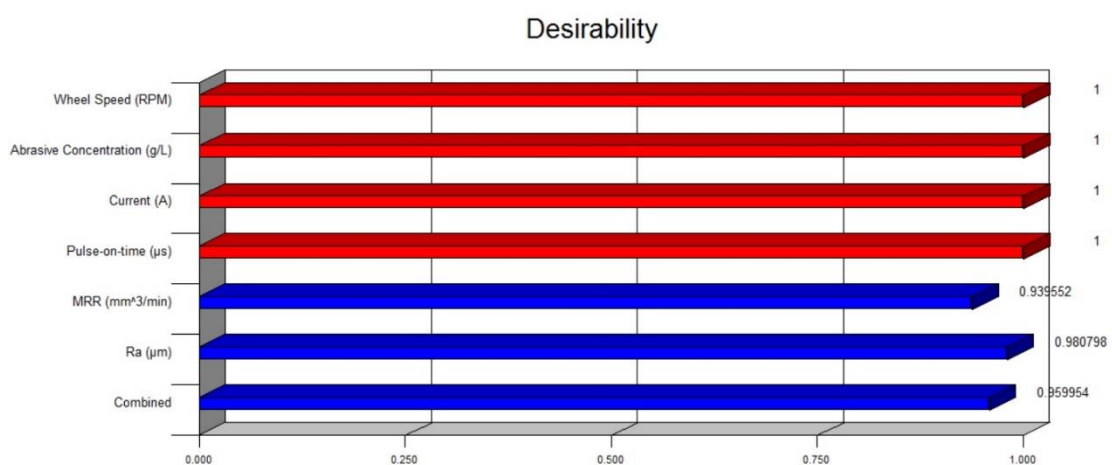
Figure 4.8 Bar graph of desirability of Inconel 718

The ramp function graph and bar graph Figure 4.7 and Figure 4.8 shows the desirability

for MRR and R_a. The point showed on every ramp reveals parameter value or response

forecast. However, the tallness of point directs its desirability. General desirability

function of the response shown by a bar graph. The values near to one in bar graph

direct towards variables satisfying the constraints.

4.8   The surface morphology of AMEDDSG machined surfaces:

Trial experiments were performed to understand the surface quality of machined

Inconel 718 using EDM process so that the observation of surfaces generated using

EDM can be compared with those by AMEDDSG. Figure 4.9 shows the images of

machining Inconel 718 using copper electrode in die-sink EDM process at two different

machining conditions. The incidence of debris and micro cracks and recast layers on the uneven surface can be clearly seen from SEM images of EDMed surfaces. The occurrence of debris, recast layers and micro-cracks increases with increase in current, and pulse-on-time as more discharge energy act on the machined surface and, therefore, results in the poor surface finish. The molten metal that cannot be removed from surface solidifies in the craters and on the surface forming increased thickness of recast layer. This is well known common phenomena reported the literature. For higher material removal rate it is required to increase the discharge energy in EDM, however, increased discharge energy at the same time results in poorer surface quality.

(a) (Current :6A, Pulse-on-time:20 μs and Duty factor: 0.67)

(b) (Current :6A, Pulse-on-time:23 μs and Duty factor: 0.67)
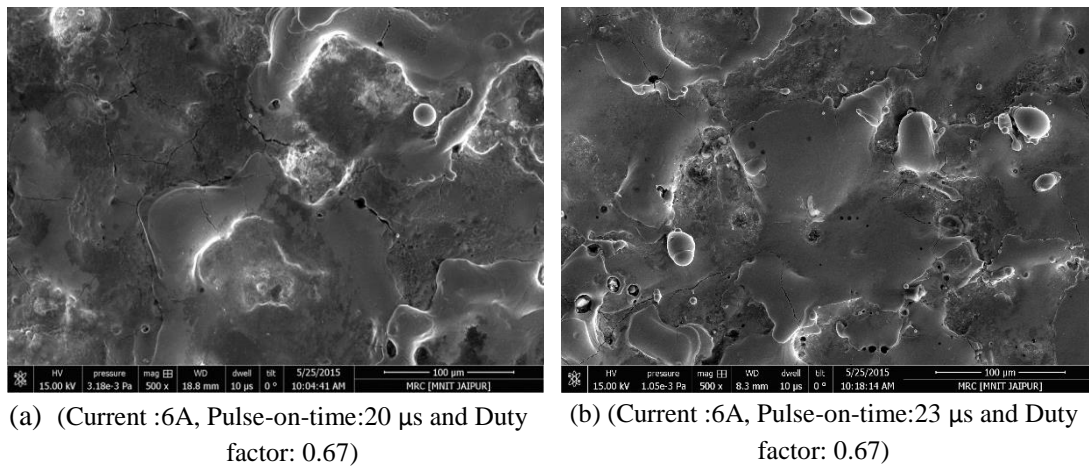
Figure 4.9 FESEM images of EDM processed surfaces of Inconel 718

The Figure 4.10 (a), (b), (c) and (d) represent the surface morphology of Inconel 718 after AMEDDSG at difference machining conditions. The surface quality of AMEDDSG processes workpiece was observed superior that EDMed surface. It can been observed that very few micro-cracks, craters and recast layer present on the surface generated by AMEDDSG process as compared to EDMed surface. In AMEDDSG processing, at low wheel speeds (at 700 rpm, Figure 4.10 (a) & (b)) more grinding wheel marks were observed as compared to higher wheel speed (at 1150 rpm, Figure 4.10 (c) & (d)). Also, as the wheel speed increases the cavities observed to be

decreasing due to more efficient dielectric flushing at inter-electrode gap. This is due to the fact that at higher wheel speed improved flushing efficiency conditions can be achieved and the molten material is effectively ejected from the workpiece surface not allowing any debris accumulation at inter-electrode gap [126]. Thus, the more uniform surface can be achieved. Further, at higher wheel speeds very few recast layers were observed as compared to those at low wheel speed. Thus, again directing towards better flushing conditions due to high wheel speed.

At low wheel speeds (at 700 rpm, Figure 4.10 (a) & (b)) more grinding wheel marks were observed as compared to higher wheel speed (at 1150 rpm, Figure 4.10 (c) & (d)). Also, as the wheel speed increases the cavities observed to be decreasing due to more efficient dielectric flushing at the inter-electrode gap. This is due to the fact that at higher wheel speed improved flushing efficiency conditions can be achieved and the molten material is effectively ejected from the workpiece surface not allowing any debris accumulation at inter-electrode gap [126]. Thus, the more uniform surface can be achieved. Further, at higher wheel speeds very few recast layers observed as compared to those at low wheel speed. Thus, again directing towards better flushing conditions due to high wheel speed.

The surface craters size observed to be increasing with increase in current and pulse-on-time; as an increase in current and pulse-on-time both will lead to evacuate more metal in molten form. This is due to the fact that at high current and high pulse-on-time more discharge energy will go in the workpiece since discharge energy is the product of pulse-current and pulse-on-time. It is also observed that the addition of powder results in smooth and narrow surface cavities. The plasma channel becomes larges and wider due to added powder in dielectric fluid resulting in a decreased spark discharge

density leading to smooth and narrow surface cavities [80, 127]. For the uniform surface, higher wheel speed and higher powder concentrations are recommended.

(a) (*WS*-700, *AC*-0, *C*-6, and T_{on}-17) (b) (*WS* -700, *AC* -0, *C*-10, and T_{on} -20)

(c) (*WS* -1150, *AC* -4, *C*-4, T_{on} -17) (d) (*WS* -1150, *AC* -6, *C*-10, T_{on} -29)
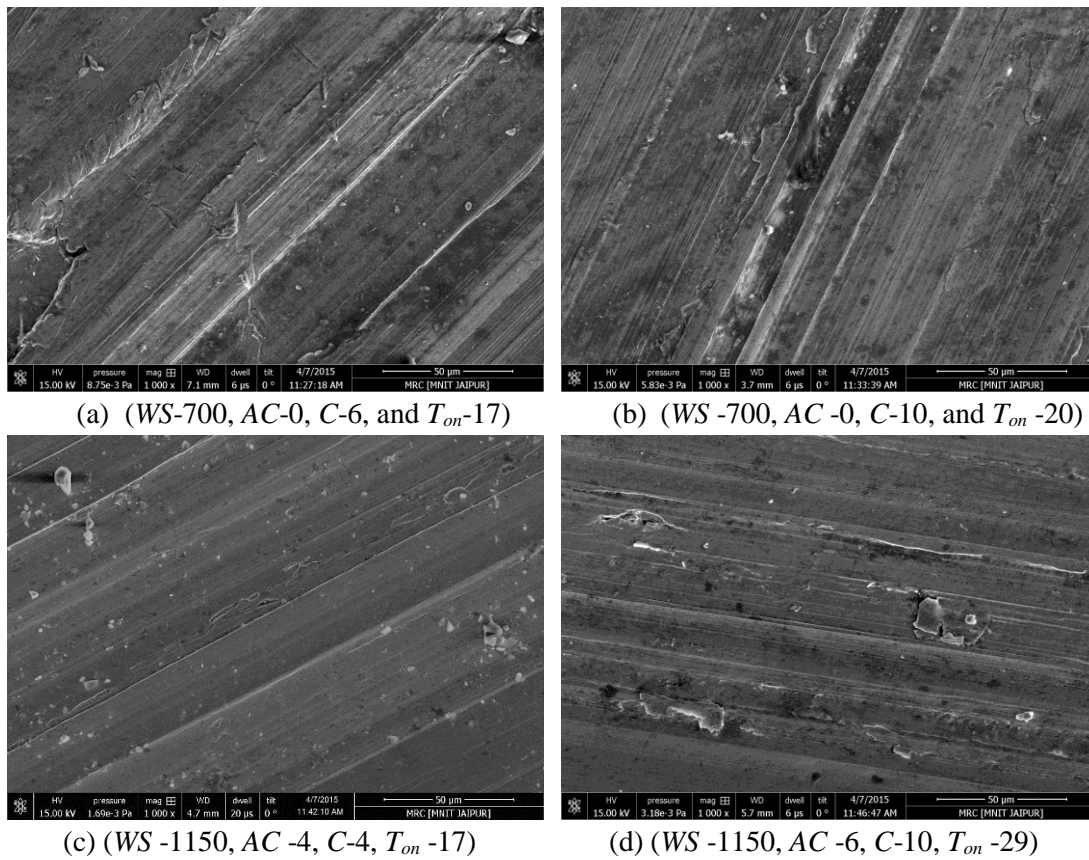
Figure 4.10 FESEM images of AMEDDG machined workpiece at different machining conditions

4.9 Summary

In this chapter, a hybrid machining process called as additive mixed surface electro discharge grinding has been used for micro-surface machining of Inconel 718 superalloy. The parametric influences on performance measures including MRR and surface roughness have been investigated.

- The empirical model for MRR and R_a have been developed as given below:

$$MRR = -62.04911 + (0.04771 \times W_s) + (0.64524 \times AC)$$
$$+ (1.04389 \times C) + (3.12916 \times T_{on})$$
$$+ (0.000815 \times W_s \times AC) - (0.000884 \times WS \times C)$$
$$- (0.000787 \times W_s \times T_{on}) + (0.17745 \times C \times T_{on})$$
$$- (0.00001 \times W_s{}^2) - (0.17943 \times AC^2) - (0.30274 \times C^2)$$
$$- (0.06344 \times T_{on}{}^2)$$

$$R_a = 22.59339 + (0.00565 \times W_s) - (0.33474 \times AC) - (1.44439 \times C)$$
$$- (1.10390 \times T_{on}) + (0.000216 \times W_s \times AC)$$
$$- (0.034812 \times C \times T_{on}) + (0.0000017 \times W_s{}^2)$$
$$+ (0.047103 \times AC^2) + (0.07240 \times C^2) + (0.021942$$
$$\times T_{on}{}^2)$$

- The above models are considerably reliable representing the experimental values with the prediction errors less than ±5 %.

- The wheel speed is the most significant factor for material removal rate for Inconel 718 contributing 16.05%. The wheel speed significantly interacts with abrasive concentration, current, and pulse-on-time for MRR. In addition, the interaction between current and POT contributes significantly in MRR.

- The MRR increases with an increase in both wheel speed and abrasive concentration up to an optimum value and then slows down with for further increase in them. The high wheel speed does not allow plasma to constitute in the process thereby slowing down the MRR. The high abrasive concentration results in plasma interference reducing the MRR.

- The pulse-on-time is the most significant factor followed by wheel speed for average surface roughness contributing by 26.57% and 19.36%, respectively. The interaction between wheel speed and abrasive concentration, abrasive concentration and POT, and current and POT are significantly affecting the average surface roughness.

- The average surface roughness decreases with increase abrasive concentration up to an optimum level and then increases with further increase in abrasive concentration.

- The results of multi-response optimization by taking equal importance to both performance measures achieved the highest material removal rate as 13.90 mm^3/min and lowest average surface response as 2.484 µm.

Overall, it is perceived that the purpose of hybridization of AEDM and EDDSG into AMEDDG resulted into better machining performance as the process yields high machining rate and the same time low surface roughness values.

5 Experimental investigation on low-frequency vibration assisted μ-ED drilling of Inconel 718

The fabrication of micro-holes in aerospace alloys like Inconel 718 is very vital from aircraft and aerospace industries perspective. Presently, micro-EDM has been established as an efficient process for drilling micro-holes in any conductive materials. However, the application of micro-EDM in deep-hole drilling is still restricted owing to the difficulty of removal of trapped debris in IEG. This chapter reports the implementation of the low-frequency workpiece vibration assisted μ-ED drilling to overcome the problem above. The next sections describe approach and results of an experimental investigation performed to analyze the effects of vibrational frequency along with the other machining parameters while drilling micro-holes in Inconel 718 based on MRR, electrode wear ratio, quality and accuracy of the micro-holes.

5.1   Experimental plan and control factors

The Box–Behnken design was utilized to plan the experiments due to its less experimental runs, the simplicity of experiments eluding extreme values of control factors causing costly or unmanageable run due to physical process constraints, and allowing the study of an interaction effect between control factors in the same number of runs [125]. The experimental procedure while performing the μ-ED drilling is discussed in section 3.2.2.

The gap voltage (V_g), capacitance (Cp), electrode rotation speed (R), and vibrational frequency (F) were designated as control factors while MRR and FEW were chosen as performance measures. The control factors and their range, shown in Table 5.1, were decided based on the literature, preliminary experiments, manufacturer's handbook, and machines constraints. Total 29 experimental runs were performed as per Box-Behnken design with four control factors each varying at three levels. Out of 29 runs, 24 runs corresponds to the side points, and five runs replicate the center position five times. The experimental plan showing a set of the control factors and resultant performance measures acquired after conducting tests are given in Table 5.2.

Table 5.1 Independent control factors, and their levels

Control factors			Level		
	Unit	Notation	-1	0	1
Gap voltage	V	V_g	80	100	120
Capacitance	µF	Cp	0.01	0.2	0.4
Electrode rotation speed	rpm	R	100	500	900
Vibrational frequency	Hz	VF	0	30	60

Table 5.2 Experimental design matrix and observed performance measures in low-frequency assisted µ-ED drilling of Inconel 718

Run order	Control factors (coded values)				Performance measures			
	Gap Voltage (V)	Capacitance (µF)	Electrode rotation speed (rpm)	Vibrational frequency (Hz)	MRR (mm³/min)	EWR (%)	Overcut (mm)	Taper angle (degree)
1	0	0	0	0	0.00945	0.238	0.014	2.473
2	0	1	-1	0	0.00548	0.236	0.024	2.512
3	0	-1	-1	0	0.00108	0.141	0.019	2.058
4	-1	-1	0	0	0.00205	0.134	0.019	1.848
5	-1	0	-1	0	0.00651	0.142	0.023	2.371
6	0	0	1	-1	0.00868	0.262	0.014	2.297
7	1	0	-1	0	0.00153	0.227	0.021	2.504

8	1	0	0	1	0.00404	0.257	0.016	2.495
9	0	0	-1	-1	0.00105	0.203	0.020	2.463
10	0	0	0	0	0.01001	0.248	0.014	2.510
11	0	1	0	-1	0.00749	0.275	0.016	2.498
12	1	0	1	0	0.00691	0.266	0.015	2.398
13	0	-1	1	0	0.00161	0.148	0.012	2.023
14	1	0	0	-1	0.00202	0.255	0.020	2.475
15	0	0	0	0	0.00899	0.230	0.013	2.553
16	-1	1	0	0	0.00978	0.275	0.011	2.494
17	0	-1	0	-1	0.00095	0.140	0.014	2.141
18	0	-1	0	1	0.00263	0.147	0.016	1.898
19	-1	0	0	-1	0.00484	0.230	0.013	2.026
20	-1	0	0	1	0.00927	0.170	0.015	2.420
21	0	1	0	1	0.00947	0.268	0.016	2.512
22	0	0	1	1	0.00938	0.264	0.012	2.418
23	0	1	1	0	0.00976	0.275	0.011	2.505
24	1	1	0	0	0.00380	0.250	0.020	2.509
25	0	0	-1	1	0.00903	0.191	0.024	2.509
26	0	0	0	0	0.00882	0.226	0.013	2.607
27	0	0	0	0	0.00985	0.250	0.014	2.339
28	-1	0	1	0	0.00858	0.257	0.011	2.382
29	1	-1	0	0	0.00124	0.230	0.013	2.136

5.2 Reproducibility

The reproducibility is checked by the performance of five center point runs. The results of experiments at center points (1,10,15,26,27) are presented separately in Table 5.3. The percentage error shown in Table 5.3 is the variability of the performance measures on its average value (sum of all terms divided by the number of terms) and is calculated by the equation (4.2).

It was observed that the results reproduced within the acceptable range of ±7%. Also, the values of experimental standard deviation and standard uncertainty were assessed for performance measures to elucidate their variations at same experimental conditions [124]. The results of standard uncertainty for MRR, EWR, overcut, and taper angle was calculated to be 0.023%, 0.479%, 0.025%, and 4.524%, respectively, which are well inside the tolerable limit.

Table 5.3 Reproducibility and percentage (%) error for performance measures

Run order	Performance measures							
	MRR (mm3/min)		EWR (%)		Overcut (mm)		Taper angle (degree)	
	Expt. value	% error	Expt. value	% error	Expt. value	% error	Expt. value	% error
1	0.00945	-0.29	0.238	0.21	0.014	-0.03	2.473	0.93
10	0.01001	-6.27	0.248	-4.04	0.014	-4.83	2.510	-0.53
15	0.00899	4.55	0.230	3.69	0.013	3.77	2.553	-2.28
26	0.00882	6.45	0.226	5.12	0.013	4.52	2.607	-4.43
27	0.00985	-4.47	0.250	-4.97	0.014	-3.44	2.339	6.30

5.3 Effects of workpiece vibration on gap distance and gap fluid pressure during vibration assisted µ-ED drilling

Figure 5.1 (a) represents the schematic diagram showing the workpiece vibration in the micro-EDM drilling process. Figure 5.1 (b) shows the variation of workpiece position, gap distance, and gap fluid pressure change with time during workpiece vibration assisted micro-EDM drilling.

(a)

Workpiece positions at different vibration phase

Resultant gap distance due to different vibration phase

Change of fluid pressure in the gap at due to vibration

(b)
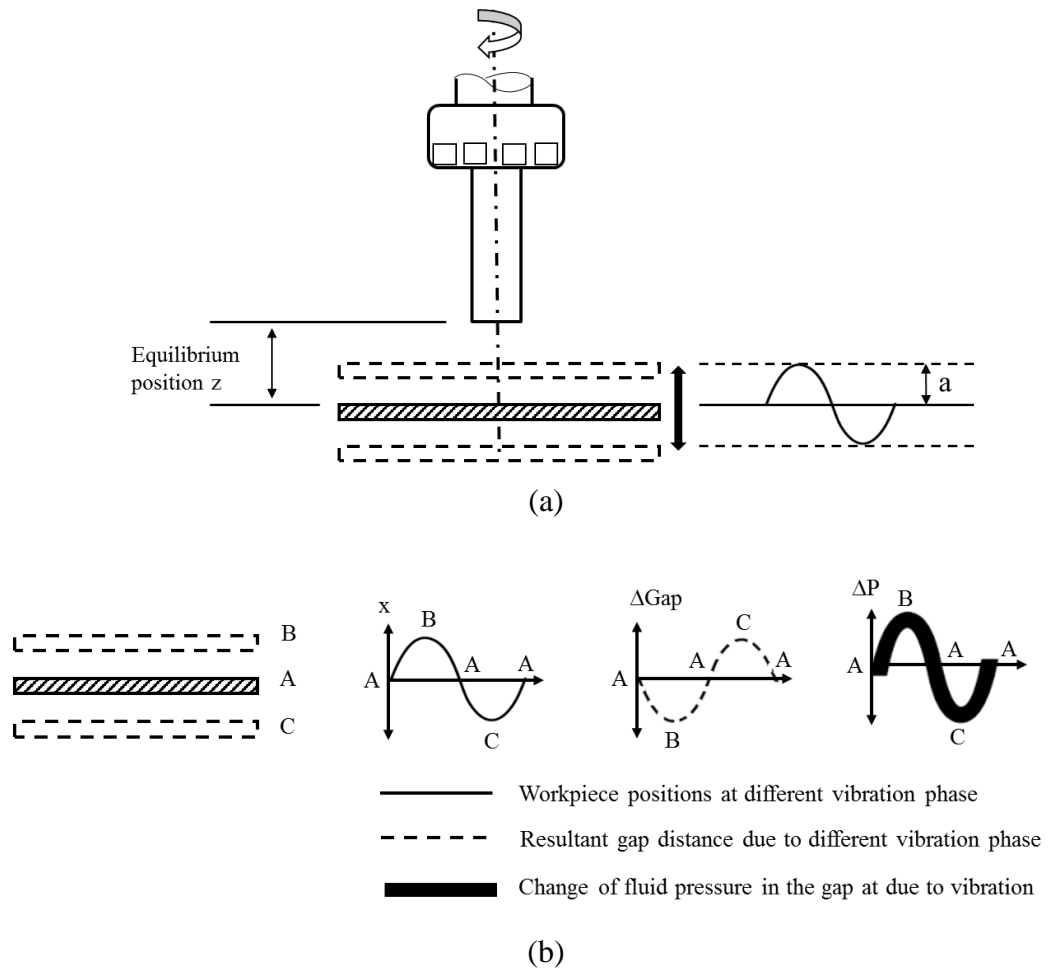
Figure 5.1 (a) Vibration assisted μ-ED drilling and (b) variation of gap distance and fluid pressure

If the maximum amplitude of the workpiece vibration is a, then the equivalent gap distance.

$$\Delta gap = z \pm a$$

The position of maximum and minimum gap distance can be obtained as:

$$\Delta gap_{max} = z + a$$

$$\Delta gap_{min} = z - a$$

The schematic representation of effects of workpiece vibration on debris and dielectric motion is shown in Figure 5.2. At position B, during the upward movement of the workpiece, the equivalent gap distance decreases. Therefore, there is an increase in the

pressure of the dielectric fluid in the gap. During the reduction of gap distance, fluid pressure increases, and the fluid comes out from the side of the tool electrode, thus helping to flush the debris particles out from the deep blind hole. Thus, the dielectric is flushed out of electrode gap when the workpiece is moving upward (decreasing IEG), whereas the dielectric is sucked in a channel for downward (increasing IEG) movement of the workpiece which makes available fresh dielectric for further machining. Overall, the vibration assists in enhancing the debris and dielectric motion during µ-ED drilling thereby enhancing the performance of the process.

(a) At A position Presence of debris at machining gap

(b) Expel of debris and fluid at B position due to pressure rise

(c) Suction of fresh dielectric at C position due to pressure drop
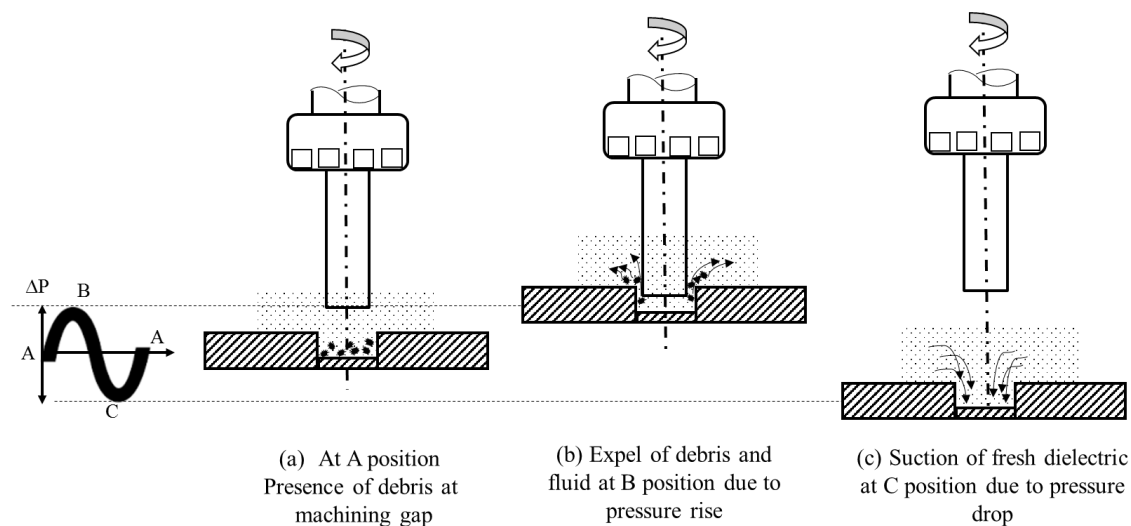
Figure 5.2 Motion of debris and dielectric fluid due to workpiece vibration in µ-ED drilling

5.4 Empirical models for performance measures

Defining the analytical model for the low-frequency vibration assisted µ-ED drilling made on process physics is very problematical due to complex and stochastic nature of the process. Therefore, to establish a mathematical relationship between the control factors and performance measures, a multi-variable regression model was established for each performance measure. ANOVA was performed to examine statistically the results of the selected model. The significant control factors were detected, and

interaction effects of these control factors on performance measures were investigated using response surface graphs.

5.4.1 ANOVA for MRR, EWR, overcut, and taper angle

The experimental results for performance measures shown in Table 5.2 were studied using Design-Expert software. The sequential model sum of squares, lack-of-fit test, and model summary statistics tests were performed to evaluate the adequacy of the models which suggested the adequacy of quadratic models. Therefore, quadratic models were analyzed using ANOVA to determine the significant model terms. The backward elimination procedure was executed to eliminate the unimportant terms from models thereby improving the models. The results of ANOVA for $MRR_{µEDD}$, EWR, overcut, and taper angle after backward elimination are summarized in Table 5.4, Table 5.5, Table 5.6, and Table 5.7, respectively.

Table 5.4 The ANOVA table for MRR model

Source	Sum of Square	df	Mean Square	F Value	p-value Prob>F		Percentage contribution
Model	3.256E-004	12	2.713E-005	35.39	< 0.0001	significant	
V_g	3.851E-005	1	3.851E-005	50.23	< 0.0001		11.81
Cp	1.093E-004	1	1.093E-004	142.56	< 0.0001		33.53
R	3.414E-005	1	3.414E-005	44.52	< 0.0001		10.47
F	2.939E-005	1	2.939E-005	38.33	< 0.0001		9.01
$V_g{\times}Cp$	6.695E-006	1	6.695E-006	8.73	0.0093		2.05
$V_g{\times}R$	2.736E-006	1	2.736E-006	3.57	0.0771		0.84
$Cp{\times}R$	3.513E-006	1	3.513E-006	4.58	0.0481		1.08
$RS{\times}F$	1.327E-005	1	1.327E-005	17.31	0.0007		4.07
$V_g{\,}^2$	3.859E-005	1	3.859E-005	50.33	< 0.0001		11.84
$Cp{\,}^2$	6.211E-005	1	6.211E-005	81.01	< 0.0001		19.05
$R{\,}^2$	1.116E-005	1	1.116E-005	14.55	0.0015		3.42
$F{\,}^2$	1.280E-005	1	1.280E-005	16.69	0.0009		3.93
Residual	1.227E-005	16	7.668E-007				

Lack of Fit	1.119E-005	12	9.323E-007	3.45	0.1210	not significant	
Pure Error	1.081E-006	4	2.702E-007				
Cor Total	3.379E-004	28					
Std. Dev.	8.756E-004			R-Squared		0.9637	
Mean	6.011E-003			Adj R-Squared		0.9365	
C.V. %	14.57			Pred R-Squared		0.8576	
PRESS	4.810E-005			Adeq. Precision		17.599	

Vg -Gap Voltage, *Cp*-Capacitance, *R*-Electrode rotation speed, *F*-Vibrational Frequency

Table 5.5 The ANOVA table for EWR model

Source	Sum of Square	df	Mean Square	F Value	p-value Prob>F		Percentage contribution
FOR EWR							
Model	0.059	8	7.385E-003	25.13	< 0.0001	significant	
V_g	6.427E-003	1	6.427E-003	21.87	0.0001		7.22
Cp	0.034	1	0.034	116.24	< 0.0001		38.34
R	9.127E-003	1	9.127E-003	31.06	< 0.0001		10.25
F	3.606E-004	1	3.606E-004	1.23	0.2811		0.40
$V_g \times Cp$	3.674E-003	1	3.674E-003	12.50	0.0021		4.12
$V_g \times RS$	1.447E-003	1	1.447E-003	4.92	0.0382		1.62
$V_g \times F$	9.468E-004	1	9.468E-004	3.22	0.0878		1.06
Cp ^2	2.939E-003	1	2.939E-003	10.00	0.0049		3.30
Residual	5.877E-003	20	2.938E-004				
Lack of Fit	5.418E-003	16	3.386E-004	2.95	0.1525	not significant	
Pure Error	4.594E-004	4	1.149E-004				
Cor Total	0.065	28					
Std. Dev.	0.017			R-Squared		0.9095	
Mean	0.22			Adj R-Squared		0.8733	
C.V. %	7.73			Pred R-Squared		0.7680	
PRESS	0.015			Adeq Precision		19.658	

Vg -Gap Voltage, *Cp*-Capacitance, *R*-Electrode rotation speed, *F*-Vibrational Frequency

Table 5.6 The ANOVA table for Overcut model

Source	Sum of Square	df	Mean Square	F Value	p-value Prob>F		Percentage contribution
Model	4.285E-004	13	3.296E-005	38.70	< 0.0001	significant	
Vg	1.436E-005	1	1.436E-005	16.86	0.0009		3.36
Cp	2.230E-006	1	2.230E-006	2.62	0.1265		0.52
R	2.666E-004	1	2.666E-004	312.97	< 0.0001		62.28
F	9.075E-009	1	9.075E-009	0.011	0.9192		0.00
$Vg{\times}Cp$	5.781E-005	1	5.781E-005	67.87	< 0.0001		13.51
$Vg{\times}R$	1.009E-005	1	1.009E-005	11.85	0.0036		2.36
$Vg{\times}F$	1.073E-005	1	1.073E-005	12.60	0.0029		2.51
$Cp{\times}R$	6.610E-006	1	6.610E-006	7.76	0.0139		1.54
$R{\times}F$	8.343E-006	1	8.343E-006	9.80	0.0069		1.95
$Vg\,{\char94}2$	1.520E-005	1	1.520E-005	17.85	0.0007		3.55
$Cp\,{\char94}2$	2.869E-006	1	2.869E-006	3.37	0.0863		0.67
$R\,{\char94}2$	4.338E-005	1	4.338E-005	50.93	< 0.0001		10.14
$F\,{\char94}2$	7.039E-006	1	7.039E-006	8.26	0.0116		1.64
Residual	1.278E-005	15	8.518E-007				
Lack of Fit	1.149E-005	11	1.045E-006	3.26	0.1327	not significant	
Pure Error	1.284E-006	4	3.209E-007				
Cor Total	4.413E-004	28					
Std. Dev.	9.229E-004			R-Squared	0.9710		
Mean	0.016			Adj R-Squared	0.9460		
C.V. %	5.78			Pred R-Squared	0.8561		
PRESS	6.348E-005			Adeq Precision	20.416		

V_g -Gap Voltage, Cp-Capacitance, R-Electrode rotation speed, F-Vibrational Frequency

Table 5.7 The ANOVA table for taper angle model

Source	Sum of Square	df	Mean Square	F Value	p-value Prob>F		Percentage contribution
Model	1.03	5	0.21	21.58	< 0.0001	significant	
Vg	0.079	1	0.079	8.32	0.0084		7.71
Cp	0.71	1	0.71	74.81	< 0.0001		69.33
F	0.010	1	0.010	1.09	0.3082		1.01
$Vg{\times}F$	0.035	1	0.035	3.68	0.0675		3.41

Cp ^2	0.19	1	0.19	20.01	0.0002		18.55
Residual	0.22	23	9.536E-003				
Lack of Fit	0.18	19	9.388E-003	0.92	0.6105	not significa nt	
Pure Error	0.041	4	0.010				
Cor Total	1.25	28					
Std. Dev.	0.098			R-Squared	0.8243		
Mean	2.36			Adj R-Squared	0.7861		
C.V. %	4.14			Pred R-Squared	0.6552		
PRESS	0.43			Adeq Precision	14.639		

V_g -Gap Voltage, Cp-Capacitance, R-Electrode rotation speed, F-Vibrational Frequency

The normal probability plot of the residuals (Figure 5.3) for MRR, EWR, overcut, and taper angle directs that residuals fall on a straight line representing that errors are normally distributed [125]. Also, from Figure 5.4, it can be seen that the actual values are in good agreement with predicted values from the model. Therefore, it has been inferred that ANOVA results for MRR$_{µEDD}$, EWR, overcut, and taper angle given in Table 5.4, Table 5.5, Table 5.6, and Table 5.7, respectively are trustworthy as the plots fulfill the error normality and prediction capability criteria.
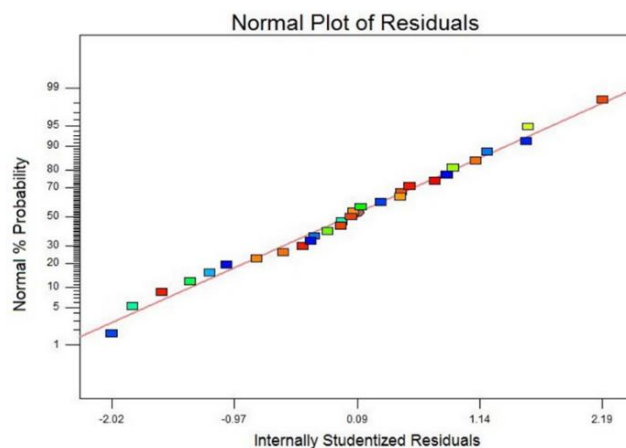
(a)
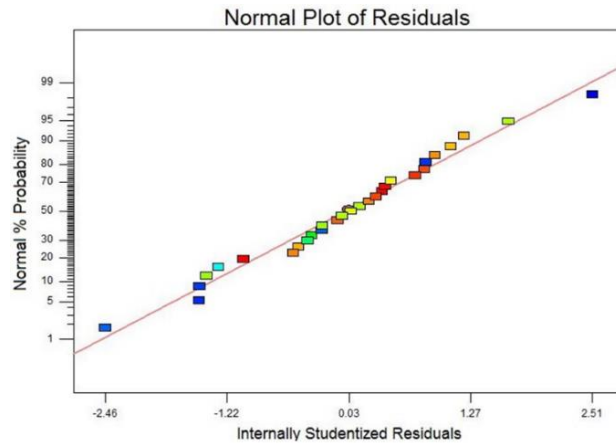
(b)
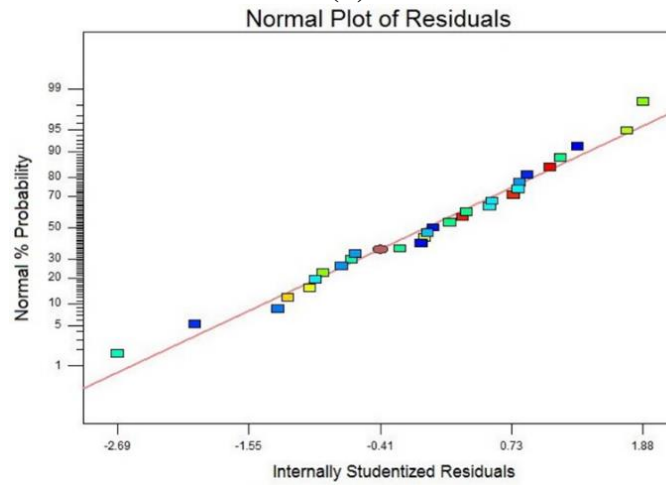
(c)
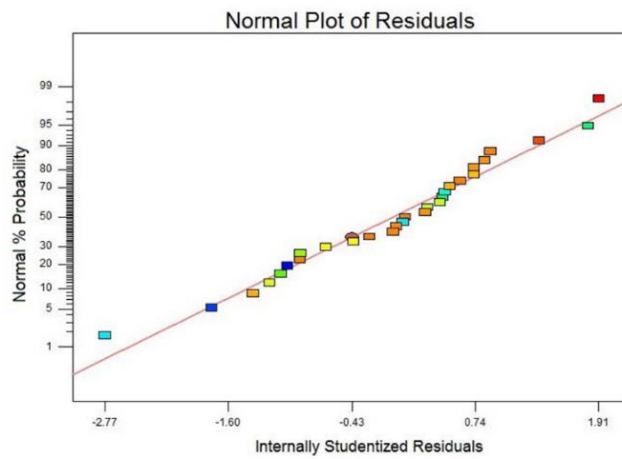
(d)

Figure 5.3 Normal probability plot of residuals for (a) MRR$_{µEDD}$, (b) EWR, (c) overcut, (d) taper angle
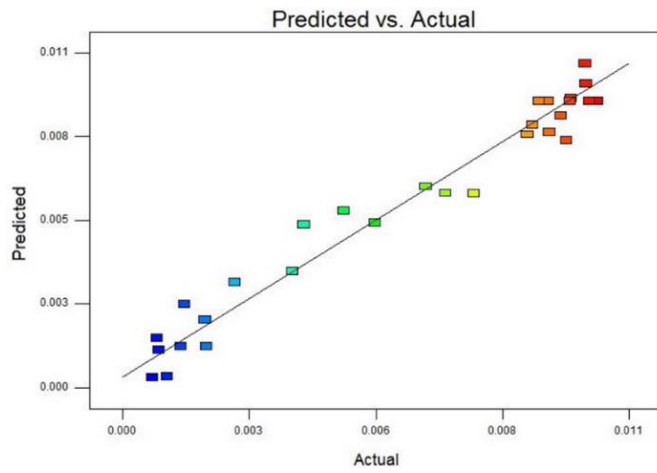
(a)
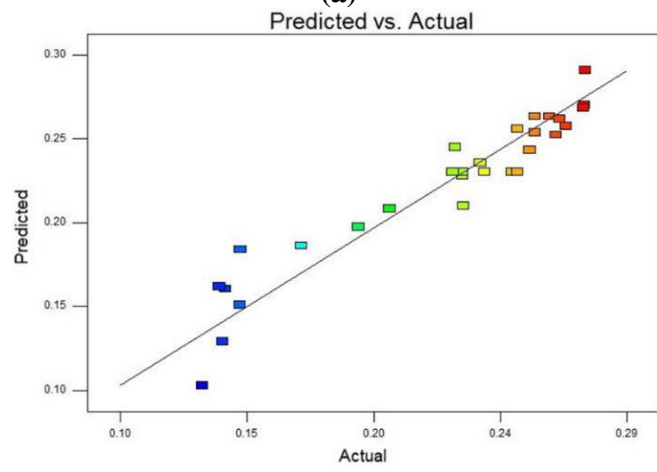
(b)
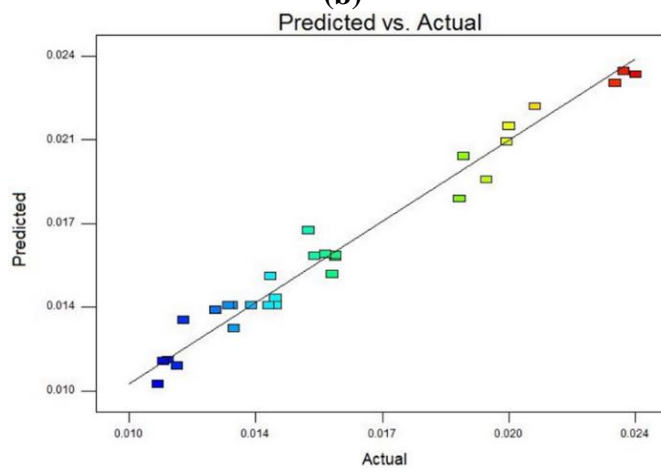
(c)
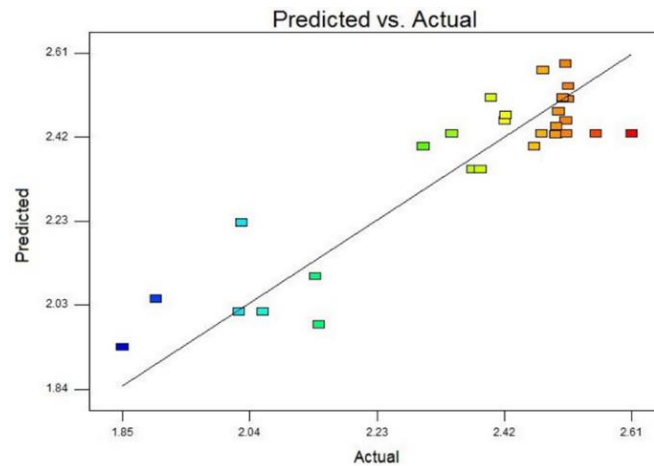
(d)

Figure 5.4 Plot of predicted vs. actual response for (a) MRR$_{μEDD}$, (b) EWR, (c) overcut, and (d) taper angle

The model F values of 35.39$_{MRR}$, 25.13$_{EWR}$, 38.70$_{overcut}$ and 21.58$_{taper\ angle}$ for MRR$_{μEDD}$, EWR, overcut, and taper angle respectively, with its Prob>F value less than 0.0001 in ANOVA tables point out that the models are significant confirming that the terms in the models have a significant effect on the performance measures. There is only a 0.01 % chance that such a large model F values could occur due to noise. The values of Prob>F less than 0.05 indicates the significance of model terms [125, 130].

For MRR$_{μEDD}$, V_g, Cp, R, F, $V_g \times Cp$, $Cp \times R$, $R \times F$, $V_g\ 2$, Cp^2, R^2, *and* F^2 are significant model terms with their percentage contribution of 11.81, 33.53, 10.47, 9.01, 2.05, 0.84, 1.08, 4.07, 11.84, 19.05, 3.42, and 3.93 respectively. The "individual (model) term" sum of squares was divided by "model" sum of squares to compute the percentage contribution. The V_g, Cp, R, F, $V_g \times Cp$, $V_g \times R$, $V_g \times F$, *and* Cp^2 are significant model terms for EWR with their percentage contribution of 7.22, 38.34, 10.25, 0.40, 4.12, 1.62, 1.06, and 3.30 respectively. The V_g, R, $V_g \times Cp$, $V_g \times R$, $V_g \times F$, $Cp \times R$, $R \times F$, $V_g\ ^2$, R^2, *and* F^2 are significant model terms for the overcut contributing 3.36, 0.52, 62.28, 0.002, 13.51, 2.36, 2.51, 1.54, 1.95, 3.55, 0.67, 10.14, and 1.64 respectively. The V_g, Cp, *and* Cp^2 contributes 7.71, 69.33, and 18.55 respectively in case of a model for taper angle.

87

The lack-of-fit values indicate its significance or non-significance relative to pure error. When lack-of-fit values are non-significant, it agrees on the model fit to the experimental data and recommends that a very small systematic difference that leftovers unaccounted for a particular model. In present study, the lack-of-fit values for were found to be 3.45, 2.95, 3.26, and 0.92 for MRR, EWR, overcut and taper angle models, respectively, which indicates that there is 12.10% $_{MRR}$, 15.25% $_{EWR}$, 13.27% $_{overcut}$, and 61.05% $_{taper\ angle}$ chance that a lack-of-fit F value this large could occur due to noise. Hence, the established models for MRR, EWR, overcut and taper angle can be accepted.

5.4.2 Regression equation for MRR, EWR, overcut and taper angle

The empirical relation between the performance measures (i.e. MRR$_{µEDD}$, EWR, overcut, and taper angle) and the control factors (actual terms) can be expressed by the following second-order polynomial equations;

$$
\begin{aligned}
MRR_{µEDD} = {} & -0.041521 + (7.583 \times 10^{-4})V_g + 0.067379\ Cp \\
& + (5.93879 \times 10^{-6})R + (2.21701 \times 10^{-4})F \\
& - (2.58820 \times 10^{-4})V_g \times Cp + (8.271 \times 10^{-8})V_g \times R \\
& + (1.17176 \times 10^{-5})Cp \times R - (1.51783 \times 10^{-7})R \\
& \times F - (3.90255 \times 10^{-6})V_g{}^2 - 0.0774\ Cp^2 \\
& - (8.19730 \times 10^{-9})R^2 - (1.56078 \times 10^{-6})F^2
\end{aligned}
\tag{5.1}
$$

$$
\begin{aligned}
EWR = {} & -0.13231 + (2.4741 \times 10^{-3})V_g + 1.10794\ Cp \\
& + (2.68658 \times 10^{-4})R - (2.33662 \times 10^{-3})F \\
& - (6.06252 \times 10^{-3})V_g \times Cp - (1.902 \times 10^{-6})V_g \times R \\
& + (2.05133 \times 10^{-5})V_g \times F - 0.51126\ Cp^2
\end{aligned}
\tag{5.2}
$$

$$\text{Overcut} = 0.06117 - (6.36691 \times 10^{-4})V_g - 0.076315\, Cp$$
$$- (3.77996 \times 10^{-5})R + (2.20965 \times 10^{-4})F$$
$$+ (7.6049 \times 10^{-4})V_g \times Cp + (1.5885 \times 10^{-7})V_g \times R$$
$$- (2.184 \times 10^{-6})V_g \times F - (1.6072 \times 10^{-5})Cp \times R \quad (5.3)$$
$$- (1.20354 \times 10^{-7})R \times VF + (2.44957 \times 10^{-6})V_g{}^2$$
$$+ 0.016636\, Cp^2 + (1.61632 \times 10^{-8})R^2$$
$$+ (1.15748 \times 10^{-6})F^2$$

$$\text{Taper angle} = 1.25279 + (6.99897 \times 10^{-3})V_g + 2.8677\, Cp$$
$$+ (0.014094)F - (1.2449 \times 10^{-4})V_g \times F \quad (5.4)$$
$$- 4.11975\, Cp^2$$

The coefficients of the control factor in above equations were calculated by Design-Expert package.

5.4.3 Validation of models

The eight additional experiments were executed at different control factors settings within the range of chosen factors in order to validate the established MRR, EWR, overcut and taper angle models. The dissimilar control factors combinations (shown in Table 5.8) were selected than the one used for forming the regression models. Table 5.9 displays the results of validation experiments. The prediction error (%) calculated using the equation (4.7).

The results of experimental validation were found to be in good agreement with the predicted results obtained from the regression equations, and prediction errors were less than ±7%. Consequently, the established models can be treated as a reliable demonstrative of the experimental results.

Table 5.8 Control factor settings

Expt. No.	Gap Voltage (V)	Capacitance (µF)	Electrode rotation speed (rpm)	Vibrational frequency (Hz)
1	100	0.1	500	60

2	100	0.4	300	30
3	120	0.1	700	0
4	100	0.1	300	30
5	105	0.4	700	30
6	105	0.4	700	60
7	100	0.1	900	30
8	120	0.1	500	0

5.5 Results and discussion

In the µ-ED drilling process, $MRR_{µEDD}$, EWR along with the overcut and taper angle of processed micro-holes are important performance measures due to their acute effects in industrial applications. In this section, Perturbation plot and three-dimensional (3D) response curves were used to discuss the impact of individual control factors as well as their interactions on the performance measures.

Table 5.9 Results of validation experiments for performance measures

Expt. no.	$MRR_{µEDD}$ (mm³/min)			EWR (%)			Overcut (mm)			Taper Angle (degree)		
	Expt. Value	Pred. value	% error	Expt. Value	Pred. value	% error	Expt. Value	Pred. value	% error	Expt. Value	Pred. value	% error
1	0.00712	0.00743	-4.32	0.173	0.182	-5.42	0.015	0.015	-1.52	2.156	2.294	-6.43
2	0.00866	0.00831	4.04	0.260	0.249	4.07	0.017	0.018	-4.34	2.446	2.489	-1.72
3	0.00431	0.00404	6.25	0.243	0.226	7.11	0.016	0.015	2.67	2.452	2.338	4.63
4	0.00664	0.00642	3.42	0.165	0.175	-6.27	0.017	0.017	5.02	2.209	2.246	-1.71
5	0.00975	0.01033	-5.99	0.281	0.277	1.43	0.012	0.012	-2.01	2.575	2.505	2.74
6	0.00938	0.00958	-2.19	0.279	0.272	2.71	0.013	0.013	2.67	2.690	2.534	5.79
7	0.00708	0.00701	0.95	0.218	0.222	-1.98	0.012	0.012	3.80	2.259	2.246	0.54
8	0.00270	0.00260	3.62	0.232	0.218	6.09	0.015	0.016	-6.24	2.361	2.338	0.96

5.5.1 Influence of control factors and their interactive effect on MRR

The comparative effects of significant control factors on $MRR_{µEDD}$ of Inconel 718 by µ-ED drilling were shown in Perturbation plot (Figure 5.5). By default, Design-Expert

package keeps the reference point at the midpoint (coded value 0) of all factors. A sharp slope for voltage (*Vg*) and capacitance (*Cp*) as compared to electrode rotations speed (*R*) and vibrational frequency (*F*) directs that the MRR is highly sensitive to voltage and capacitance. The reasons for above results have been discussed in successive paragraphs while explaining the interactive effects.
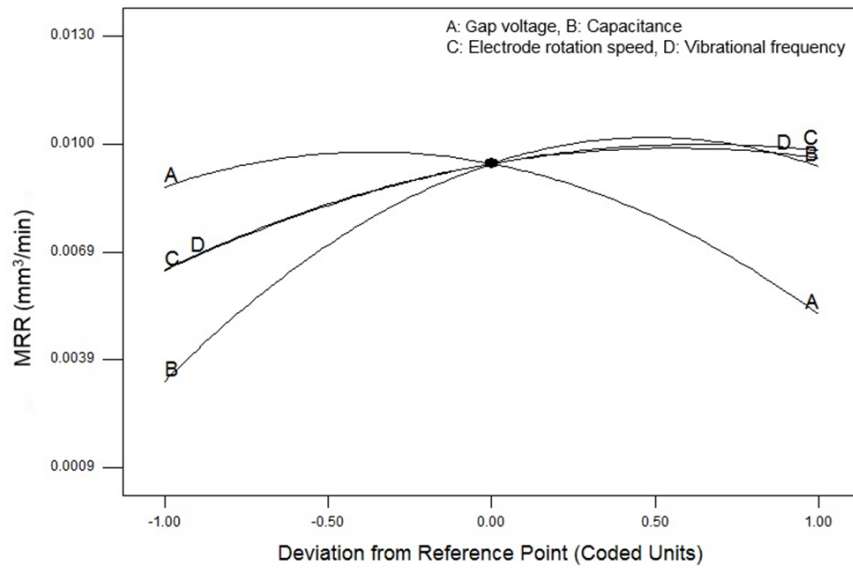
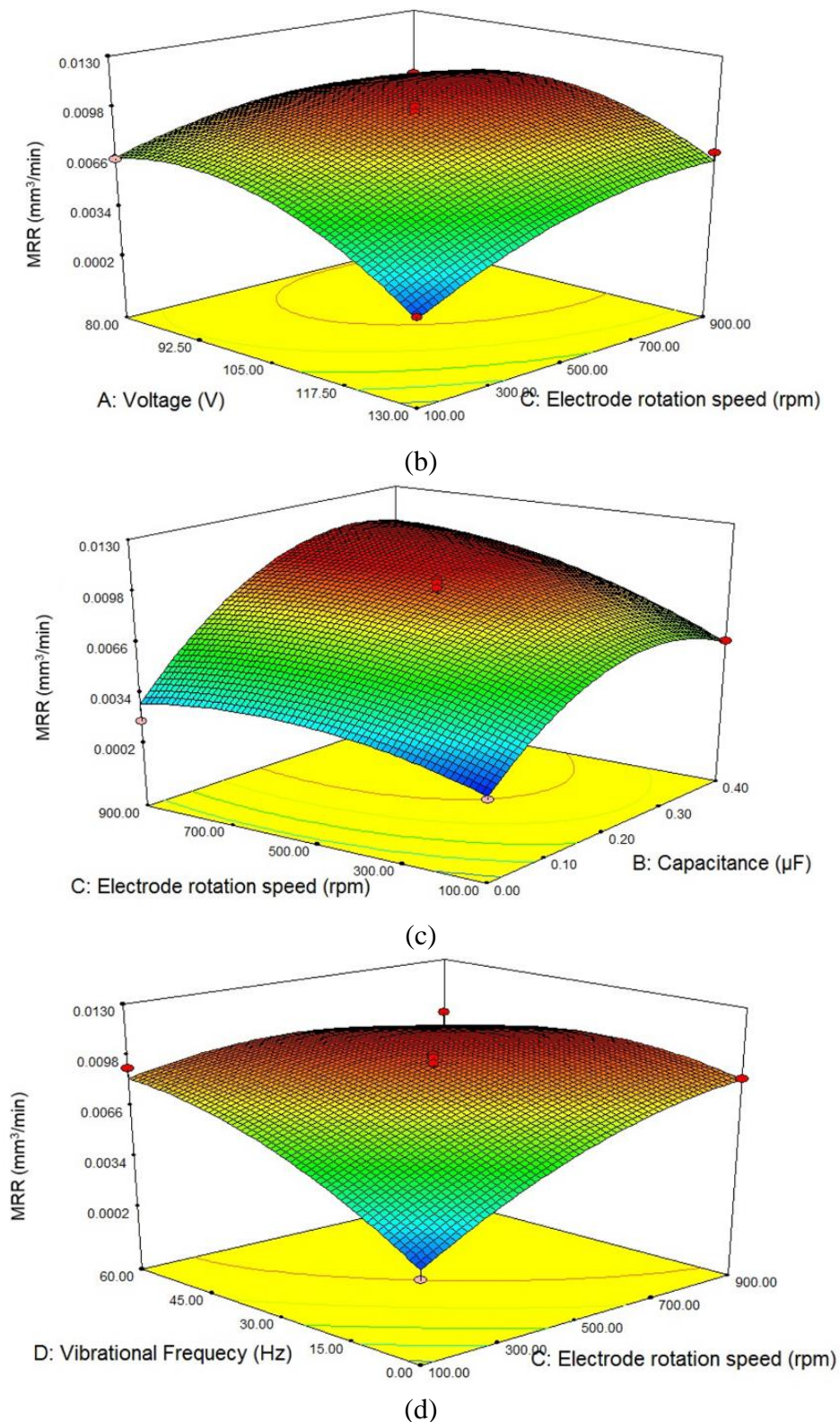*Figure 5.5 Perturbation plot for MRR$_{µEDD}$*

(a)

(b)

(c)

(d)
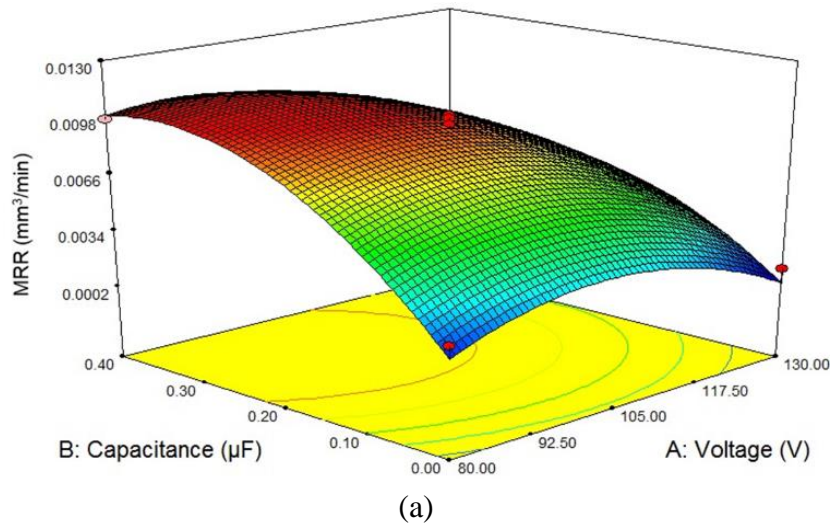
Figure 5.6 (a), (b), (c), and (d) shows the response graph of MRR$_{μEDD}$

It is perceived from the Table 5.4 that the interactions which significantly contributes

to the MRR model are those between the voltage and capacitance '$Vg×Cp$', voltage and

ERS '$Vg×R$', capacitance and ERS '$Cp×R$' and ERS and VF '$R×VF$' and the

interaction plots corresponding to these interaction terms are shown in Figure 5.6 (a), (b), (c), and (d) respectively.

The interaction effect of voltage and capacitance at all other control factors at middle values in shown in Figure 5.6 (a). It can also be witnessed from Figure 5.6 (a) is that the MRR increases with increase in capacitance. However, MRR initially increases with increase in gap voltage but after an optimal value decreases with further increase in gap voltage value. The voltage determines the breakdown value upon which the current streams through the gap to initiate the plasma channel. The interelectrode gap (IEG) for spark actuation predominantly governed by the gap voltage rather than governing the MRR. The similar observation regarding effects of capacitance and gap voltage on MRR also reported by [109]. Upon reach of optimal value, the gap voltage leads to secondary sparking among the trapped debris in spark gap and electrode and thus reduces the MRR. The similar observation of voltage also noted in interaction voltage and ERS (Figure 5.6 (b)). The discharge energy (DE) engendered in RC pulse circuit is multiplication of capacitance and voltage ($DE = \frac{1}{2} Cp \times V_g{}^2$). The DE stored by capacitor is released when voltage reaches breakdown voltage. The capacitance value determines the extent of the energy deposited and therefore, with increase in capacitance, the amount of DE, pulse current and pulse interval also increases boosting the MRR. Therefore, the MRR increases prominently at high values of capacitance (Figure 5.6).

The response surface in Figure 5.6 (b, c, and d) exemplifies that the increase in ERS stimulates the rise in MRR. The higher centrifugal force generated at high-ERS aids the dielectric to evacuate the debris trapped in between IEG. An agitation effects attributed by higher ERS drives the dielectric into discharge zone [108]. Also, the increased ERS

promotes the disturbance of dielectric due to increased tangential velocities [29]. Therefore, along with evacuating the debris and molten metal in discharge zone, the agitation effect results in more efficient sparks in machining zone and attributes in increase MRR.

The Figure 5.6 (d) shows the interaction effect between the ERS and VF. It is observed that very low MRR is achieved at lower values of ERS and VF. The adhesion i.e. coupling between the workpiece and electrode could lead to above results. The molten metal and debris causes adhesion leading to electrical short among electrode and workpiece and constrains the insulation recovery of the machine tool [59]. To overcome the short circuit, the machine has to retract the spindle opposite to feed direction to maintain the gap distance between electrode and workpiece. Thus, frequent short circuits attribute to higher machining time. With higher VF, the faster recovery from adhesion can be achieved. The higher speed of the expansion and contraction of vibration device at high VF avoids adhesion between electrode and workpiece and also, causes the ejection of debris and molten metal from machining zone.

5.5.2 Influence of control factors and their interactive effect on EWR

The Perturbation plot for EWR is shown in Figure 5.7. A steep slope for capacitance indicates that the EWR is very sensitive to capacitance as compared to other factors. The EWR increases with increase in voltage, capacitance, and ERS, however, decreases with increase in VF. The reasons behind these observations are discussed in next paragraph.
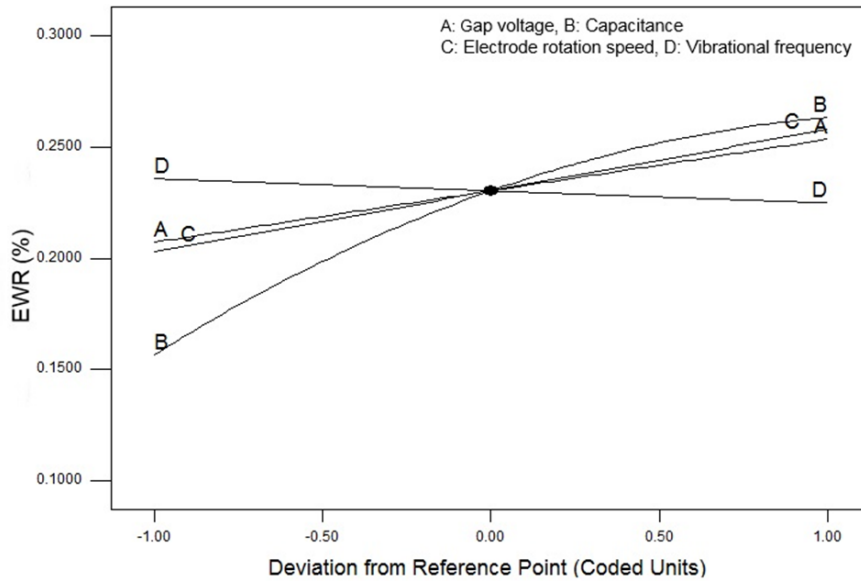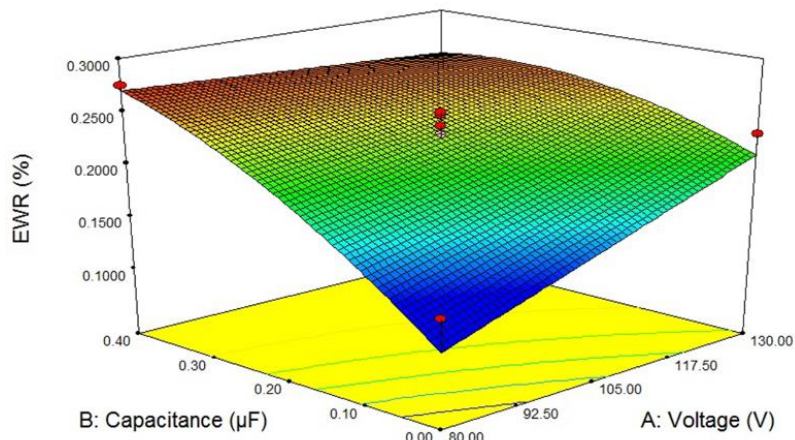
Figure 5.7 Perturbation plot for EWR

The ANOVA results (Table 5.5) shows that the interactions contributing significantly to the EWR model are those between voltage and capacitance '$Vg \times Cp$', voltage and ERS '$Vg \times R$', and voltage and VF '$Vg \times F$'. It is observed from Figure 5.8 (a) that the EWR has increased with increase in both voltage as well capacitance, but EWR is highly sensitive to capacitance. The capacitor controls the charging and discharging process along with the frequency of discharging in RC circuit and thus, it is a most significant factor in micro-EDM [131]. At high values of capacitance, deeper craters formed in workpiece enhancing MRR as more DE acts in the gap, and thereby also increasing the relative electrode wear. It is also noticed that from Figure 5.8 (a) and (b), EWR increases with increase in gap voltage. As already discussed, the more discharge energy will wear more electrode at higher voltage values.

The EWR decreases slightly with an increase in VF. The normal discharge pulses rose by 40% and short pulses reduced by 80% as compared to without vibration assisted µ-ED drilling reported by Jahan et al. [29] attributed due to effective flushing of debris and reduced adhesion between electrode and workpiece in the presence of vibration. The increased normal pulses and decreased short pulses results in stable machining and

95

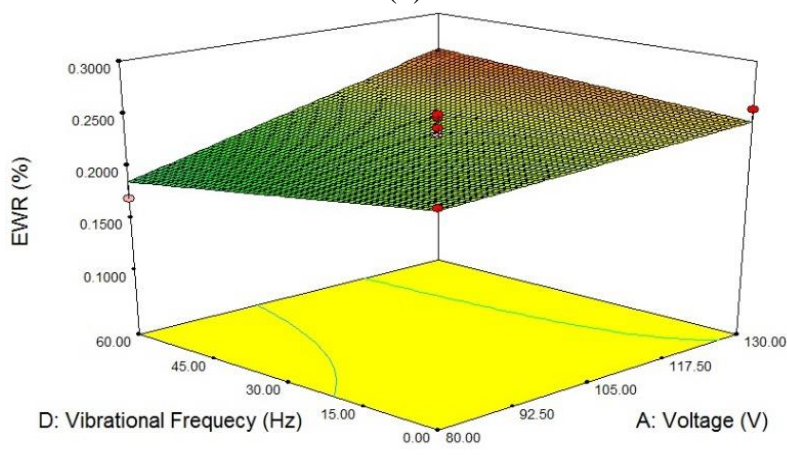reduced EWR. The EWR increases with increase in ERS (Figure 5.8 (b)) due to effective sparking condition attributed at higher ERS leading to more wear of electrode.

(a)
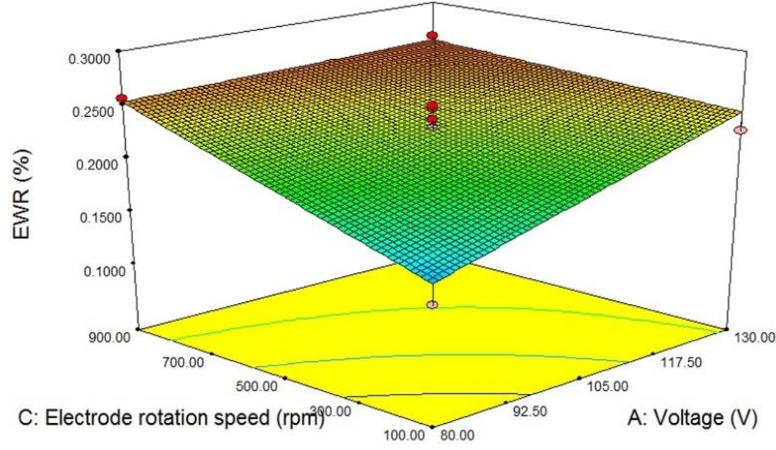
(b)

(c)

Figure 5.8 (a), (b), and (c) shows the response graph of EWR

5.5.3 Influence of control factors and their interactive effect on overcut

The Perturbation plot for overcut is shown in Figure 5.9. It indicates that the overcut is more sensitive to ERS as compared to other factors. The overcut decreases with increase in ERS. The overcut initially decreases up to center points of voltage, capacitance, and VF, but then increases will further increase of these factors.

The interaction effect between the voltage and capacitance '$Vg \times Cp$', voltage and ERS '$Vg \times R$', voltage and VF '$Vg \times F$', capacitance and ERS '$Cp \times R$', and ERS and VF '$R \times F$' are significant in overcut model and are shown in Figure 5.10 (a, b, c, d, and e) respectively. The overcut influence the capability of a workpiece to attain better dimensional accuracy along with finishing. By observing, capacitance and voltage effect on overcut from Figure 5.10 (a, b, and c), it can be inferred that lower amount of discharge energy is more appropriate to yield lower overcut. The similar observation also reported by [120, 132].
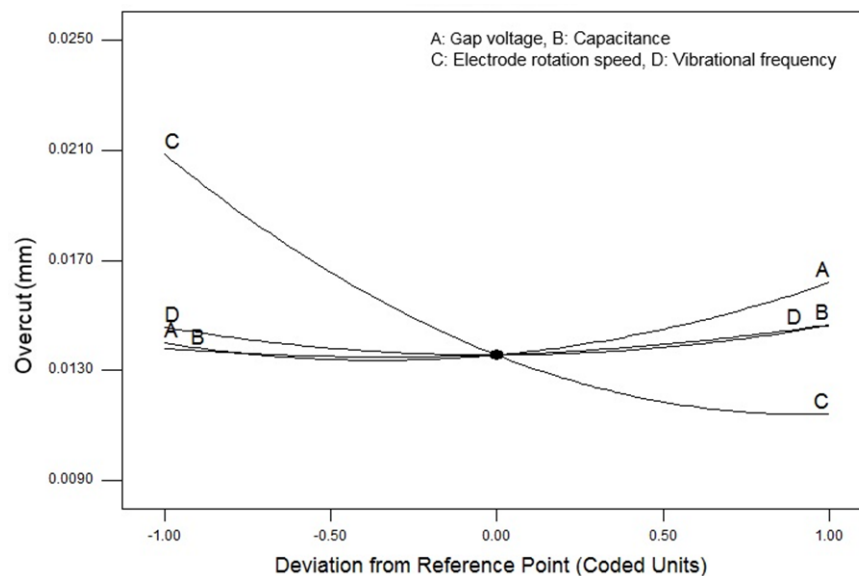
Figure 5.9 Perturbation plot for overcut

At low DE, lower workpiece volume will be ejected per discharge generating narrower crates and thus, resulting in lower overcut. Also, the discharge column built at higher

DE continued for longer as compared to one at poor DE results in bigger ionization effect and expanded micro-hole [120]. Recently, Dave et al. [133] reported that stationary electrode condition is better for lower overcut. However, they did not report reasons behind such observation. In this study, we found that the overcut decreases with increase in ERS and high-ERS values are appropriate for lower overcut while µ-ED drilling of Inconel 718. The overcut increases while drilling deep micro-holes as it becomes problematic to expel all the debris using side flushing and due to trapped debris, the increased width of discharge column along with secondary sparking results in widened overcut. As discussed earlier, the higher ERS expel debris due to centrifugal force, provide fresh dielectric in IEG, and causes turbulence of dielectric and therefore, reduces the overcut. Similarly, high VF is recommended for lower overcut as high VF also attributes in effective debris evacuation and reduced workpiece-electrode adhesion (Figure 5.10 (e)).
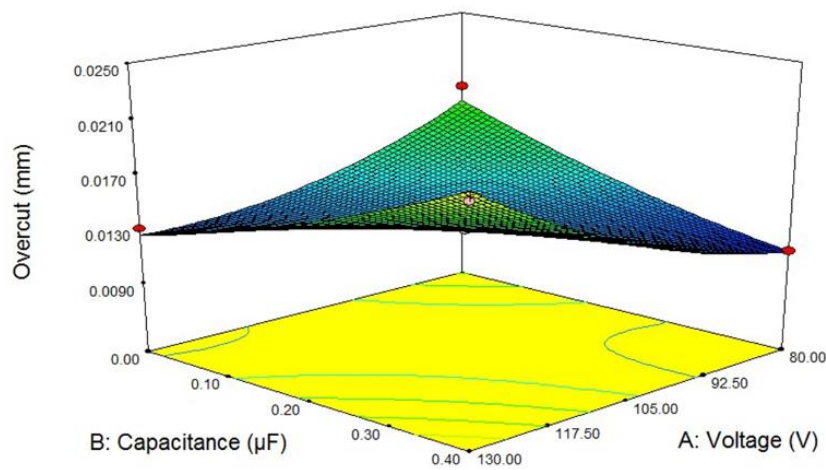
(a)
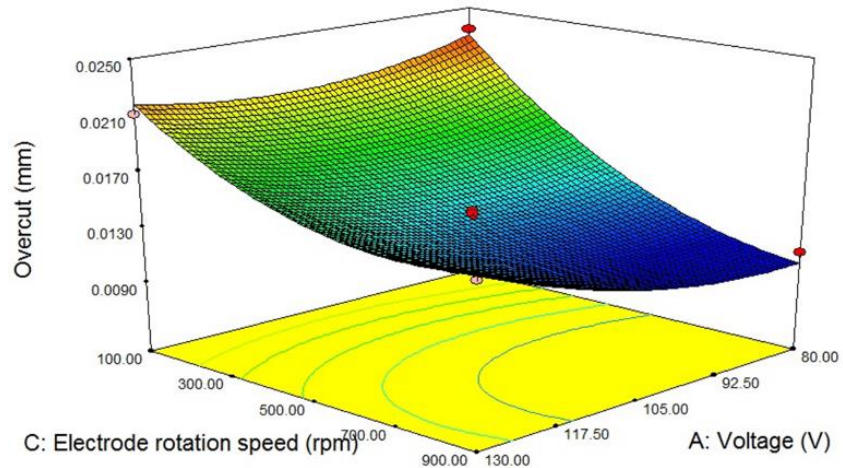
(b)
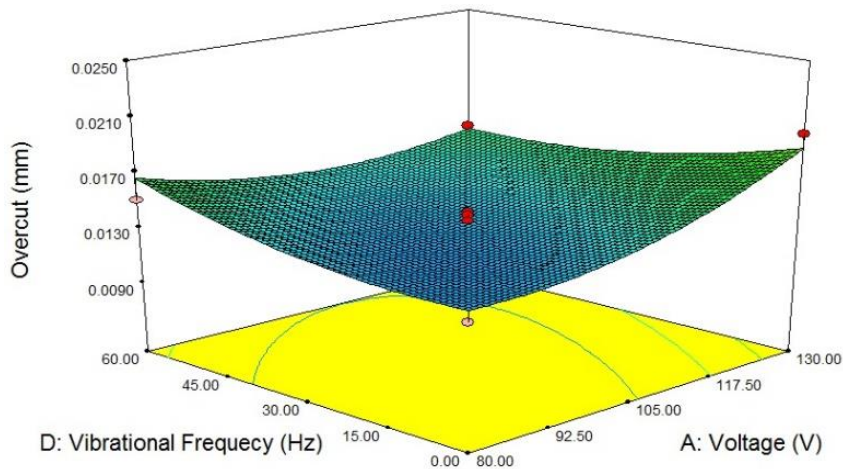
(c)
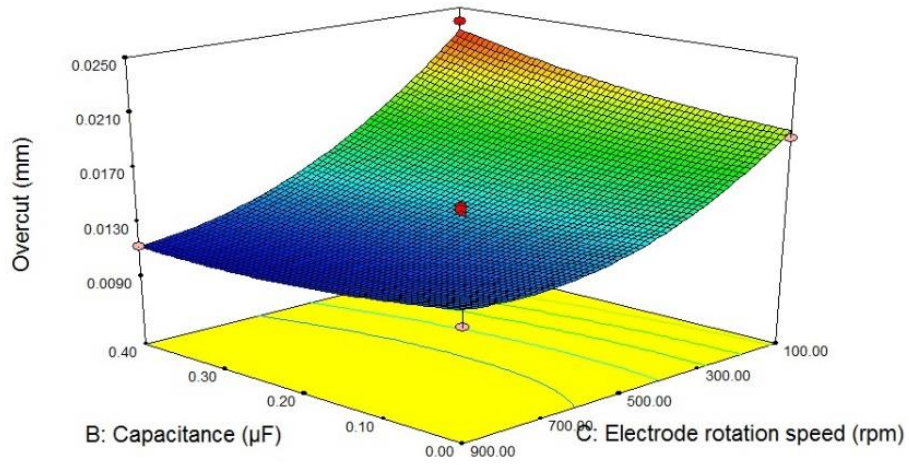
(d)
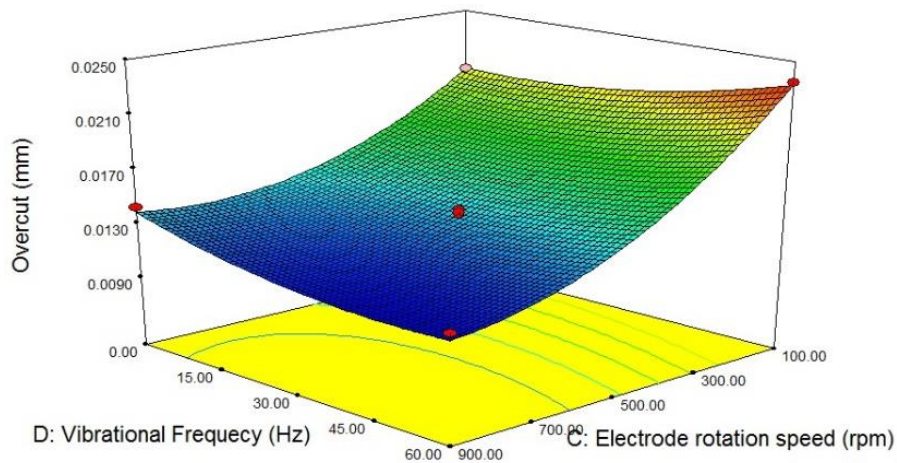
(e)

Figure 5.10 (a), (b), (c), (d), and (e) shows the response graph of overcut

5.5.4 Influence of control factors and their interactive effect on taper angle

Figure 5.11 shows the Perturbation plot for taper angle. It indicates that the overcut is more sensitive to ERS as compared to other factors. The ANOVA results show that only the interaction effect between voltage and VF '$Vg \times F$' is significant in taper angle model that is shown in Figure 5.12. The corner wear of the electrode results in taperness of micro-holes. From Figure 5.11 and Figure 5.12, it can be studied that taper angle increases with DE. The wide and deep craters formed in workpiece due to higher DE accrues leads to short circuits and arcing into secondary sparking [134].

From Figure 5.12, it is perceived that taper angle increases with increase in VF. The similar observation also reported by [29]. The reason behind this could be with higher VF values the debris inside the micro-hole travels from the bottom of the hole towards the top of the hole along edges of the electrode and causes the secondary sparking among debris and workpiece again, thereby, increasing diameter at the top of the hole [29, 59].
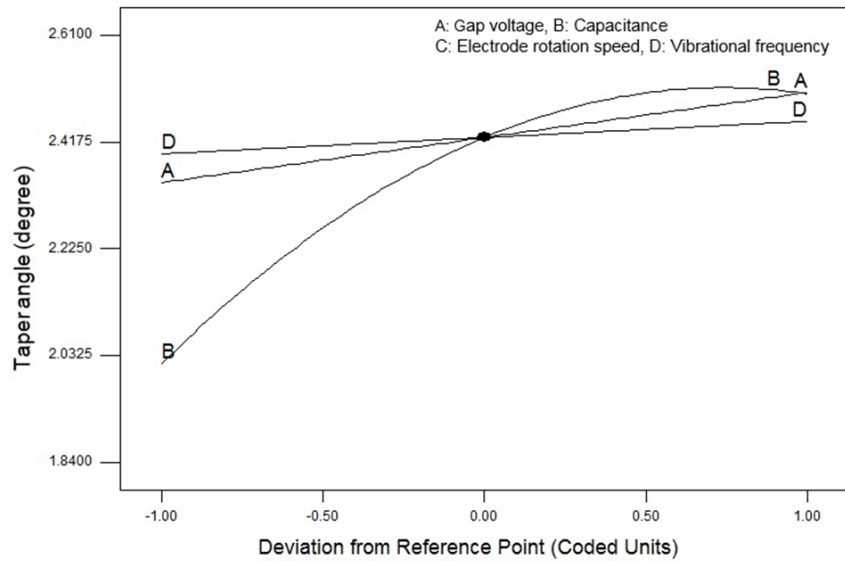
Figure 5.11 Perturbation plot for taper angle
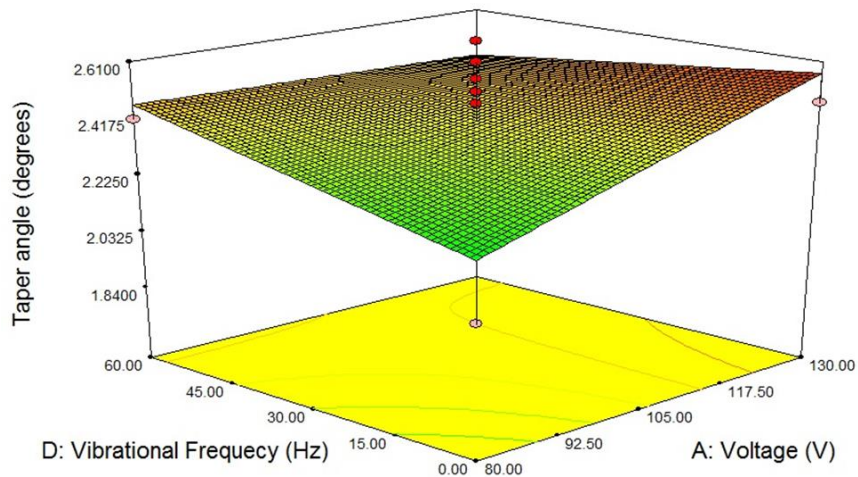
Figure 5.12 The response graph of taper angle

5.6 Desirability based multi-response optimization

Desirability function technique is one of the common techniques practiced in the optimization of single and multiple performance measures problem [124, 125]. In this technique, the desirability that ranges between zero and one is calculated by transforming the projected responses. The optimal conditions are decided based on the settings of control factors which provides the maximum desirability, and the respective values of control factors are the optimal one. The design expert optimization module

was used to find the combination of control factors, i.e., voltage, capacitance, ERS, and VF, which fulfills the constraint imposed on each of the control factors and performance measures. This technique evaluates the optimal values of control factors by maximizing the MRR while minimizing the EWR, overcut and taper angle at all together as well as separately. The constraints for control factors and performance measures are given in Table 5.10. Table 5.11 shows the optimization results with corresponding settings of control factors. In single response optimization, the other three responses were ignored. However, each performance measure was assigned an equal weight of 3 while performing multi-response optimization.

Table 5.10 The constraints for control factors and performance measures

Factor	Goal	Lower constraint	Upper constraint	Importance
Gap Voltage	is in range	80	130	3
Capacitance	is in range	0.01	0.4	3
Electrode rotation speed	is in range	100	900	3
Vibrational Frequency	is in range	0	60	3
$MRR_{µEDD}$	maximize	0.00095434	0.0100146	3
EWR	minimize	0.13351	0.27521	3
Overcut	minimize	0.011055	0.023873	3
Taper angle	minimize	1.8484	2.60706	3

Table 5.11 Optimal settings of control factors for single and multi-response optimization
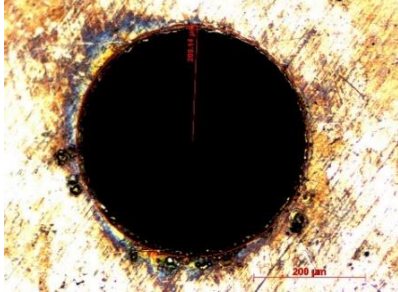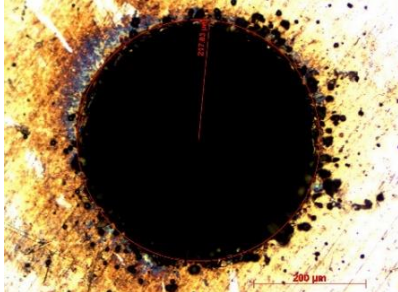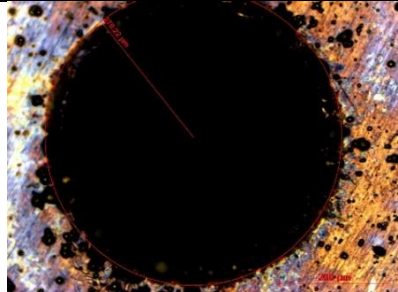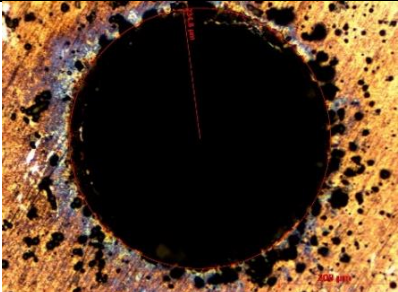
Type of optimization	Objective	Optimum control factor values				Performance measure (Predicted)	Performance measure (Experimental)	Desirability
		Gap Voltage (V)	Capacitance (µF)	ERS (rpm)	VF (Hz)			
Single response	Maximize $MRR_{µEDD}$	97	0.33	714	13	0.0106334 mm³/min	0.0112 mm³/min	1.0
Single response	Minimize EWR	90	0.01	301	58	0.100864 %	0.1050 %	1.0
Single response	Minimize overcut	96	0.19	883	48	0.0106907 mm	0.0101 mm	1.0

Single response	Minimize taper angle	80	0.00	109	6	1.84747 degree	1.9717 degree	1.0
Multiple response	Maximize MRR$_{\mu EDD}$, while minimize EWR, overcut and taper angle	95	0.05	577	36	0.00581264 mm^3/min, 0.16702%, 0.0138689 mm, 2.14294 degree,	0.0060 mm^3/min, 0.172%, 0.0132 mm, 2.036 degree	0.665

5.7 Effects of machining parameters on accuracy of micro-holes

The microscopic images of micro-holes fabricated at different VF, ERS and DE settings and are presented in Table 5.12. The diameter of fabricated holes along with its deviation from expected value of 300 µm is also presented. These images were taken from top side of the micro-holes. By observing images of the micro-holes at different DE and different frequency, it is clear that both DE and VF have considerable effects on accuracy of micro-holes fabricated. With increase in DE, the diameter of micro-holes found to be increasing i.e. increase in overcut. At low DE, lower workpiece volume will be removed per discharge, thereby generating narrower crates. This result in lower overcut as compared to one at high DE. Also, the discharge column built at high DE continues for longer as compared to one at small DE resulting in bigger ionization effect and expanded micro-hole.

Table 5.12 Microscopic images at different energy and vibration conditions

Energy	Vibrational Frequency & electrode rotational speed.		
	Without vibration & 100 rpm	40 Hz & 500 rpm	60 Hz & 900 rpm
50 µJ	Diameter: 447 µm (Deviation: 147)	Diameter: 437.2 µm (Deviation: 137)	Diameter: 418.2 µm (Deviation: 118)
500 µJ	Diameter: 509 µm (Deviation: 200)	Diameter: 460 µm (Deviation: 160)	Diameter:435 µm (Deviation: 135)
1280 µJ	Diameter:540 µm (Deviation: 240)	Diameter:468 µm (Deviation: 168)	Diameter:488 µm (Deviation: 188)

At the rim of the hole, more burrs due to resolidification of debris and craters were observed at high DE. Therefore, it is recommended that low DE values are suitable for achieving micro-holes with better accuracy and surface quality.

It is also observed that with an increase in ERS and vibrational frequency the overcut of fabricated micro-hole decreases i.e. diameter of fabricated holes decreases. In EDM drilling, the debris, and molten metal get trapped in IEG at side flushing conditions and result in expanded discharge column width. Therefore, causes increase in the diameter of micro-holes. As discussed earlier, the higher ERS and VF results in efficient expelling of debris and subsequently generating accurate micro-holes due to reasons including high centrifugal force, the supply of fresh dielectric in IEG, and turbulence of dielectric, etc.

5.8   Surface quality of fabricated micro-holes

The surface quality at the entrance of the micro-holes fabricated by the µ-ED drilling on Inconel 718 with different settings of control factors is shown in Figure 5.13 (a and b). Figure 5.13 (a) shows effects of voltage, capacitance, and ERS at different combinations without low-frequency vibrations. It was clearly witnessed that at higher DE values the surface quality of micro-holes was poor as compared those at low DE. As already discussed, at higher DE the discharge column remains for longer resulting expanded holes, thus, it can be observed that with an increase in discharge energy the diameter at the entrance of micro-holes increased significantly. At the rim of the hole, more burrs due to resolidification of debris and craters were observed at high DE without vibration assistance.

The surface quality of micro-holes with vibration assisted µ-ED drilling was significant improved (Figure 5.13 (b)) as compared with those without vibration assistance. At low

DE and with middle values of vibrational frequency, the best surface quality without any burrs at the rim of micro-holes perceived. The low-frequency vibration assists in expelling debris and molten metal during the µ-ED drilling process and also reduces the adhesion of workpiece and electrode.

V_g:80 C_p:0.2 R:500 F:0 V_g:105 C_p:0.2 R:100 F:0 V_g:105 C_p:0.4 R:500 F:0

(a)

V_g:105 C_p:0.2 R:500 F:30 V_g:80 C_p:0.2 R:900 F:30 V_g:130 C_p:0.2 R:500 F:60

(b)
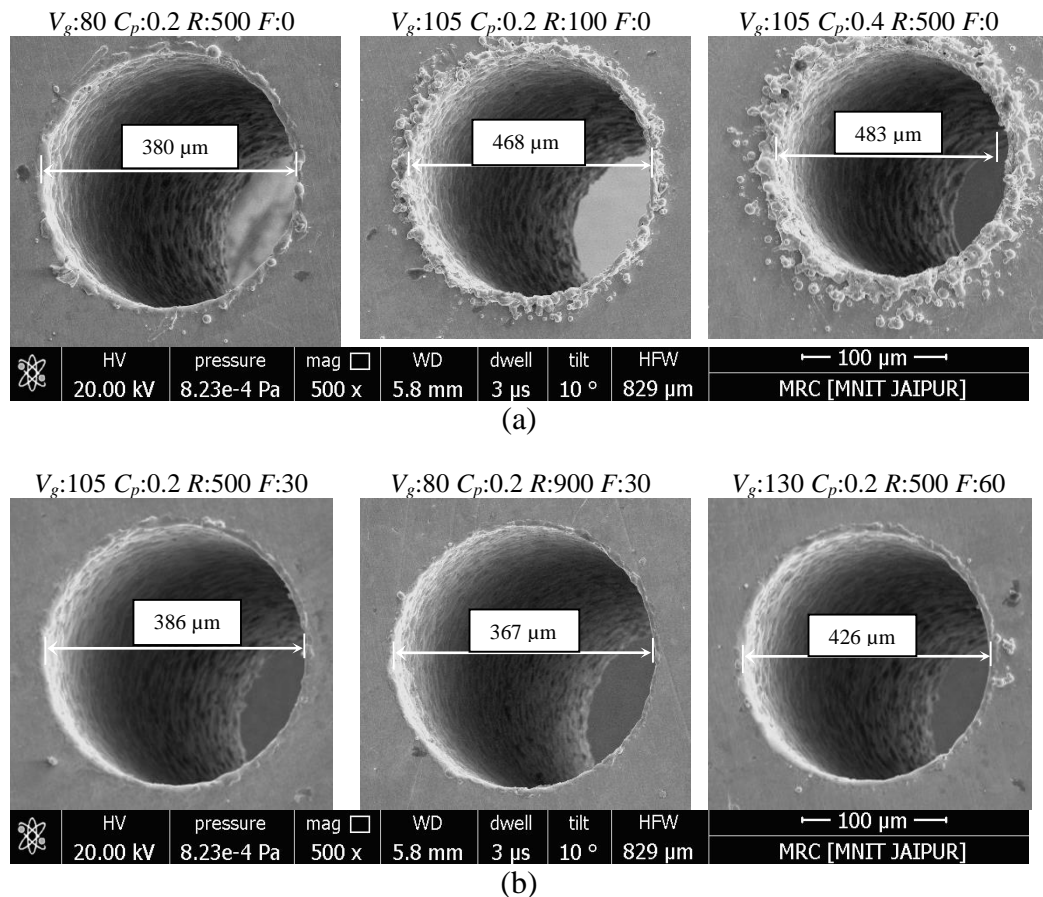
Figure 5.13 Surface quality of fabricated micro-holes (a) without low-frequency assistance, (b) with low-frequency assistance

The cross-sectional view of micro-holes fabricated with and without vibration assistance in µ-ED drilling is shown in Figure 5.14. It has been observed that the surface obtained without vibration has resolidified debris and craters attached to the rims of the micro-holes. Moreover, the surface is heat-affected and contains black spots or pin holes in different positions (Fig. 5.14 (a)). On the other hand, the surface obtained using vibration-assisted µ-ED drilling at same electrical settings is smoother and almost free

of burrlike recast layer. There are less black spots on the surface obtained using the vibration-assisted µ-ED drilling (Figure 5.14 (b)).

V_g:105 C_p:0.2 R:500 F:0

(a)
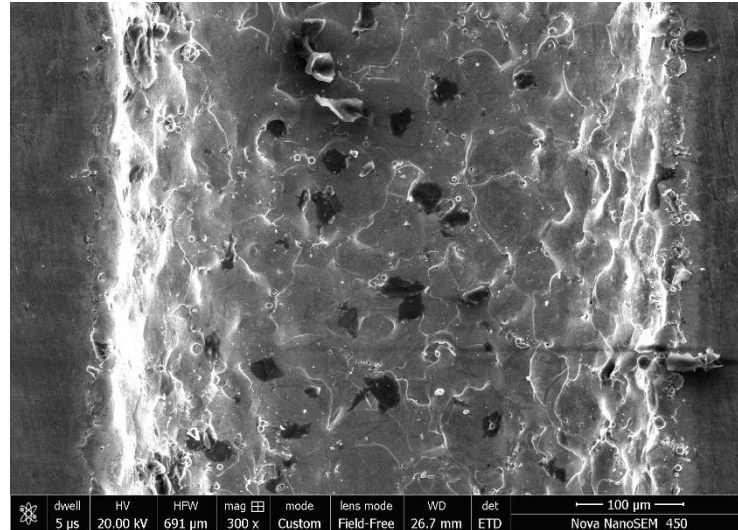
V_g:105 C_p:0.2 R:500 F:30
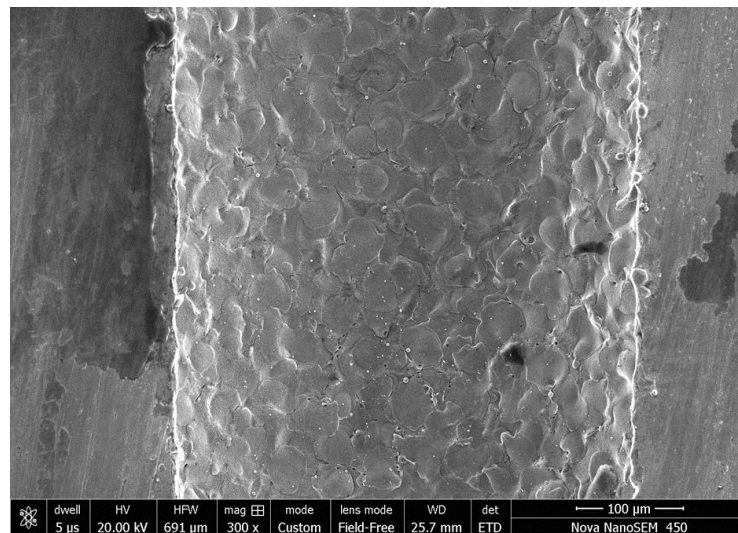
(b)

Figure 5.14 Quality of the inner surface of the microholes (a) without vibration assistance (b) with vibration assistance

When vibration is applied at same energy settings, the inner surface of micro-holes is observed to be smooth as comparatively smaller craters are formed at lower discharge energy levels. Moreover, the small working gap is subjected to periodical changes due to workpiece vibration, which helps in flushing out of debris effectively and generating

the smooth and defect-free surface. It has been observed that the craters are of comparatively broader sizes on the surface obtained without vibration due to the secondary discharging. The broader crater sizes are responsible for hole-expansion when machining without vibration. Moreover, there are resolidified craters attached on the surface, which makes the surface faulty. On the other hand, the surface obtained using vibration-assisted µ-ED drilling is smoother and composed of comparatively smaller size craters at the same discharge energy setting.

Finally, arrays of high-aspect-ratio micro-holes were fabricated on Inconel 718. Figure 5.15 shows an array of high-aspect-ratio micro-holes fabricated on 8 mm thick workpiece at setting of gap voltage 110V, capacitance 0.2 µF, and VF 30Hz. The high-aspect-ratio value of approximately 21 for fabricated micro-holes was achieved.
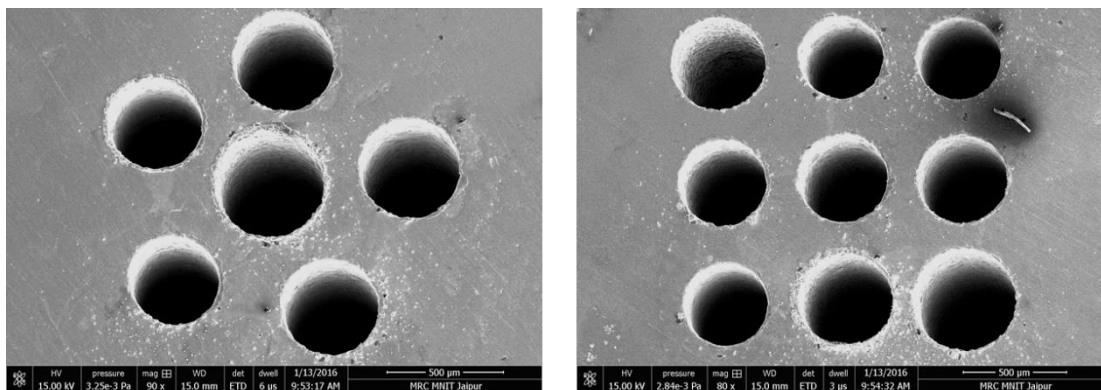
Figure 5.15 Array of high-aspect ratio micro-holes fabricated in Inconel 718

5.9   Comparison with previous studies

A comparative study of a low-frequency vibration assisted µ-ED drilling is compared with without vibration assisted µ-ED drilling to broaden the study and validate the results. Mondol et al. recently performed the µ-ED drilling on Ti–6Al–4V alloy using same machine tool DT 100. The similar machining condition used by Mondol et al. [135] are considered for comparison purpose and results obtained are shown in Table

5.13. The RC circuit power supply, electrode material, dielectric, voltage and capacitance values are nearly similar.

Table 5.13 Comparison of low-frequency vibration assisted µ-ED drilling with without vibration assistance

Sr. no.	Description		Mondol et al. [135]	Without vibration	With vibration assistance (60 Hz)
1	Experimental conditions	Workpiece material	Ti–6Al–4V	Inconel 718	
		Electrode material	Tungsten (⌀0.3mm)	Tungsten (⌀0.3mm)	
		Dielectric	Not mentioned	EDM oil (Total®)	
		Electrode rpm	Not mentioned	900 rpm	
2	Machining condition 1	Vg: 90 V, Cp: 0.1 µF	MRR: 0.0055927 mm^3/min	MRR: 0.005295 mm^3/min	MRR: 0.006357 mm^3/min
3	Machining condition 2	Vg: 110 V, Cp: 0.1 µF	MRR: 0.0055259 mm^3/min	MRR: 0.005814 mm^3/min	MRR: 0.006884 mm^3/min
4	Machining condition 3	Vg: 90 V, Cp: 0.01 µF	MRR: 0.0011308 mm^3/min	MRR: 0.001059 mm^3/min	MRR: 0.002417 mm^3/min

Initially, the machining time for µ-ED drilling at stationary workpiece condition is compared with the similar condition reported in Mondol et al., and nearly same MRR is observed in both cases is nearly same. Then, experiments were performed with low-frequency vibration assistance at similar setting and it was noted that vibration assistance noticeably enhanced the process performance. At medium discharge energy settings (condition 1 and condition 2) the percentage increase in MRR was observed around ~15 to 20%. However, vibration assistance substantially increased MRR in µ-ED drilling by ~48% at low DE (condition 3). Therefore, it can be claimed that the low-frequency vibration assisted µ-ED drilling is appropriated for fabrication of micro-holes at high machining speed.

5.10 Summary

In this chapter, the µ-ED drilling of Inconel 718 was performed with low-frequency workpiece vibration assistance to examine effects of vibrational frequency along with

other control factors viz. gap voltage, capacitance, and electrode rotation speed on MRR, EWR, overcut, and taper angle. The results observed are summarized as following:

- The quadratic models given below for MRR, EWR, overcut, and taper angle were established which represents the experimental results reliably with prediction errors less than ±7 %.

$$
\begin{aligned}
MRR_{\mu EDD} = {}& -0.041521 + (7.583 \times 10^{-4})V_g + 0.067379\,Cp \\
& + (5.93879 \times 10^{-6})R + (2.21701 \times 10^{-4})F \\
& - (2.58820 \times 10^{-4})V_g \times Cp + (8.271 \times 10^{-8})V_g \times R \\
& + (1.17176 \times 10^{-5})Cp \times R - (1.51783 \times 10^{-7})R \times F \\
& - (3.90255 \times 10^{-6})V_g{}^2 - 0.0774\,Cp^2 \\
& - (8.19730 \times 10^{-9})R^2 - (1.56078 \times 10^{-6})F^2
\end{aligned}
$$

$$
\begin{aligned}
EWR = {}& -0.13231 + (2.4741 \times 10^{-3})V_g + 1.10794\,Cp \\
& + (2.68658 \times 10^{-4})R - (2.33662 \times 10^{-3})F \\
& - (6.06252 \times 10^{-3})V_g \times Cp - (1.902 \times 10^{-6})V_g \times R \\
& + (2.05133 \times 10^{-5})V_g \times F - 0.51126\,Cp^2
\end{aligned}
$$

$$
\begin{aligned}
Overcut = {}& 0.06117 - (6.36691 \times 10^{-4})V_g - 0.076315\,Cp \\
& - (3.77996 \times 10^{-5})R + (2.20965 \times 10^{-4})F \\
& + (7.6049 \times 10^{-4})V_g \times Cp + (1.5885 \times 10^{-7})V_g \times R \\
& - (2.184 \times 10^{-6})V_g \times F - (1.6072 \times 10^{-5})Cp \times R \\
& - (1.20354 \times 10^{-7})R \times VF + (2.44957 \times 10^{-6})V_g{}^2 \\
& + 0.016636\,Cp^2 + (1.61632 \times 10^{-8})R^2 \\
& + (1.15748 \times 10^{-6})F^2
\end{aligned}
$$

$$
\begin{aligned}
Taper\ angle = {}& 1.25279 + (6.99897 \times 10^{-3})V_g + 2.8677\,Cp \\
& + (0.014094)F - (1.2449 \times 10^{-4})V_g \times F - 4.11975\,Cp^2
\end{aligned}
$$

- The capacitance was found to be a most significant factor for MRR, EWR, and taper angle models contributing 33.53%, 38.34%, and 62.28%, respectively. With an increase in capacitance value, the discharge energy acting on the workpiece increase significantly, therefore, appropriate choice of capacitance values is very crucial in the micro-EDM process.

- The ERS was found to be a significant factor in deciding the amount of overcut of micro-hole generated. The higher speed of electrode rotation is recommended for low overcut.

- The workpiece vibrations result in variation in gap distance and gap fluid pressure and improve the machining efficiency while deep hole drilling. The vibrational frequency observed to beneficial for improvement in MRR, EWR, and accuracy of micro-holes. The accurate micro-holes with better surface quality can be produced at a range of 30-40 Hz vibrational frequency, low discharge energy values and high-ERS.

- The workpiece vibrations also reduce the HAZ while µ-ED drilling of Inconel 718. The microhardness values were found to be increased with workpiece vibration during µ-ED drilling as compared to that of without workpiece vibrations.

The application of low-frequency vibration play a vital role in improving the performance of µ-ED drilling process due to enhanced flushing conditions in the spark gap, effective debris evacuation, and reduced arcing and short-circuits. The better machining stability along with enhanced machining efficiency leads to the improved µ-ED drilling performance with application of low-frequency workpiece vibration. The low-frequency vibration assisted µ-ED drilling was found to be an efficient method for fabrication of high-aspect-ratio micro-holes with improved surface quality and burr free surface.

6 Experimental investigation on low-frequency vibration assisted µ-ED milling

The µ-ED milling is a competent process for fabricating high-aspect-ratio micro-features with the good surfaces finish. However, the low material removal rate (MRR) limits its applications in micro-feature fabrication as compared to other micro-fabrication processes. Therefore, this chapter attempts to address the issues of long machining time through the application of low-frequency workpiece vibration in the µ-ED milling while fabricating micro-channels in Inconel 718. Initially, the effects of control variable are observed on response variables viz. MRR and electrode wear. Then, the effects of vibrational frequency surface quality and accuracy of the fabricated micro-channels are examined. Finally, the proposed approach is compared with previous studies and used to fabricate complex shapes of micro-channels.

6.1 Experimental plan and control factors

The Box–Behnken design was utilized to plan the experiments. The gap voltage (V_g), capacitance (Cp), electrode rotation speed (R), and vibrational frequency (F) were designated as control factors while MRR and frontal electrode wear (FEW) chosen as performance measures. The control factors and their range, shown in Table 6.1, were decided based on the literature, preliminary experiments, manufacturer's handbook, and machines constraints. Total 29 experimental runs were performed as per Box-Behnken design with four control factors each varying at three levels. Out of 29 runs, 24 runs corresponds to the side points, and five runs replicate the center position five

times. The experimental plan showing a set of the control factors and resultant performance measures acquired after conducting tests are given in Table 6.2.

Table 6.1 Independent control factors, and their levels

Control factors			Level		
	Symbol	**Notation**	**-1**	**0**	**1**
Gap voltage (A)	V	*Vg*	80	105	130
Capacitance (B)	µF	*Cp*	0.01	0.2	0.4
Electrode rotation speed (C)	rpm	*R*	100	500	900
Vibrational frequency (D)	Hz	*F*	0	30	60

Table 6.2 Experimental design matrix and observed performance measures in low-frequency assisted µ-ED milling of Inconel 718

Run order	Control factors				Performance measures	
	Gap Voltage (V)	Capacitance (µF)	Electrode rotation speed (rpm)	Vibrational frequency (Hz)	MRR$_{µEDm}$ (gm/min)	FEW (mm)
1	120	0.10	500	60	0.01831	0.5220
2	100	0.10	900	60	0.02919	0.6371
3	120	0.10	500	0	0.02599	0.6301
4	100	0.10	500	30	0.01794	0.6158
5	100	0.10	500	30	0.02115	0.6824
6	100	0.01	500	0	0.00214	0.5071
7	80	0.10	500	0	0.01018	0.5659
8	120	0.01	500	30	0.00487	0.5215
9	80	0.10	500	60	0.04112	0.6462
10	100	0.10	500	30	0.01983	0.6045
11	100	0.01	500	60	0.01045	0.4926
12	100	0.40	900	30	0.02559	0.7115
13	100	0.10	100	60	0.00726	0.5174
14	80	0.01	500	30	0.01549	0.5104
15	120	0.40	500	30	0.03132	0.7253

16	80	0.10	900	30	0.02719	0.7243
17	100	0.10	500	30	0.02183	0.6118
18	100	0.40	500	60	0.02877	0.6810
19	80	0.10	100	30	0.00282	0.5231
20	100	0.10	100	0	0.00198	0.5075
21	100	0.40	100	30	0.02266	0.7194
22	80	0.40	500	30	0.02519	0.7108
23	100	0.01	900	30	0.02720	0.7315
24	100	0.40	500	0	0.02096	0.7223
25	120	0.10	100	30	0.00381	0.5228
26	120	0.10	900	30	0.02554	0.6998
27	100	0.10	900	0	0.02213	0.7201
28	100	0.10	500	30	0.02254	0.6158
29	100	0.01	100	30	0.00216	0.5059

6.2 Reproducibility

The reproducibility is checked by the performance of five center point runs. The results of experiments at center points (1,10,15,26,27) are presented separately in Table 6.3. The percentage error shown in Table 6.3 is the variability of the performance measures on its average value and is calculated by the equation (4.2).

Table 6.3 Reproducibility and percentage (%) error for performance measures

Run order	Performance measures			
	$MRR_{µEDm}$ (gm/min)		FEW (mm)	
	Expt. value	% error	Expt. value	% error
1	0.01894	9.20	0.61584	1.64
10	0.021153	-3.39	0.6824	-8.99
15	0.019833	3.06	0.60453	3.44
26	0.021833	-6.71	0.61184	2.28
27	0.022541	-10.17	0.61584	1.64

It was observed that the results reproduced within the acceptable range. Also, the values of experimental standard deviation and standard uncertainty were assessed for performance measures to elucidate their variations at same experimental conditions. The results of standard uncertainty for $MRR_{\mu EDm}$, and FEW were calculated to be 0.073, and 1.42%, respectively, which are well inside the tolerable limit.

6.3 Empirical models for performance measures

Defining the analytical model for the μ-ED milling made on process physics is very problematical due to complex and stochastic nature of the process. Therefore, to establish a mathematical relationship between the control factors and performance measures, a multi-variable regression model was established for each performance measure. Analysis of variance (ANOVA) was performed to examine statistically the results of the selected model. The significant control factors were detected, and interaction effects of these control factors on performance measures were investigated using response surface graphs.

6.3.1 ANOVA for MRR, and FEW

The experimental results for performance measures shown in Table 6.2 were studied using Design-Expert software. The sequential model sum of squares, lack-of-fit test, and model summary statistics tests were performed to evaluate the adequacy of the models which suggested the adequacy of quadratic models. Therefore, quadratic models were analyzed using ANOVA to determine the significant model terms. The backward elimination procedure was executed to eliminate the unimportant terms from models thereby improving the models. The results of ANOVA for $MRR_{\mu EDm}$, and FEW after backward elimination are summarized in Table 6.4 and Table 6.5, respectively.

Table 6.4 The ANOVA table for MRR model

Source	Sum of Square	df	Mean Square	F Value	p-value Prob>F		Percentage contribution
Model	2.753E-003	9	3.058E-004	19.88	< 0.0001	significant	
V_g	4.783E-007	1	4.783E-007	0.031	0.8619		0.02
Cp	7.080E-004	1	7.080E-004	46.02	< 0.0001		25.72
R	5.209E-004	1	5.209E-004	33.85	< 0.0001		18.92
F	2.227E-004	1	2.227E-004	14.47	0.0012		8.09
$V_g \times Cp$	5.707E-005	1	5.707E-005	3.71	0.0692		2.07
$V_g \times F$	3.730E-004	1	3.730E-004	24.24	< 0.0001		13.55
$Cp \times R$	1.630E-004	1	1.630E-004	10.60	0.0042		5.92
$Cp \wedge 2$	1.671E-004	1	1.671E-004	10.86	0.0038		6.07
$R \wedge 2$	8.894E-005	1	8.894E-005	5.78	0.0266		3.23
Residual	2.924E-004	19	1.539E-005				
Lack of Fit	2.791E-004	15	1.861E-005	5.62	0.0537	not significant	
Pure Error	1.324E-005	4	3.310E-006				
Cor Total	3.045E-003	28					
Std. Dev.	3.923E-003			R-Squared	0.9040		
Mean	0.018			Adj R-Squared	0.8585		
C.V. %	21.24			Pred R-Squared	0.7363		
PRESS	8.029E-004			Adeq. Precision	18.004		

V_g -Gap Voltage, Cp-Capacitance, R-Electrode rotation speed, F-Vibrational Frequency

The normal probability plot of the residuals (Figure 6.1) for MRR$_{\mu EDm}$ and FEW directs that residuals falls on a straight line representing that errors are normally distributed [125]. Also, from Figure 6.2, it can be seen that the actual values are in good agreement with predicted values from the model. Therefore, it has been inferred that ANOVA results for MRR$_{\mu EDm}$, EWR, overcut, and taper angle given in Table 6.4 and Table 6.5, respectively are trustworthy as the plots fulfil the error normality and prediction capability criteria.

Table 6.5 The ANOVA table for FEW model

Source	Sum of Square	df	Mean Square	F Value	p-value Prob>F		Percentage contribution
Model	0.19	8	0.024	23.24	< 0.0001	significant	
V_g	2.923E-004	1	2.923E-004	0.28	0.6023		0.15
Cp	0.084	1	0.084	80.13	< 0.0001		43.10
R	0.028	1	0.028	27.33	< 0.0001		14.70
F	2.045E-003	1	2.045E-003	1.96	0.1767		1.06
$V_g F$	8.864E-003	1	8.864E-003	8.50	0.0085		4.57
$Cp R$	0.017	1	0.017	16.07	0.0007		8.64
Cp ^2	5.290E-003	1	5.290E-003	5.07	0.0357		2.73
F ^2	7.858E-003	1	7.858E-003	7.54	0.0125		4.05
Residual	0.021	20	1.043E-003				
Lack of Fit	0.017	16	1.050E-003	1.04	0.5459	not significant	
Pure Error	4.049E-003	4	1.012E-003				
Cor Total	0.21	28					
Std. Dev.	0.032			R-Squared		0.9029	
Mean	0.62			Adj R-Squared		0.8640	
C.V. %	5.24			Pred R-Squared		0.8007	
PRESS	0.043			Adeq Precision		15.962	

V_g -Gap Voltage, Cp-Capacitance, R-Electrode rotation speed, F-Vibrational Frequency

The model F values of 19.88$_{MRR}$, and 23.24$_{EWR}$ for MRR$_{μEDm}$, and EWR, respectively, with its Prob>F value less than 0.0001 in ANOVA tables point out that the models are significant confirming that the terms in the models have a significant effect on the performance measures. There is only a 0.01 % chance that such a large model F values could occur due to noise. The values of Prob>F less than 0.05 indicates the significance of model terms [125, 130].
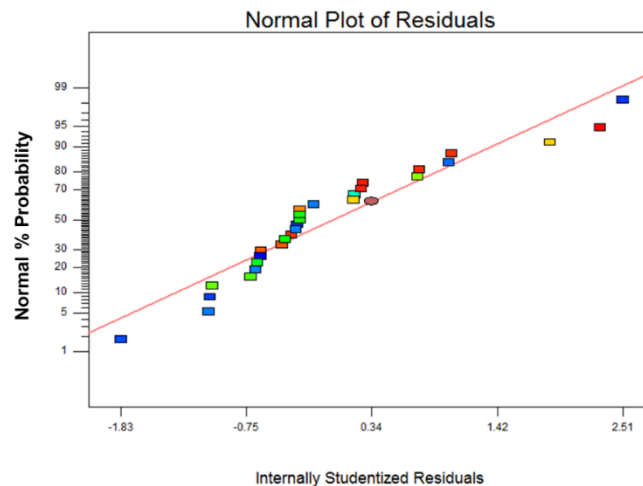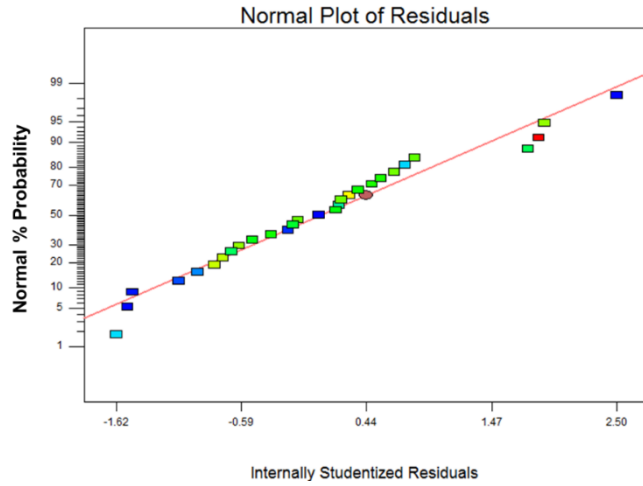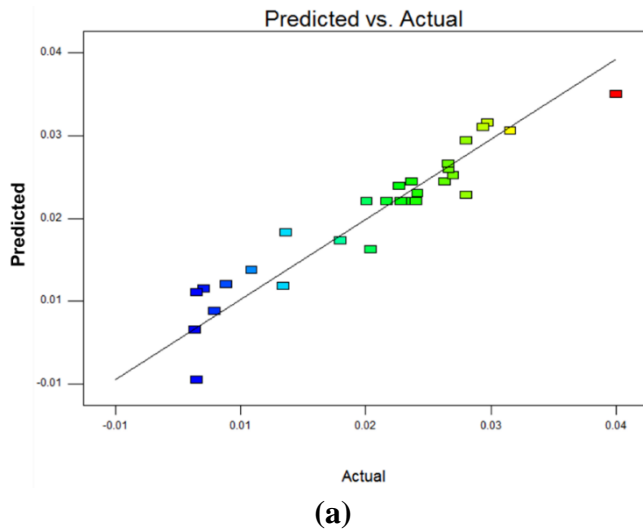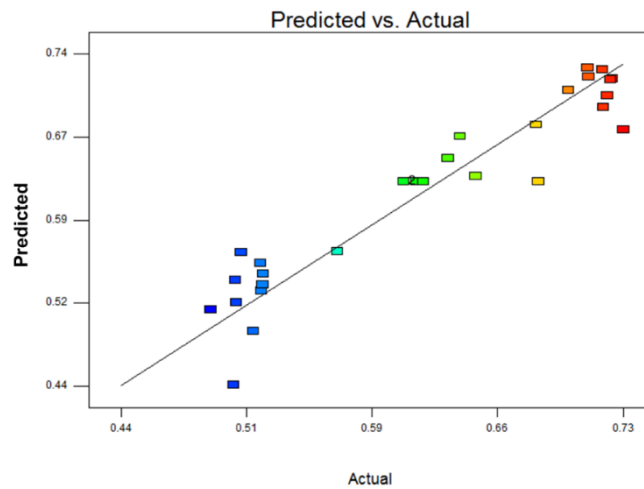
(a)

(b)

Figure 6.1 Normal probability plot of residuals for (a) MRR$_{µEDm}$, (b) FEW

(a)

119

(b)

Figure 6.2 Plot of predicted vs. actual response for (a) MRR$_{\mu EDm}$, (b) FEW

For MRR$_{\mu EDm}$, *Cp, E, F, V$_g$ F, Cp$\times$R, Cp^2, and R^2* are significant model terms with their percentage contribution of 25.78, 18.96, 8.11, 13.58, 5.94, 5.87 and 3.07 respectively. The *Cp, R, V$_g$$\times$F, Cp$\times$R, Cp^2 and F^2* are significant model terms for EWR with their percentage contribution of 43.10, 14.70, 4.57, 8.64, 2.73, and 4.05 respectively. The lack-of-fit values indicate its significance or non-significance relative to pure error. When lack-of-fit values are non-significant, it agrees on the model fit to the experimental data and recommends that a very small systematic difference that leftovers unaccounted for a particular model. In the present study, the lack-of-fit values for were found to be 5.62, and 1.04 for MRR, and FEW, respectively, indicating small chance that a lack-of-fit F value this large could occur due to noise. Hence, the established models for MRR, FEW are accepted.

6.3.2   Regression equation for MRR and FEW

The empirical relation between the performance measures (i.e. MRR, and EWR) and the control factors (actual terms) can be expressed by the following second-order polynomial equations;

120

$$MRR_{\mu EDm} = -0.047927 + (3.1254 \times 10^{-4})V_g + 0.068906\, Cp$$

$$+ (5.67487 \times 10^{-5})R + (1.75298 \times 10^{-3})F$$

$$+ (8.8659 \times 10^{-4})V_g \times Cp - (1.60938 \times 10^{-5})V_g \times F \quad (6.1)$$

$$- (7.49299 \times 10^{-5})Cp \times R - 0.19685\, Cp^2$$

$$- (2.24361 \times 10^{-9})R^2$$

$$\text{FEW} = +0.16804 + (2.1070 \times 10^{-3})V_g + 1.26179\, Cp$$

$$+ (2.95894 \times 10^{-4})R + (9.66017 \times 10^{-3})F$$

$$- (7.84583 \times 10^{-5})V_g \times F - (7.5958 \times 10^{-4})Cp \times R \tag{6.2}$$

$$- 1.10754\, Cp^2 - (3.74921 \times 10^{-5})\, F^2$$

6.3.3 Validation of models

The five additional experiments were executed at different control factors settings within the range of chosen factors in order to validate the established MRR$_{\mu EDm}$ and FEW. The dissimilar control factors combinations were chosen than the one used for forming the regression models. The prediction errors were calculated using equation (4.7).

Table 6.6 Results of validation experiments for MRR and FEW

Expt. No.	Gap Volatage (V)	Capaci tance (μF)	ERS (rpm)	VF (HZ)	MRR$_{\mu EDm}$ (gm/min)			FEW (mm)		
					Experime ntal value	Predict ed value	Predicti on error %	Experimen tal value	Predict ed value	Predicti on error %
1	100	0.1	500	60	0.0309	0.0298	3.57	0.367	0.376	2.23
2	100	0.4	900	60	0.0436	0.0458	-4.94	0.463	0.462	-0.09
3	120	0.01	500	0	0.0181	0.0187	-3.59	0.325	0.310	-4.95
4	100	0.01	500	30	0.0176	0.0166	5.57	0.346	0.364	5.08
5	80	0.4	500	60	0.0395	0.0423	-6.85	0.560	0.593	5.63

Table 6.6 displays the results of validation experiments. The results of experimental validation were found to be in good agreement with the predicted results obtained from the regression equations. Consequently, the established models can be treated as a reliable demonstrative of the experimental results.

6.4   Results and discussion

In this section, Perturbation plot and 3D response curves were used to discuss the impact of individual control factors as well as their interactions on the performance measures.

6.4.1   Influence of control factors and their interactive effect on MRR

The comparative effects of significant control factors on MRR of Inconel 718 by µ-ED milling were shown in Perturbation plot (Figure 6.3). By default, Design-Expert package keeps the reference point at the midpoint (coded value 0) of all factors. A sharp slope for capacitance (Cp) and electrode rotations speed (R) directs that the MRR is highly sensitive to these factors.
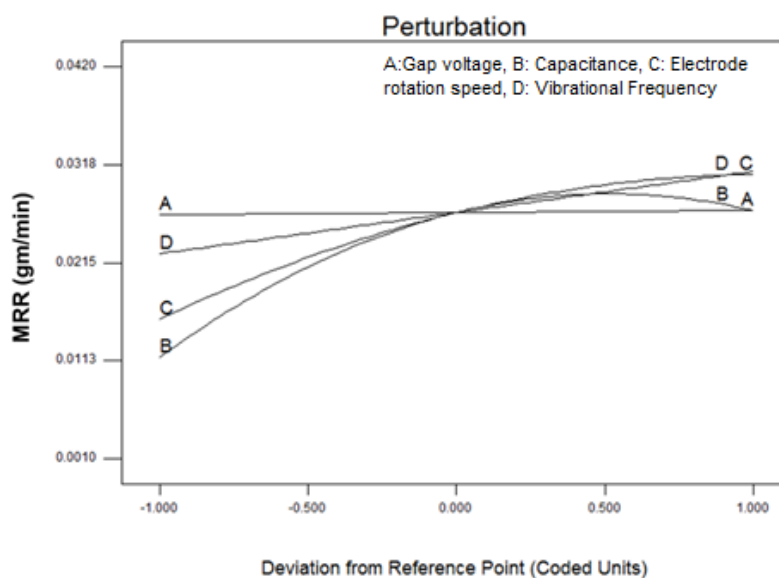

Figure 6.3 Perturbation plot for MRR

It is perceived from the Table 6.4 that the interactions which significantly contributes to the MRR$_{\mu EDm}$ model are those between the voltage and capacitance '$V_g \times Cp$', voltage and vibrational frequency '$V_g \times F$', and capacitance and ERS '$Cp \times R$' and the interaction plots corresponding to these interaction terms are shown in Figure 6.4 (a), (b), and (c) respectively.

The interaction effect of voltage and capacitance at all other control factors at middle values. It can be seen from Figure 6.4 (a) is that the MRR increases with increase in capacitance. It was noted that at low capacitance values, the MRR decreases with increase in gap voltage. However, at higher capacitance values, the MRR initially increases with increase in gap voltage. The similar observation regarding effects of capacitance and gap voltage on MRR also reported by [109]. The reasons behind these trends as discusses in section 5.5.1. As discussed previously, the discharge energy (DE) engendered in RC pulse circuit is multiplication of capacitance and voltage ($DE = \frac{1}{2}Cp \times V_g{}^2$). The DE stored by capacitor is released when voltage reaches breakdown voltage. The capacitance value determines the extent of the energy deposited and therefore, with increase in capacitance, the amount of DE, pulse current and pulse interval also increases boosting the MRR. Therefore, the MRR increases prominently at high values of capacitance (Figure 6.4).
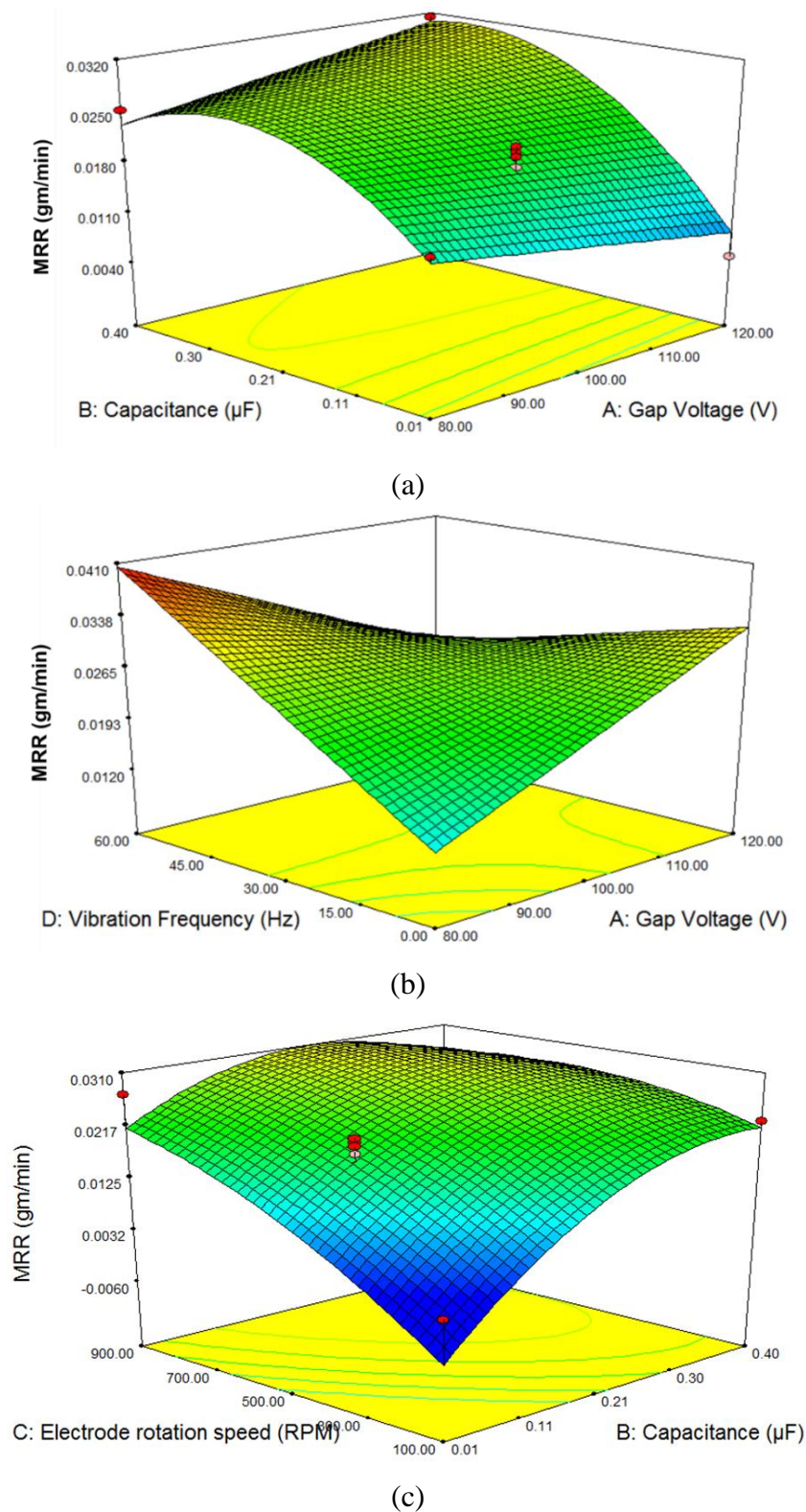
(a)

(b)

(c)

Figure 6.4 (a), (b), and (c) shows the response graph of MRR

It is evident from the Figure 6.4 (b) and that the vibration frequency has an important

effect in improving the MRR. The molten metal and debris present in spark gap lead to

adhesion and causes short circuits. At evidence of short circuit, the machine retracts the

electrode to maintain the spark gap and then again directs electrode in feed direction [114]. Thus, frequent adhesion and short circuits lead to higher machining time as the machine has to retract and feed electrode repeatedly. As vibration device expands and contracts faster at a higher frequency, the workpiece moves up and down continuously. Therefore, the adhesion between electrode and workpiece recovered effectively. Also, vibration frequency aids in effect removal of debris and molten metal from IEG, thereby, aiding improved MRR.

The response surface in Figure 6.4 (c) exemplifies that the increase in ERS promotes the growth in MRR. The higher centrifugal force is developed at high-ERS, which aids in effective the dielectric circulation and thereby effective evacuation of the debris trapped in between IEG. An agitation effects attributed by higher ERS drives the dielectric into discharge zone [108]. Also, higher ERS promotes the disturbance of dielectric due to increased tangential velocities [29]. Therefore, along with evacuating the debris and molten metal in discharge zone, the agitation effect results in more efficient sparks in machining zone and attributes in increase MRR.

6.4.2 Influence of control factors and their interactive effect on FEW
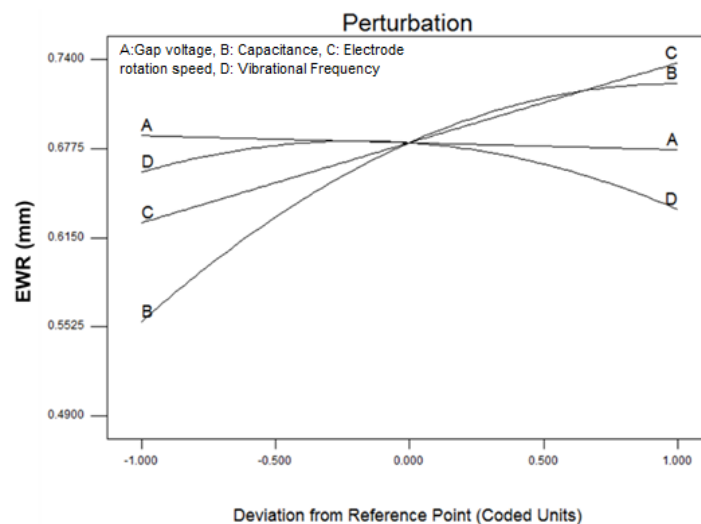

Figure 6.5 Perturbation plot for FEW

The Perturbation plot for FEW is shown in Figure 6.5. A steep slope for capacitance indicates that the FEW is very sensitive to capacitance as compared to other factors. The FEW increases with increase in capacitance, and ERS, however, decreases with increase in gap voltage and VF. With the increase in capacitance, the extent of DE, pulse current and, pulse interval also rises causing more wear of electrode [107]. The VF also found to effective in reducing the FEW. The FEW increases with increase in ERS (Figure 6.6 (b)) due to effective sparking condition attributed at higher ERS leading to more wear of electrode. The higher ERS results in assisting the dielectric to pull out the debris from the IEG with the influence of centrifugal force. Also, it causes an agitation effects helpful for dielectric fluid to go into the discharge zone as discussed previously in section 5.5.2.
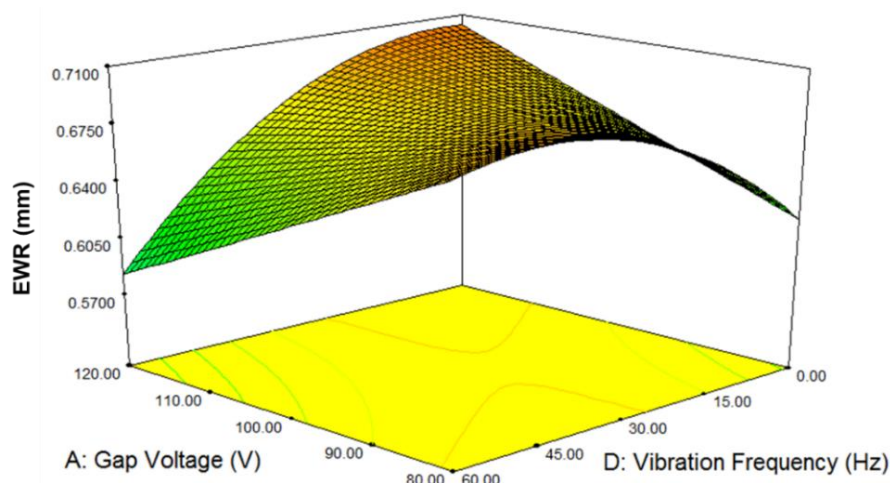
(a)
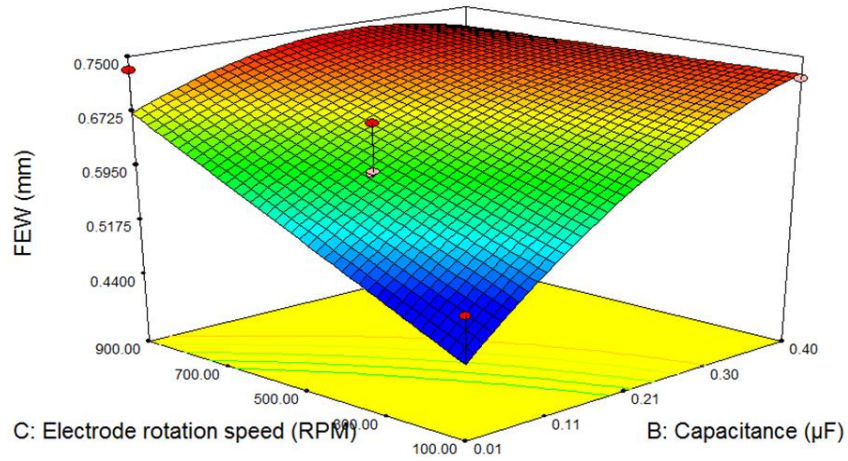
(b)

Figure 6.6 (a), and (b) shows the response graph of EWR

6.5 Desirability based multi-response optimization

The design expert optimization module was used to find the combination of control factors, i.e., voltage, capacitance, ERS, and VF, which fulfills the constraint imposed on each of the control factors and performance measures. The desirability based multi-response optimization was performed to find the optimal values of control factors by maximizing the MRR while minimizing the EWR. The constraints for control factors and performance measures are given in Table 6.7. Table 6.8 shows the optimization results with corresponding settings of control factors.

Table 6.7 The constraints for control factors and performance measures

Factor	Goal	Lower constraint	Upper constraint	Importance
Gap Voltage	is in the range	80	120	3
Capacitance	is in range	0.01	0.4	3
Electrode rotation speed	is in range	100	900	3
Vibrational Frequency	is in range	0	60	3
MRR	maximize	0.0019796	0.041117	5
FEW	minimize	0.49262	0.7315	3

127

Table 6.8 Optimal settings of control factors for single and multi-response optimization

Type of optimization	Objective	Optimum control factor values				Performance measure value (Measured)	Performance measure value (Expt.)	Desirability
		Gap Voltage (V)	Capacitance (μF)	Electrode rotation speed (rpm)	Vibrational frequency (Hz)			
Single response	Maximize MRR$_{μEDm}$	84	0.2	772	58	0.0411 gm/min	0.0391gm/min	1.0
Single response	Minimize FEW	111	0.06	236	58	0.4615	0.4685	1.0
Multiple response	Maximize MRR$_{μEDm}$, while minimize FEW	80	0.02	522	60	0.0308 gm/min, 0.5790	0.0312 gm/min, 0.5821	0.698

6.6 Microscopic investigation on effects on vibrational frequency on shape and dimensions of micro-channel

The microscopic images of micro-channels were taken after each machining pass at different vibrational frequency values. These micro-channels were fabricated at constant discharge energy value of 500 μJ, electrode rotational speed of 500rpm, and different workpiece vibrational frequency values. The bulk machining approach as described in section 3.2.3 was employed for fabrication of micro-channels and three number of passes were performed as shown in Figure 6.7. The dimension of micro-channel was observed after each pass.

For the first pass images of micro-channels from entry side, exit side, and top side are presented in Table 6.9. Similarly, for a second pass and third pass, images of micro-channels from entry side, exit side and top side are presented in Table 6.10 and Table 6.11, respectively.
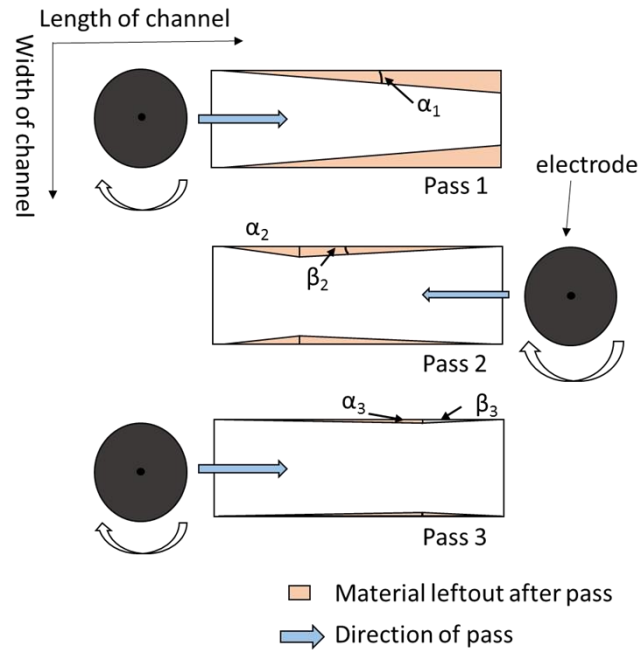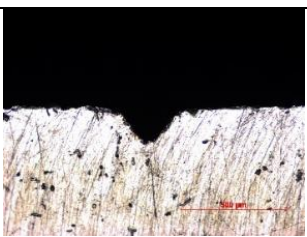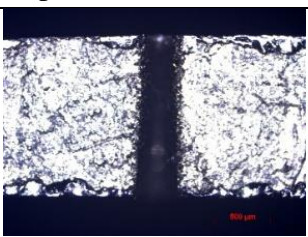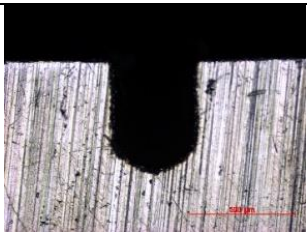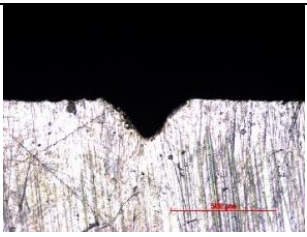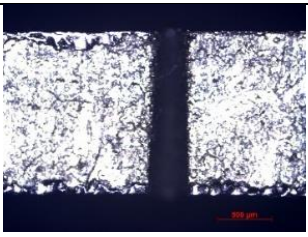
Figure 6.7 Three passes in bulk machining approach

By observing the micro-channel images at different passes at a different frequency, it was found that vibrational frequency has notable effects on shape and dimensions of fabricated micro-channels. From images of micro-channels at entry side for the first pass, it was noted that both the width and depth of micro-channels decreases by applying workpiece vibration up to the level of vibrational frequency of 40Hz. The width and depth of micro-channel increase slightly with a further increase in vibrational frequency values. While fabricating micro-channels using µ-EDM process, the trapped debris particle in IEG results in secondary sparking and arcing [99]. This trapped debris if not removed from IEG results in overcutting at the side wall and the bottom surface of the micro-channel. The application of low-frequency workpiece vibration results in efficient evacuation of debris particles and molten metal from IEG attributed due to enhanced dielectric flow in machining zone. This phenomenon assists in reduced ineffective pulses and thereby improving the accuracy of micro-channel. From exit side images of micro-channels after the first pass, it was observed that with the application of workpiece vibration the depth of micro-channels at exit side increased. The reason

behind this observation is with an increase in workpiece vibration the electrode wear reduces as secondary sparking between electrode and debris is reduced. Therefore, additional material removal takes place resulting in increased depth of micro-channels. Similarly, the taper angle (α_1) also decreases with an increase in vibrational frequency up to the value of 40Hz due to reduced electrode wear and increased material removal rate attributed due to reduced arcing and adhesion, and efficient dielectric flow.

The similar observations regarding the width, depth and a taper angle (β_2) also found from microscopic investigations of micro-channels after the second pass. From images of micro-channels at entry side for the second pass, it was noted that both the width, depth and a taper angle (β_2) of micro-channels decreases by applying workpiece vibration up to the level of vibrational frequency of 40Hz. The width and depth of micro-channel increase slightly with a further increase in vibrational frequency values. From microscopic images of the micro-channels after the third pass, it was observed that vibration frequency values of 40Hz results in accurate micro-channel in terms of correct dimensions and least taper angles.

Table 6.9 Microscopic images of micro-channels after the first pass

	First pass		
	Entry Side	Exit Side	Top side
VF 0 Hz	 W=442, D=530	 D=178	 α_1= 4.1°
VF 20 Hz	 W=411, D= 505	 D=195	 α_1= 3.1°
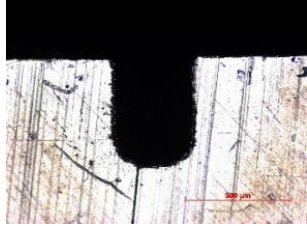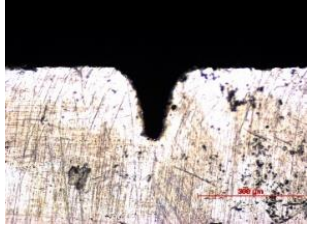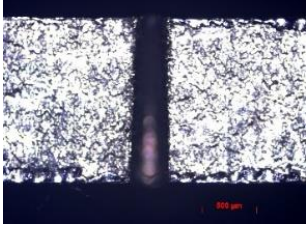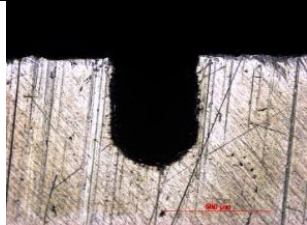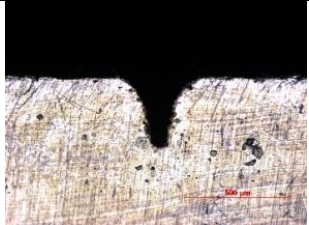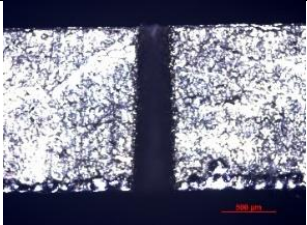
	Entry Side	Exit Side	Top Side
VF 40 Hz	W=402, D=497	D=345	α_1= 2.2°
VF 60 Hz	W=421, D=506	D=317	α_1= 2.6°

Table 6.10 Microscopic images of micro-channels after the second pass
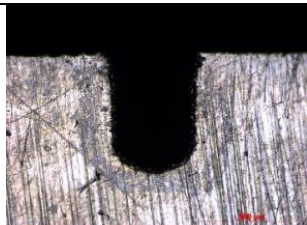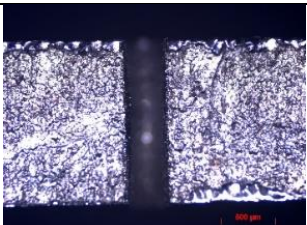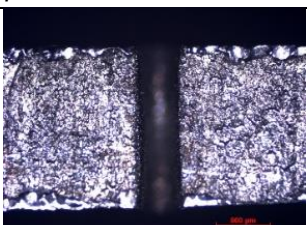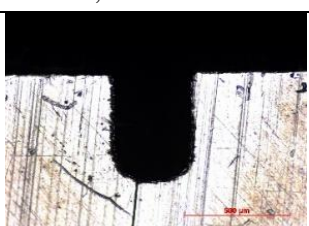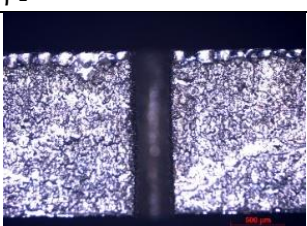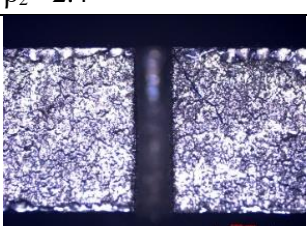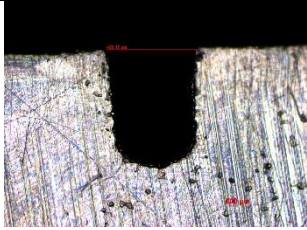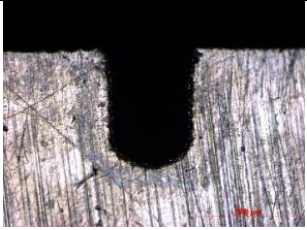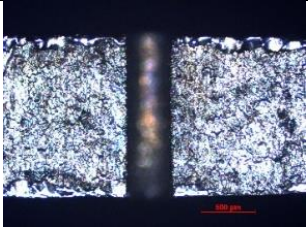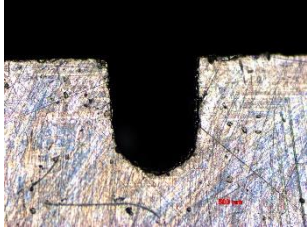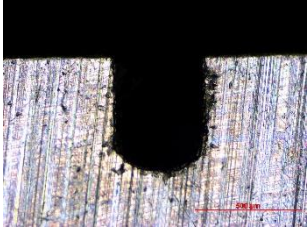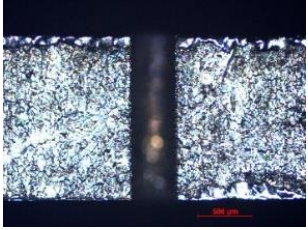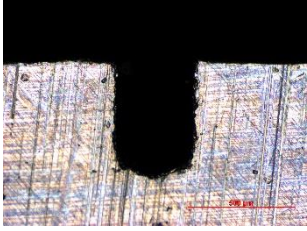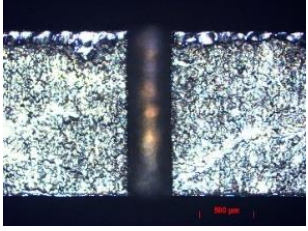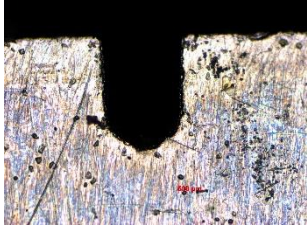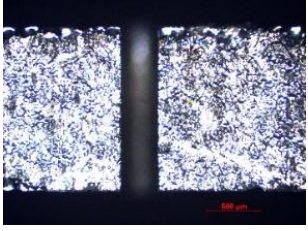
	Second pass		
	Entry Side	Exit Side	Top Side
VF 0 Hz	W=443, D=535	W=442, D=530	β_1= 4.2°
VF 20 Hz	W=419, D=509	W=411, D= 505	β_2= 3.2°
VF 40 Hz	W=398, D=504	W=402, D=502	β_2= 2.4°
VF 60 Hz	W=399, D=513	W=421, D=515	β_2= 2.5°

Table 6.11 Microscopic images of micro-channels after the third pass

	Third pass		
	Entry Side	Exit Side	Top side
VF 0 Hz	W=442, D=530	W= 443, D=535	α_3= 1.2°, β_3= 1.3°
VF 20 Hz	W=411, D=525	W= 421, D=521	α_3= 0.7°, β_3= 0.8°
VF 40 Hz	W=408, D=497	W=406, D=502	α_3= 0.6°, β_3= 0.7°
VF 60 Hz	W=421, D=520	W=399, D=518	α_3= 0.6°, β_3= 0.8°
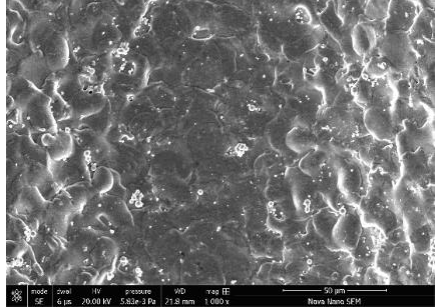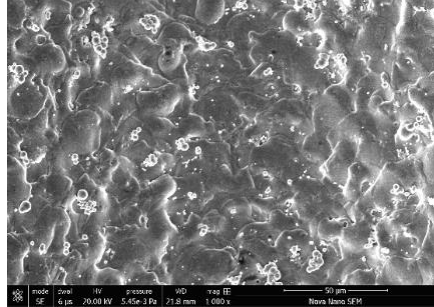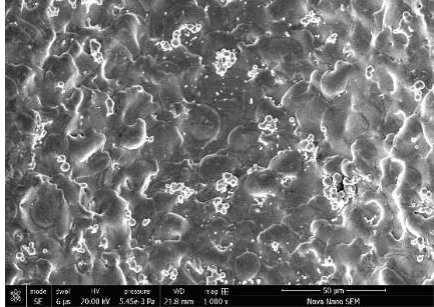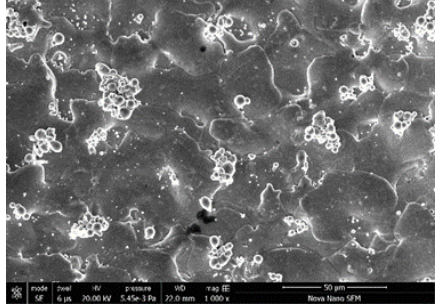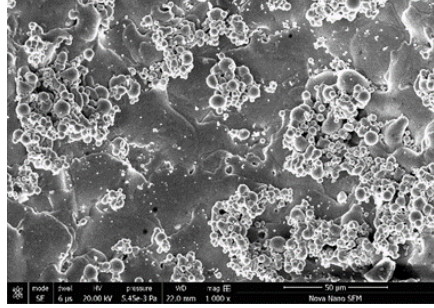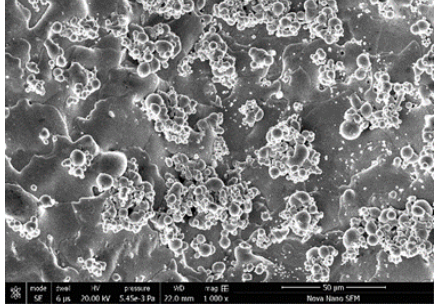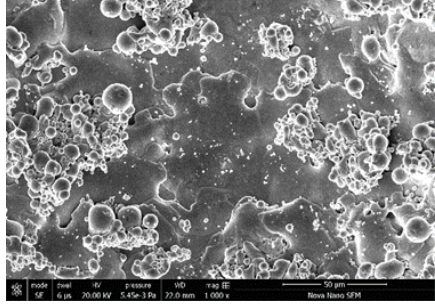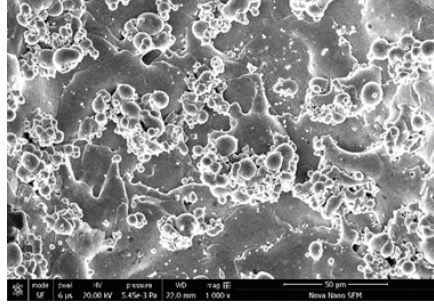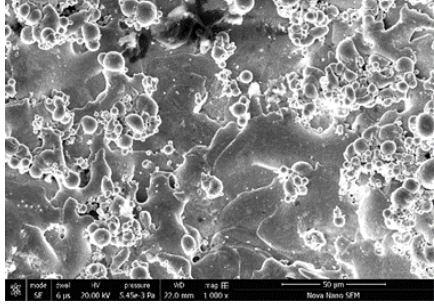
6.7 Surface morphology of micro-channels at different discharge energy and vibrational frequencies

The surface quality of micro-channels was investigated using the images captured at a magnification of 1000X using FESEM. Table 6.12 shows the images of micro-channels fabricated at different discharge energy and vibrational frequency settings. It was

recognized that the discharge energy has a considerable effect on surface quality of micro-channel produced. The discharge energy removes the material from the workpiece by melting and evaporation of material leaving behind the craters. The dielectric fluid causes the rapid cooling and quenching of molten metal and thus leading to the formation of globules which are non-crystalline sphere-shaped specks [108]. The discharge energy is acting onto the workpiece notably affects the shape and size of the globule formed. At lower discharge energy, the globules size appear to be tiny as compared to the globules at high discharge energy. Moreover, the size of the globules was not same at particular energy level owing to superimposing of craters and rotation of electrode. The more number of globules were formed with an increase in the extent of discharge energy at same vibration setting.

It was observed that at same discharge energy setting, with an increase of vibration frequency the number of globules formed increases. The workpiece vibrations improve the dielectric circulation and also causes turbulence in the dielectric flow. Moreover, with workpiece vibration, the dielectric present in machining zone will be pulled in and pushed out effectively. Therefore, the enhanced dielectric flow conditions lead to instant cooling and quenching of molten metal in machining zone causing increased globule formation.

Table 6.12 Surface morphology of micro-channels at different conditions

Energy	Vibrational Frequency		
	Without vibration	40 Hz	60 Hz
50 µJ			
500 µJ			
2000 µJ			

6.8   Comparison with previous studies
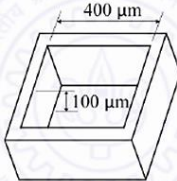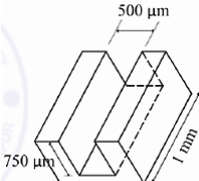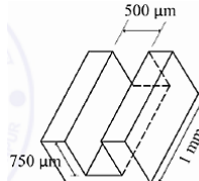
As discussed in the literature review, the µ-ED milling carried out with two different approaches, one layer-by-layer machining and second bulk machining approach. To broaden the analysis and justify the results, a comparative study of a low-frequency vibration assisted bulk machining approach in µ-ED milling is compared with without vibration assisted bulk machining approach, and layer-by-layer approach. Kathikeyan [9] demonstrated the combined advantage of lower machining time, and better surface finish through multiple pass machining with varying machining conditions (i.e. different parametric settings for subsequent passes). He reported that multiple pass machining in bulk machining approach results in better performance of µ-ED milling. The results of the comparison of a low-frequency vibration assisted bulk machining approach for µ-ED milling with results presented by Yu et al. [136] for layer-by-layer approach and Karthikeyan [9] for bulk machining approach are shown in Table 6.13.

The similar machining condition used by Yu et al. [136] and Karthikeyan et al. [9] were considered for comparison purpose and are shown in Table 6.13. The RC circuit power supply, electrode material, dielectric, voltage and capacitance values are nearly similar. Yu et al. considered square pocket shape and Karthikeyan considered rectangular channel in their study. The channel shape dimension which is slightly larger than pocket shape, therefore, channel shape chose for fabrication and comparison.

Initially, the machining time for bulk machining approach is compared with the layer-by-layer approach, and it is observed that bulk machining approach saves nearly 130 mins. Then, bulk machining approach with multiple machining conditions is compared with bulk machining approach with single machining condition. It has been noted that

bulk machining with multiple machining conditions saves nearly 130 mins. Nearly similar time recorded as that by Karthikeyan for bulk machining approach with single machining condition and multiple machining conditions.

Table 6.13 Comparison of low-frequency vibration machining approach with bulk machining approach and layer-by-layer approach

Sr. no.	Description		Layer-by-layer approach [136]	Bulk approach [9]		Vibration-assisted bulk approach	
1	Shape and dimension of feature considered						
2	Choice of conditions	Workpiece material	Stainless steel AISI 304	EN 24		Inconel 718	
		Electrode material	Tungsten	Tungsten		Tungsten	
		Voltage (V)	80V	100V		100V	
		Capacitance (nF)	0.1	10		10	
		Dielectric	Mineral oil	EDM oil (Total®)		EDM oil (Total®)	
3.	Machining Time		354 mins	229 mins (A1)		224 mins (without vibration) (A2)	
4.	Multiple machining conditions (Proposed by [9])		-	2000μJ & 500 rpm	91 mins (B1)	2000 μJ & 500 rpm	90 mins
				500 μJ & 500 rpm		500 μJ & 500 rpm	
				50 μJ & 800 rpm		50 μJ & 800 rpm	
5.	Multiple machining conditions with low-frequency vibration assistance		-	-		2000 μJ & 500 rpm & 40Hz	69 mins (B2)
						500 μJ & 500 rpm & 40 Hz	
						50 μJ & 800 rpm & 40 Hz	
6.	Saving in Time		-	A1-B1= 138 mins (i.e. 2 hours & 18 mins)		A1-B2= 285 mins (i.e. 4 hours & 45 mins) A2-B2 = 155 mins (i.e. 2 hours & 35 mins)	

Finally, the low-frequency vibration assistance for bulk machining with multiple machining conditions is examined for its effectiveness. It was observed that vibration assistance reduced the machining time. Overall, as compared to layer-by-layer

approach and bulk machining approach, the low-frequency vibration assisted bulk machining approach with multiple machining conditions saves 4 hours & 45 mins and 2 hours and 35 mins. Therefore, it can be claimed that the low-frequency vibration assisted bulk machining approach with multiple machining conditions is appropriate for faster fabrication of 3D micro-features. The low-frequency vibration µ-ED milling is used for fabrication of different complex shapes of micro-channels and discussed in next section.

6.9 Fabrication of complex shaped micro-channels

The low-frequency vibration assisted µ-ED milling was employed for fabrication of complex shaped micro-channels. The same setup as shown in Figure 3.8 was utilized for channel fabrication in workpiece and workpiece positive setting used. The block-EDG process was used for the dressing of electrode after each pass, and electrode dressing is performed as positive tool polarity setting.

Different complex shapes of micro-channels were fabricated on Inconel 718 superalloy using ∅300 µm electrode. The machining carried out at a constant machining condition of 500 µJ and 500 RPM for all passes. Figure 6.8 shows the different micro-channels shapes fabricated using low-frequency vibration assisted µ-ED milling (bulk machining) approach.
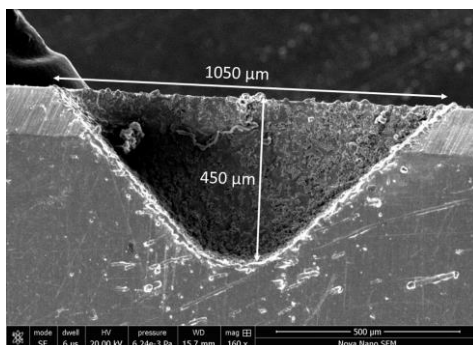
| (a) 2-way micro-channel | (b) 3-way micro-channel |
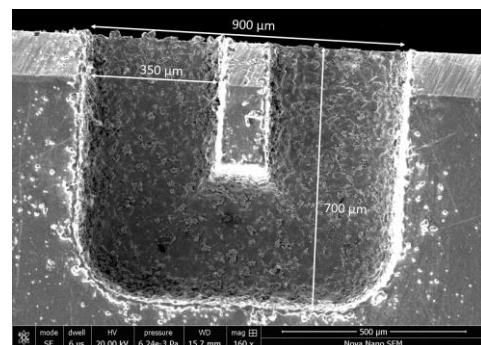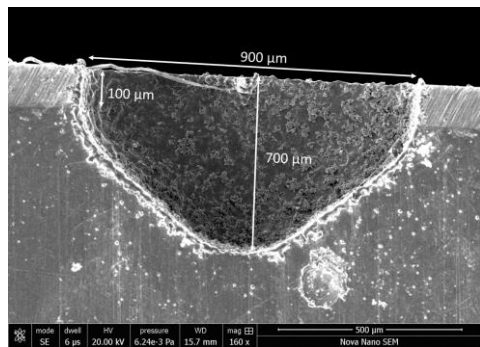
(c) 3-way micro-channel
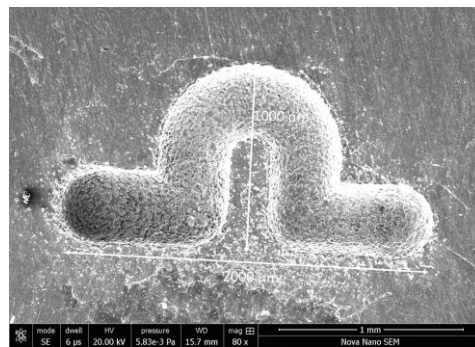
(d) Serpentine curved connection
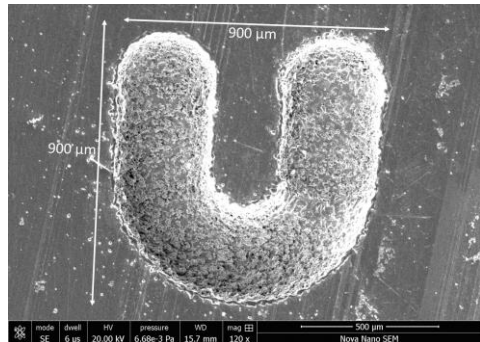
(e) 'U' type micro-channel
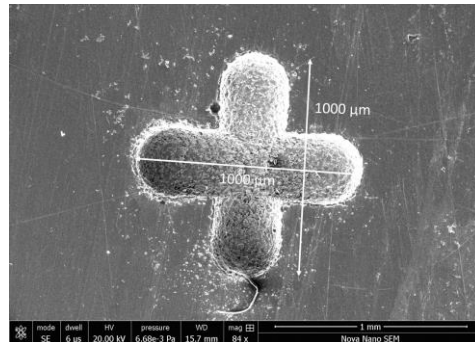
(f) '+' connection micro-channel
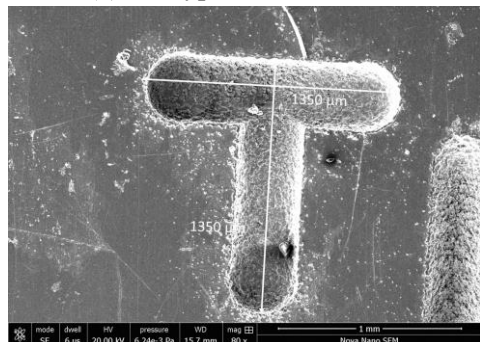
(g)'T' type micro-channel
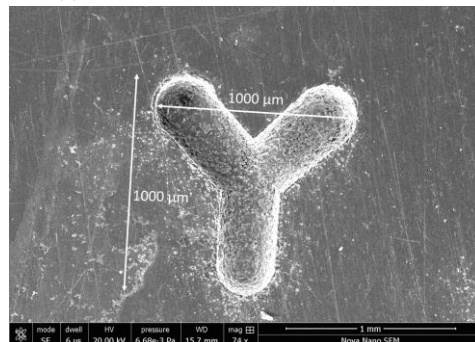
(h) 'Y' type micro-channel

Figure 6.8 Complex shaped micro-channels fabricated using low-frequency vibration assisted micro-ED milling

6.10 Summary

In this chapter, an approach of low-frequency workpiece vibration assisted µ-ED milling was proposed. The effects of gap voltage, capacitance, ERS, and vibration frequency were analyzed on MRR and FEW while producing micro-channels in Inconel 718. The results achieved after experimentation are summarized as follows:

- The capacitance was found to be the most influencing factor for both MRR and FEW contributing 25.72% and 43.10% respectively. The both MRR and FEW increase with an increase in capacitance values.

- The electrode rotational speed also observed to be influencing the MRR and FEW significantly by 18.92% and 14.70%. The MRR and FEW increases with an increase in rotational speed of the electrode.

- The low-frequency vibration assistance found to be improving the machining condition suitable for increasing the MRR and reducing the FEW. The vibration frequency contributes 8.09% on MRR indicating its positive influence on reducing the machining time in the µ-ED milling.

- The application of low-frequency vibration assists in effective debris evacuation from machining zone, thereby, reduced taper angle and reduced overcut of width and depth of micro-channels. The vibrational frequency of 40Hz was found to be optimum for fabricating dimensionally accurate micro-channels in less machining time.

- Microscopic investigation of produce micro-channel reveals that low values of discharge energy are more suitable for achieving uniform and smooth micro-channel surface.

- The comparison of proposed low-frequency vibration assisted bulk machining approach with other previous approach shows that the proposed approach is appropriate for achieving micro-channels at reduced machining time.

7 Conclusions and future scope

7.1 Conclusions

In present work, the fabrication of micro-features based on the EDM based hybrid machining processes have been demonstrated. It has been perceived that hybridizing EDM could overcome the limitations associated with EDM variant processes. The conclusions obtained from this research on hybrid EDM based machining of Inconel 718 while fabricating common micro-features like micro-surfaces, micro-holes and micro-channels are gathered in the following headings:

- Abrasive mixed electro discharge diamond grinding
- Low-frequency vibration assisted μ-ED drilling
- Low-frequency vibration assisted μ-ED milling

7.1.1 Abrasive mixed electro discharge diamond grinding

- The outcomes of ANOVA and assessments of experimental data signifies that the developed mathematical models for the material removal rate and average surface roughness are well fitted with the experimental values with the prediction errors less than ±5 %.

- The wheel speed is found to be the most significant factor for both the MRR and R_a. With the increase in wheel speed, the MRR found to be increasing and R_a decreasing. High wheel speed removes a higher volume of material uniformly improving process performance. It also attributes in enhancing the flushing efficiency and removal of recast layers and molten metal formed during EDM.

141

- With an increase in abrasive concentration, the MRR increases while surface roughness decreases. For the uniform surface, high wheel speed and high abrasive concentration and low value of pulse-on-time are recommended.

- The results of multi-response optimization by providing equal importance to both performance measures achieved the material removal rate of 15.960 mm^3/min and average surface roughness of 2.441 μm

The hybrid process AMEDDSG found to be competent for achieving high machining rate and good surface finish while machining difficult-to-cut Inconel 718 superalloy serving its purpose of hybridization.

7.1.2 Low-frequency vibration assisted μ-ED drilling

- The empirical models developed for MRR, EWR, overcut and taper angle found to be reliable in representing the experimental results with prediction errors less than ±7 %.

- The capacitance was found to be the most significant factor affecting the overall performance of μ-ED drilling process. Higher electrode rotational speed results in conditions favorable for higher machining rate and accuracy of drilled holes.

- The application of low-frequency vibration assistance results in enhanced debris evacuation and flushing conditions during μ-ED drilling due to variation in gap distance and dielectric pressure.

- The workpiece vibrations also reduce the HAZ while μ-ED drilling of Inconel 718. The microhardness values were found to be increased with workpiece vibration during μ-ED drilling as compared to that of without workpiece vibrations.

- For generating micro-holes with better surface quality and dimensional accuracy, the low discharge energy, high electrode rotational speed and vibrational frequency in the range of 30-40 Hz are recommended.

The low-frequency vibration assisted μ-ED drilling is an appropriate method to fabricate good surface quality and burr free high-aspect-ratio micro-holes in Inconel 718.

7.1.3 Low-frequency vibration assisted μ-ED milling

- The empirical models developed for MRR, FEW found to be trustworthy in representing the experimental results with prediction errors less than ±7 %.

- The MRR and FEW increases with an increase in both gap voltage as well as capacitance.

- The application of low-frequency vibration assists results in reduced taper angle and overcut in width and depth of micro-channels. The vibrational frequency of 40Hz was found to be optimum for fabricating accurate micro-channels in less machining time.

- The discharge energy significantly affects the amount and size of the globules formed during μ-ED milling. The amount of globules slightly increases with increase in vibrational frequency at the same energy level.

- Microscopic investigation reveals that low discharge energy along with low-frequency vibration yields in uniform and smooth microchannel surface.

- The comparison of proposed low-frequency vibration assisted bulk machining approach with other previous approach shows that the proposed approach is best suitable for achieving micro-channels at reduced machining time.

143

The low-frequency vibration assistance played a vital role in improving the MRR and reducing the FEW in the μ-ED milling and served the purpose of hybridization.

The assistance of low-frequency vibration found to be attributing enhanced machining performance through effective removal of debris and molten material from inter-electrode gap, effective flushing conditions, reduced electrode-workpiece adhesion, etc. of both μ-ED drilling and μ-ED milling. To complement and verify the usefulness of low-frequency vibration assistance in micro-EDM, the performance of vibration-assisted micro-WEDM process also assessed (see, Appendix-C) and found to be effective in improving the process performance.

7.2 Research contributions

The contributions from this research in the field of fabrication of micro-features using hybrid EDM machining of Inconel 718 along with scientific interests and practical application of this research are provided below from the manufacturing perspective:

- In this work, experimental investigations were performed fabricating most common micro-features viz. micro-surfaces, micro-holes, and micro-channels in a difficult-to-cut material Inconel-718 superalloy.

- This work emphasized on achieving improved process performance of EDM-based processes by hybridizing them to overcome their limitations.

- Fine surfaces finish was achieved on Inconel 718 at high machining rate with abrasive mixed electro discharge diamond grinding process.

- For fabricating high-aspect-ratio micro-holes in difficult-to-cut Inconel 718, a hybrid machining process of a low-frequency vibration assisted micro-ED drilling was successfully employed.

- Introducing low-frequency workpiece vibration is an effective approach for the micro-EDM drilling. Most of the previous studies used ultrasonic vibration with micro-EDM for drilling micro-holes in different materials.

- High aspect ratio (~21) micro-holes in Inconel 718 with good surface quality and dimensional accuracy have been fabricated using the vibration assisted micro-ED drilling. High-aspect-ratio micro-holes in difficult-to-cut materials may have significant contribution in the industries.

- For fabricating micro-channels in difficult-to-cut Inconel 718, a hybrid machining process of a low-frequency vibration assisted micro-ED milling was successfully employed.

- To best the knowledge of the author, no study has been conducted elsewhere on workpiece-vibration-assisted micro-ED milling for machining of Inconel 718. With vibration assisted micro-ED milling improved process performance was observed and then process used for fabrication of different complex micro-channel shapes.

7.3 Future scope

This research work was focused on the generation of micro-features in Inconel 718 super alloy utilizing hybrid-EDM processes. As hybrid-EDM is a newer area of research; there may be many issues which could be taken up for further research. A few directions in which further research and development can be carried out are as follows:

- Future studies can focus on the application of hybrid EDM based processes for different materials and study of their effectiveness. Materials like ceramics and composites can be explored.

- Study on effects of hybrid machining processes such as AMEDDG, μ-ED drilling, μ-ED milling, and μ-WEDM on properties of processed materials can be incorporated.

- A product-specific study on fabrication and performance of micro-device e.g. micro-heat exchanger, micro-reactor fabricated using the hybrid EDM processes can be included.

- Tool shapes such as hollow, spline shafts, etc. along with different electrode materials can be incorporated to study their performances in the μ-EDM process. The performance of such tools along with the assistance of vibration may provide further enhanced machining condition as these shapes will further aid in effective flushing of the debris in the machining zone.

- Tool wear is responsible for achieving an accuracy of generated micro-features. Hence, online tool wear monitoring and compensation are essential steps to perform in order to maintain the geometrical accuracy of machined parts. This way the desired profile may be achieved with less error.

- The development of grinding attachment for micro-EDM to establish micro-EDDG process could open up new avenues in the micro-EDM process by reducing the machining time and improving surface finish.

References

[1] E. O. Ezugwu, "Key improvements in the machining of difficult-to-cut aerospace superalloys," *International Journal of Machine Tools and Manufacture,* vol. 45, pp. 1353-1367, 2005.

[2] P. N. Rao, *Manufacturing Technology: Metal Cutting and Machine Tools* vol. 2. India: Tata McGraw-Hill Education, 2013.

[3] S. Pervaiz, A. Rashid, I. Deiab, and M. Nicolescu, "Influence of Tool Materials on Machinability of Titanium- and Nickel-Based Alloys: A Review," *Materials and Manufacturing Processes,* vol. 29, pp. 219-252, 2014.

[4] M. Anderson, R. Patwa, and Y. C. Shin, "Laser-assisted machining of Inconel 718 with an economic analysis," *International Journal of Machine Tools and Manufacture,* vol. 46, pp. 1879-1891, 2006.

[5] W. Akhtar, J. Sun, P. Sun, W. Chen, and Z. Saleem, "Tool wear mechanisms in the machining of Nickel based super-alloys: A review," *Frontiers of Mechanical Engineering,* vol. 9, pp. 106-119, 2014.

[6] D. Zhu, X. Zhang, and H. Ding, "Tool wear characteristics in machining of nickel-based superalloys," *International Journal of Machine Tools and Manufacture,* vol. 64, pp. 60-77, 2013.

[7] D. Dudzinski, A. Devillez, A. Moufki, D. Larrouquère, V. Zerrouki, and J. Vigneau, "A review of developments towards dry and high speed machining of Inconel 718 alloy," *International Journal of Machine Tools and Manufacture,* vol. 44, pp. 439-456, 2004.

[8] J. P. Davim, *Nontraditional Machining Processes*. London: Springer, 2013.

[9]   G. Karthikeyan, "Micro electric discharge milling (µED-milling) process for fabrication of complex micro-features," Ph.D., Department of Mechanical Engineering, Indian Institute of Technology, Kanpur, IIT Kanpur, 2011.

[10]   K. F. Ehmann, D. Bourell, M. L. Culpepper, T. J. Hodgson, T. R. Kurfess, M. Madou*, et al.*, *Micromanufacturing*. Dordrecht: Springer Netherlands, 2007.

[11]   M. Beidaghi and Y. Gogotsi, "Capacitive energy storage in micro-scale devices: recent advances in design and fabrication of micro-supercapacitors," *Energy & Environmental Science,* vol. 7, p. 867, 2014.

[12]   H. Wang and M. Pumera, "Fabrication of Micro/Nanoscale Motors," *Chemical Reviews,* vol. 115, pp. 8704-8735, 2015.

[13]   E. Luong-Van, I. Rodriguez, H. Y. Low, N. Elmouelhi, B. Lowenhaupt, S. Natarajan*, et al.*, "Review: Micro- and nanostructured surface engineering for biomedical applications," *Journal of Materials Research,* vol. 28, pp. 165-174, 2012.

[14]   W. Gao and J. Wang, "The Environmental Impact of Micro/Nanomachines: A Review," *ACS Nano,* vol. 8, pp. 3170-3180, 2014.

[15]   M. Vaezi, H. Seitz, and S. Yang, "A review on 3D micro-additive manufacturing technologies," *The International Journal of Advanced Manufacturing Technology,* vol. 67, pp. 1721-1754, 2012.

[16]   X. Liu, R. E. DeVor, S. G. Kapoor, and K. F. Ehmann, "The Mechanics of Machining at the Microscale: Assessment of the Current State of the Science," *Journal of Manufacturing Science and Engineering,* vol. 126, p. 666, 2004.

[17]   D. Allen, P. T. Tang, L. Staemmler, H. Oosterling, A. Ivanov, A. Herrero*, et al.*, "Comparison between microfabrication technologies for metal tooling," *Proceedings of the Institution of Mechanical Engineers, Part C: Journal of Mechanical Engineering Science,* vol. 220, pp. 1665-1676, 2006.

[18]   K. P. Rajurkar, M. M. Sundaram, and A. P. Malshe, "Review of Electrochemical and Electrodischarge Machining," *Procedia CIRP,* vol. 6, pp. 13-26, 2013.

[19]   M. P. Jahan, M. Rahman, and Y. S. Wong, "A review on the conventional and micro-electrodischarge machining of tungsten carbide," *International Journal of Machine Tools and Manufacture,* vol. 51, pp. 837-858, 2011.

[20]   C. Prakash, H. K. Kansal, B. Pabla, S. Puri, and A. Aggarwal, "Electric discharge machining - A potential choice for surface modification of metallic implants for orthopedic applications: A review," *Proceedings of the Institution of Mechanical Engineers, Part B: Journal of Engineering Manufacture,* vol. 230, pp. 331-353, 2015.

[21]   D. Kanagarajan, R. Karthikeyan, K. Palanikumar, and J. P. Davim, "Application of goal programming technique for Electro Discharge Machining (EDM) characteristics of cemented carbide (WC/Co)," *International Journal of Materials and Product Technology,* vol. 35, p. 216, 2009.

[22]   A. Manna and B. Bhattacharyya, "Taguchi and Gauss elimination method: A dual response approach for parametric optimization of CNC wire cut EDM of PRAlSiCMMC," *The International Journal of Advanced Manufacturing Technology,* vol. 28, pp. 67-75, 2005.

[23]   S. Z. Chavoshi and X. Luo, "Hybrid micro-machining processes: A review," *Precision Engineering,* vol. 41, pp. 1-23, 2015.

[24]   R. K. Garg, K. K. Singh, A. Sachdeva, V. S. Sharma, K. Ojha, and S. Singh, "Review of research work in sinking EDM and WEDM on metal matrix composite materials," *The International Journal of Advanced Manufacturing Technology,* vol. 50, pp. 611-624, 2010.

[25]   K. H. Ho, S. T. Newman, S. Rahimifard, and R. D. Allen, "State of the art in wire electrical discharge machining (WEDM)," *International Journal of Machine Tools and Manufacture,* vol. 44, pp. 1247-1259, 2004.

[26]   G.-L. Chern and Y. Chuang, "Study on vibration-EDM and mass punching of micro-holes," *Journal of Materials Processing Technology,* vol. 180, pp. 151-160, 2006.

[27]   P. Kuppan, S. Narayanan, A. Rajadurai, and M. Adithan, "Effect of EDM parameters on hole quality characteristics in deep hole drilling of Inconel 718 superalloy," *International Journal of Manufacturing Research,* vol. 10, p. 45, 2015.

[28]   C. Gao and Z. Liu, "A study of ultrasonically aided micro-electrical-discharge machining by the application of workpiece vibration," *Journal of Materials Processing Technology,* vol. 139, pp. 226-228, 2003.

[29]   M. P. Jahan, M. Rahman, Y. S. Wong, and L. Fuhua, "On-machine fabrication of high-aspect-ratio micro-electrodes and application in vibration-assisted micro-electrodischarge drilling of tungsten carbide," *Proceedings of the Institution of Mechanical Engineers, Part B: Journal of Engineering Manufacture,* vol. 224, pp. 795-814, 2010.

[30]   M. Ohadi, K. Choo, S. Dessiatoun, and E. Cetegen, "Emerging Applications of Microchannels," pp. 67-105, 2013.

[31]   G. Hang, G. Cao, Z. Wang, J. Tang, Z. Wang, and W. Zhao, "Micro-EDM Milling of Micro Platinum Hemisphere," pp. 579-584, 2006.

[32]   G. Karthikeyan, K. Sambhav, J. Ramkumar, and S. Dhamodaran, "Simulation and experimental realization of μ-channels using a ED-milling process," *Proceedings of the Institution of Mechanical Engineers, Part B: Journal of Engineering Manufacture,* vol. 225, pp. 2206-2219, 2011.

[33]   D. R. Unune and H. S. Mali, "Current status and applications of hybrid micro-machining processes: A review," *Proceedings of the Institution of Mechanical Engineers, Part B: Journal of Engineering Manufacture,* vol. 229, pp. 1681-1693, 2014.

[34]   B. Lauwers, "Surface Integrity in Hybrid Machining Processes," *Procedia Engineering,* vol. 19, pp. 241-251, 2011.

[35]   H. Kurafuji and T. Masuzawa, "Micro-EDM of cemented carbide alloys," *Japanese Society of Electronics and Machining Engineering,* vol. 2, pp. 1-16, 1968.

[36]   M. Jahan, "Micro-Electrical Discharge Machining," in *Nontraditional Machining Processes*, J. P. Davim, Ed., ed: Springer London, 2013, pp. 111-151.

[37]   N. M. Abbas, D. G. Solomon, and M. F. Bahari, "A review on current research trends in electrical discharge machining (EDM)," *International Journal of Machine Tools & Manufacture,* vol. 47, pp. 1214-1228, Jun 2007.

[38]   T. Masuzawa, "State of the Art of Micromachining," *CIRP Annals - Manufacturing Technology,* vol. 49, pp. 473-488, 2000.

[39]   E. Gentili, L. Tabaglio, and F. Aggogeri, "Review on Micromachining Techniques," in *AMST'05 Advanced Manufacturing Systems and Technology*. vol. 486, E. Kuljanic, Ed., ed Vienna: Springer, 2005, pp. 387-396.

[40]   B. M. Schumacher, "After 60 years of EDM the discharge process remains still disputed," *Journal of Materials Processing Technology,* vol. 149, pp. 376-381, 2004.

[41]   M. Rahman, A. B. M. A. Asad, T. Masaki, T. Saleh, Y. S. Wong, and A. Senthil Kumar, "A multiprocess machine tool for compound micromachining," *International Journal of Machine Tools and Manufacture,* vol. 50, pp. 344-356, 2010.

[42]   K. Heinz, "Fundamental study of magnetic field-assisted micro-edm for Non-magnetic materials," Master of Science, Mechanical Engineering, University of Illinois, Urbana-Champaign, 2010.

[43]   S. Mahendran, R. Devarajan, T. Nagarajan, and A. Majdi, "A Review of Micro-EDM," in *Procedings of the International MultiConference of Engineers and Computer Scientist* Hong Kong, 2010.

[44]   E. Uhlmann, S. Piltz, and U. Doll, "Machining of micro/miniature dies and moulds by electrical discharge machining—Recent development," *Journal of Materials Processing Technology,* vol. 167, pp. 488-493, 2005.

[45]   Z. Katz and C. J. Tibbles, "Analysis of micro-scale EDM process," *The International Journal of Advanced Manufacturing Technology,* vol. 25, pp. 923-928, 2004.

[46]   K. P. Rajurkar, G. Levy, A. Malshe, M. M. Sundaram, J. McGeough, X. Hu*, et al.*, "Micro and Nano Machining by Electro-Physical and Chemical Processes," *CIRP Annals - Manufacturing Technology,* vol. 55, pp. 643-666, 2006.

[47]   M. P. Jahan, "Micro-EDM-based multi-process machining of tungsten carbide," PhD, Department of Mechanical Engineering, National University of Singapore, Singapore, 2009.

[48]   D. Reynaerts, P.-H. s. Heeren, and H. Van Brussel, "Microstructuring of silicon by electro-discharge machining (EDM) — part I: theory," *Sensors and Actuators A: Physical,* vol. 60, pp. 212-218, 1997.

[49]   H. R. Shih and K. M. Shu, "A study of electrical discharge grinding using a rotary disk electrode," *The International Journal of Advanced Manufacturing Technology,* vol. 38, pp. 59-67, 2007.

[50]   R. N. Yadav and V. Yadava, "Electric discharge grinding: a review," in *Proceedings of the National Conference on Trends and Advances in Mechanical Engineering*, Faridabad, Haryana, 2012, pp. 590-597.

[51]   L. Dąbrowski and M. Marciniak, "Investigation into hybrid abrasive and electrodischarge machining," *Archives of Civil and Mechanical Engineering,* vol. 5, pp. 5-12, 2005.

[52]   S. K. S. Yadav, V. Yadava, and V. L. Narayana, "Experimental study and parameter design of electro-discharge diamond grinding," *International Journal of Advanced Manufacturing Technology,* vol. 36, pp. 34-42, Feb 2008.

[53]   R. Swiecik, "Experimental investigation of abrasive electrodischarge grinding of Ti6Al4V titanium alloy," *Journal of Achievements in Meterials and Manufacturing Engineering,* vol. 27, pp. 706-711, 2009.

[54]   C. S. Jawalkar, A. K. Sharma, A. Kumar, and P. Kumar, "Micromachining with ECDM: Research Potentials and Experimental Investigations," *World Academy of Science, Engineering & Technology,* vol. 6, pp. 7-12, 2012.

[55]   B. R. Sarkar, B. Doloi, and B. Bhattacharyya, "Parametric analysis on electrochemical discharge machining of silicon nitride ceramics," *The International Journal of Advanced Manufacturing Technology,* vol. 28, pp. 873-881, 2006.

[56]   C. Wei, K. Xu, J. Ni, A. J. Brzezinski, and D. Hu, "A finite element based model for electrochemical discharge machining in discharge regime," *The International Journal of Advanced Manufacturing Technology,* vol. 54, pp. 987-995, 2010.

[57]   Z. P. Zheng, K. L. Wu, and Y. S. Hsu, "Feasibility of 3D surface machining on Pyrex glass by electrochemical discharge machining," in *AEMS07*, Nagoya, Japan, 2007, pp. 98-103.

[58]   J. W. Liu, T. M. Yue, and Z. N. Guo, "Grinding-aided electrochemical discharge machining of particulate reinforced metal matrix composites," *The International Journal of Advanced Manufacturing Technology,* vol. 68, pp. 2349-2357, 2013.

[59]   T. Endo, T. Tsujimoto, and K. Mitsui, "Study of vibration-assisted micro-EDM—The effect of vibration on machining time and stability of discharge," *Precision Engineering,* vol. 32, pp. 269-277, 2008.

[60]   L. Zhang, Z. Jia, W. Liu, and L. Wei, "A study of electrode compensation model improvement in micro-electrical discharge machining milling based on large monolayer thickness," *Proceedings of the Institution of Mechanical Engineers, Part B: Journal of Engineering Manufacture,* vol. 226, pp. 789-802, 2012.

[61]   M. R. Shabgard and H. Alenabi, "Ultrasonic Assisted Electrical Discharge Machining of Ti–6Al–4V Alloy," *Materials and Manufacturing Processes,* vol. 30, pp. 991-1000, 2015.

[62]   D. Kremer, J. L. Lebrun, B. Hosari, and A. Moisan, "Effects of Ultrasonic Vibrations on the Performances in EDM," *CIRP Annals - Manufacturing Technology,* vol. 38, pp. 199-202, 1989.

[63]   H. E. De Bruijn, T. H. Delft, and A. J. Pekelharing, "Effect of a magnetic field on the gap cleaning in EDM," *CIRP Annals: Manufacturing Technology,* vol. 27, pp. 93–95, 1978.

[64]   Y.-C. Lin and H.-S. Lee, "Machining characteristics of magnetic force-assisted EDM," *International Journal of Machine Tools and Manufacture,* vol. 48, pp. 1179-1186, 2008.

[65]   Y.-C. Lin and H.-S. Lee, "Optimization of machining parameters using magnetic-force-assisted EDM based on gray relational analysis," *The International Journal of Advanced Manufacturing Technology,* vol. 42, pp. 1052-1064, 2008.

[66]   P. Koshy, V. K. Jain, and G. K. Lal, "Experimental investigations into electrical discharge machining with a rotating disk electrode," *Precision Engineering,* vol. 15, pp. 6-15, 1993.

[67]   B. Mohan, A. Rajadurai, and K. G. Satyanarayana, "Effect of SiC and rotation of electrode on electric discharge machining of Al–SiC composite," *Journal of Materials Processing Technology,* vol. 124, pp. 297-304, 2002.

[68]   P. Koshy, V. K. Jain, and G. K. Lal, "Mechanism of material removal in electrical discharge diamond grinding," *International Journal of Machine Tools & Manufacture,* vol. 36, pp. 1173-1185, Oct 1996.

[69]   D. R. Unune and H. S. Mali, "Current status and applications of hybrid micro-machining processes: A review," *Proceedings of the Institution of Mechanical Engineers, Part B: Journal of Engineering Manufacture,* 2014.

[70]   J. Kozak, "Abrasive electro discharge grinding (AEDG) of advanced materials," *Arch. Civil Mech. Eng,* vol. 2, pp. 83-101, 2002.

[71]   R. N. Yadav and V. Yadava, "Experimental Study of Erosion and Abrasion based Hybrid Machining of Hybrid Metal Matrix Composite," *International Journal of Precision Engineering and Manufacturing,* vol. 14, pp. 1293-1299, Aug 2013.

[72]   G. K. Singh, V. Yadava, and R. Kumar, "Multiresponse Optimization of Electro-Discharge Diamond Face Grinding Process Using Robust Design of Experiments," *Materials and Manufacturing Processes,* vol. 25, pp. 851-856, 2010.

[73]   G. K. Singh, V. Yadava, and R. Kumar, "Diamond Face Grinding of WC-Co Composite with Spark Assistance: Experimental Study and Parameter Optimization," *International Journal of Precision Engineering and Manufacturing,* vol. 11, pp. 509-518, Aug 2010.

[74]   G. K. Singh, V. Yadava, and R. Kumar, "Robust parameter design and multi-objective optimisation of electro-discharge diamond face grinding of HSS," *International Journal of Machining and Machinability of Materials,* vol. 11, p. 1, 2012.

[75]   S. S. Agrawal and V. Yadava, "Modeling and Prediction of Material Removal Rate and Surface Roughness in Surface-Electrical Discharge Diamond Grinding Process of Metal Matrix Composites," *Materials and Manufacturing Processes,* vol. 28, pp. 381-389, Apr 1 2013.

[76]   H. Kumar, R. Choudhary, and S. Singh, "Experimental and Morphological Investigations Into Electrical Discharge Surface Grinding (EDSG) of 6061Al/Al2O3p 10% Composite by Composite Tool Electrode," *Journal of Materials Engineering and Performance,* vol. 23, pp. 1489-1497, 2014.

[77]   F. Klocke, D. Lung, G. Antonoglou, and D. Thomaidis, "The effects of powder suspended dielectrics on the thermal influenced zone by electrodischarge machining with small discharge energies," *Journal of Materials Processing Technology,* vol. 149, pp. 191-197, 2004.

[78]   H. K. Kansal, S. Singh, and P. Kumar, "Parametric optimization of powder mixed electrical discharge machining by response surface methodology," *Journal of Materials Processing Technology,* vol. 169, pp. 427-436, 2005.

[79]   A. Kumar, S. Maheshwari, C. Sharma, and N. Beri, "A Study of Multiobjective Parametric Optimization of Silicon Abrasive Mixed Electrical Discharge Machining of Tool Steel," *Materials and Manufacturing Processes,* vol. 25, pp. 1041-1047, 2010.

[80]   A. Kumar, S. Maheshwari, C. Sharma, and N. Beri, "Analysis of Machining Characteristics in Additive Mixed Electric Discharge Machining of Nickel-Based Super Alloy Inconel 718," *Materials and Manufacturing Processes,* vol. 26, pp. 1011-1018, 2011.

[81]   S. Kumar and U. Batra, "Surface modification of die steel materials by EDM method using tungsten powder-mixed dielectric," *Journal of Manufacturing Processes,* vol. 14, pp. 35-40, 2012.

[82]   X. Tian, J. Zhao, J. Zhao, Z. Gong, and Y. Dong, "Effect of cutting speed on cutting forces and wear mechanisms in high-speed face milling of Inconel 718 with Sialon ceramic tools," *The International Journal of Advanced Manufacturing Technology,* vol. 69, pp. 2669-2678, 2013.

[83]   M. S. Cheong, D.-W. Cho, and K. F. Ehmann, "Identification and control for micro-drilling productivity enhancement," *International Journal of Machine Tools and Manufacture,* vol. 39, pp. 1539-1561, 1999.

[84]   J. Chae, S. S. Park, and T. Freiheit, "Investigation of micro-cutting operations," *International Journal of Machine Tools and Manufacture,* vol. 46, pp. 313-332, 2006.

[85]   L. Li, D. K. Y. Low, M. Ghoreshi, and J. R. Crookall, "Hole Taper Characterisation and Control in Laser Percussion Drilling," *CIRP Annals - Manufacturing Technology,* vol. 51, pp. 153-156, 2002.

[86]   M. Imran, P. T. Mativenga, A. Gholinia, and P. J. Withers, "Evaluation of surface integrity in micro drilling process for nickel-based superalloy," *The*

International Journal of Advanced Manufacturing Technology, vol. 55, pp. 465-476, 2010.

[87]   K. P. Rajurkar and Z. Y. Yu, "3D Micro-EDM Using CAD/CAM," *CIRP Annals - Manufacturing Technology,* vol. 49, pp. 127-130, 2000.

[88]   P. Kuppan, A. Rajadurai, and S. Narayanan, "Influence of EDM process parameters in deep hole drilling of Inconel 718," *The International Journal of Advanced Manufacturing Technology,* vol. 38, pp. 74-84, 2007.

[89]   O. Yilmaz and M. A. Okka, "Effect of single and multi-channel electrodes application on EDM fast hole drilling performance," *The International Journal of Advanced Manufacturing Technology,* vol. 51, pp. 185-194, 2010.

[90]   E. Bassoli, L. Denti, A. Gatto, and L. Iuliano, "Influence of electrode size and geometry in electro-discharge drilling of Inconel 718," *The International Journal of Advanced Manufacturing Technology,* 2016.

[91]   M. Ay, U. Çaydaş, and A. Hasçalık, "Optimization of micro-EDM drilling of inconel 718 superalloy," *The International Journal of Advanced Manufacturing Technology,* vol. 66, pp. 1015-1023, 2012.

[92]   D. R. Unune and H. S. Mali, "Performance Investigations of Different Electrode Materials in Micro-EDM Drilling of Inconel-718," presented at the International Conference on Precision, Meso, Micro and Nano Engineering (Copen-9), Victor Menezes Convocation Centre, IIT Bombay, 2015.

[93]   G. D'Urso, G. Maccarini, and C. Ravasio, "Process performance of micro-EDM drilling of stainless steel," *The International Journal of Advanced Manufacturing Technology,* vol. 72, pp. 1287-1298, 2014.

[94]   G. D'Urso, G. Maccarini, and C. Ravasio, "Influence of electrode material in micro-EDM drilling of stainless steel and tungsten carbide," *The International Journal of Advanced Manufacturing Technology,* 2015.

[95]   G. D'Urso, G. Maccarini, M. Quarto, and C. Ravasio, "Investigation on power discharge in micro-EDM stainless steel drilling using different electrodes," *Journal of Mechanical Science and Technology,* vol. 29, pp. 4341-4349, 2015.

[96]   L. Li, C. Diver, J. Atkinson, R. Giedl-Wagner, and H. J. Helml, "Sequential Laser and EDM Micro-drilling for Next Generation Fuel Injection Nozzle Manufacture," *CIRP Annals - Manufacturing Technology,* vol. 55, pp. 179-182, 2006.

[97]   A. M. A. Al-Ahmari, M. S. Rasheed, M. K. Mohammed, and T. Saleh, "A Hybrid Machining Process Combining Micro-EDM and Laser Beam Machining of Nickel–Titanium-Based Shape Memory Alloy," *Materials and Manufacturing Processes,* pp. 1-9, 2015.

[98]   G. S. Prihandana, M. Mahardika, M. Hamdi, Y. S. Wong, and K. Mitsui, "Effect of micro-powder suspension and ultrasonic vibration of dielectric fluid in micro-EDM processes—Taguchi approach," *International Journal of Machine Tools and Manufacture,* vol. 49, pp. 1035-1041, 2009.

[99]   M. P. Jahan, Y. S. Wong, and M. Rahman, "Evaluation of the effectiveness of low frequency workpiece vibration in deep-hole micro-EDM drilling of tungsten carbide," *Journal of Manufacturing Processes,* vol. 14, pp. 343-359, 2012.

[100]   K. Heinz, S. G. Kapoor, R. E. DeVor, and V. Surla, "An Investigation of Magnetic-Field-Assisted Material Removal in Micro-EDM for Nonmagnetic Materials," *Journal of Manufacturing Science and Engineering,* vol. 133, p. 021002, 2011.

[101]   P. A. Lee, Y. Kim, and B. H. Kim, "Effect of low frequency vibration on micro EDM drilling," *International Journal of Precision Engineering and Manufacturing,* vol. 16, pp. 2617-2622, 2015.

[102]   L. Li, Y. B. Guo, X. T. Wei, and W. Li, "Surface Integrity Characteristics in Wire-EDM of Inconel 718 at Different Discharge Energy," *Procedia CIRP,* vol. 6, pp. 220-225, 2013.

[103] J. Wang, F. Yang, J. Qian, and D. Reynaerts, "Study of alternating current flow in micro-EDM through real-time pulse counting," *Journal of Materials Processing Technology,* vol. 231, pp. 179-188, 2016.

[104] J. W. Murray, J. Sun, D. V. Patil, T. A. Wood, and A. T. Clare, "Physical and electrical characteristics of EDM debris," *Journal of Materials Processing Technology,* vol. 229, pp. 54-60, 2016.

[105] X. Chu, K. Zhu, C. Wang, Z. Hu, and Y. Zhang, "A Study on Plasma Channel Expansion in Micro-EDM," *Materials and Manufacturing Processes,* vol. 31, pp. 381-390, 2015.

[106] R. Mehfuz and M. Y. Ali, "Investigation of machining parameters for the multiple-response optimization of micro electrodischarge milling," *The International Journal of Advanced Manufacturing Technology,* vol. 43, pp. 264-275, 2008.

[107] G. Karthikeyan, J. Ramkumar, S. Dhamodaran, and S. Aravindan, "Micro electric discharge milling process performance: An experimental investigation," *International Journal of Machine Tools and Manufacture,* vol. 50, pp. 718-727, 2010.

[108] G. Karthikeyan, A. K. Garg, J. Ramkumar, and S. Dhamodaran, "A microscopic investigation of machining behavior in μED-milling process," *Journal of Manufacturing Processes,* vol. 14, pp. 297-306, 2012.

[109] B. Kuriachen and J. Mathew, "Experimental Investigations into the Effects of Microelectric-Discharge Milling Process Parameters on Processing Ti–6Al–4V," *Materials and Manufacturing Processes,* vol. 30, pp. 983-990, 2014.

[110] Z. Y. Yu, T. Masuzawa, and M. Fujino, "Micro-EDM for Three-Dimensional Cavities - Development of Uniform Wear Method," *CIRP Annals - Manufacturing Technology,* vol. 47, pp. 169-172, 1998.

[111] Z. Y. Yu, T. Masuzawa, and M. Fujino, "3D micro-EDM with simple shape electrode Part1: Machining of cavities with sharp corners and electrode wear

compensation," in *Proceedings of The 4th Korea-Russia International Symposium on Science and Technology*, KORUS, 2000.

[112] Z. Y. Yu, J. Kozak, and K. P. Rajurkar, "Modelling and Simulation of Micro EDM Process," *CIRP Annals - Manufacturing Technology,* vol. 52, pp. 143-146, 2003.

[113] W. Zhao, Y. Yang, Z. Wang, and Y. Zhang, "A CAD/CAM system for micro-ED-milling of small 3D freeform cavity," *Journal of Materials Processing Technology,* vol. 149, pp. 573-578, 2004.

[114] V. Shukla, S. N. Akhtar, S. K. Subbu, and J. Ramkumar, "Fabrication of Complex Micro Channels by Micro Electric Discharge Milling (µ-ED Milling)," p. V02BT02A072, 2013.

[115] J. M. Jafferson, P. Hariharan, and J. Ram Kumar, "Effects of Ultrasonic Vibration and Magnetic Field in Micro-EDM Milling of Nonmagnetic Material," *Materials and Manufacturing Processes,* vol. 29, pp. 357-363, 2014.

[116] M. Kunleda, Y. Miyoshi, T. Takaya, N. Nakajima, Y. ZhanBo, and M. Yoshida, "High Speed 3D Milling by Dry EDM," *CIRP Annals - Manufacturing Technology,* vol. 52, pp. 147-150, 2003.

[117] S. Su, Q. B. Zhang, Q. Zhang, and J. H. Zhang, "Investigation and simulation of ultrasonic vibration electrical discharge milling in gas," in *International Technology and Innovation Conference* Hangzhou, 2006.

[118] (2013, 6 June 2014). *MIKROTOOLS: Hybrid µ-EDM*. Available: http://mikrotools.com/hybriduedm/hybrid-uedm-introduction/

[119] M. Modi and G. Agarwal, "Design, Development & Experimental Investigation of Electro-Discharge Diamond Surface Grinding of Ti-6Al-4V," *International Journal of Advanced Materials Research,* vol. 418- 420, pp. 1478-1481, 2012.

[120] M. P. Jahan, Y. S. Wong, and M. Rahman, "A comparative experimental investigation of deep-hole micro-EDM drilling capability for cemented carbide

(WC-Co) against austenitic stainless steel (SUS 304)," *The International Journal of Advanced Manufacturing Technology,* vol. 46, pp. 1145-1160, 2009.

[121] B. Kuriachen and J. Mathew, "Effect of Powder Mixed Dielectric on Material Removal and Surface Modification in Microelectric Discharge Machining of Ti-6Al-4V," *Materials and Manufacturing Processes,* vol. 31, pp. 439-446, 2015.

[122] P. Koshy, V. K. Jain, and G. K. Lal, "Grinding of cemented carbide with electrical spark assistance," *Journal of Materials Processing Technology,* vol. 72, pp. 61-68, 1997.

[123] S. Youssefi, Z. Emam-Djomeh, and S. M. Mousavi, "Comparison of Artificial Neural Network (ANN) and Response Surface Methodology (RSM) in the Prediction of Quality Parameters of Spray-Dried Pomegranate Juice," *Drying Technology,* vol. 27, pp. 910-917, 2009.

[124] V. Aggarwal, S. S. Khangura, and R. K. Garg, "Parametric modeling and optimization for wire electrical discharge machining of Inconel 718 using response surface methodology," *The International Journal of Advanced Manufacturing Technology,* vol. 79, pp. 31-47, 2015.

[125] D. C. Montgomery, *Design and Analysis of Experiments*, 8 ed. New York: John Wiley & Sons, Inc., 2013.

[126] R. N. Yadav and V. Yadava, "Influence of Input Parameters on Machining Performances of Slotted-Electrical Discharge Abrasive Grinding of Al/SiC/Gr Metal Matrix Composite," *Materials and Manufacturing Processes,* vol. 28, pp. 1361-1369, Dec 2 2013.

[127] P. Peças and E. Henriques, "Electrical discharge machining using simple and powder-mixed dielectric: The effect of the electrode area in the surface roughness and topography," *Journal of Materials Processing Technology,* vol. 200, pp. 250-258, 2008.

[128] T. A. El-Taweel and S. A. Gouda, "Performance analysis of wire electrochemical turning process—RSM approach," *The International Journal of Advanced Manufacturing Technology,* vol. 53, pp. 181-190, 2010.

[129] A. Kumar, V. Kumar, and J. Kumar, "Multi-response optimization of process parameters based on response surface methodology for pure titanium using WEDM process," *The International Journal of Advanced Manufacturing Technology,* vol. 68, pp. 2645-2668, 2013.

[130] R. O. Kuehl, *Design of experiments: statistical principles of research design and analysis*, 2nd ed. Pacific Grove: Duxbury/Thomson Learning, 2000.

[131] M. P. Jahan, Y. S. Wong, and M. Rahman, "A study on the quality micro-hole machining of tungsten carbide by micro-EDM process using transistor and RC-type pulse generator," *Journal of Materials Processing Technology,* vol. 209, pp. 1706-1716, 2009.

[132] K. P. Maity and R. K. Singh, "An optimisation of micro-EDM operation for fabrication of micro-hole," *The International Journal of Advanced Manufacturing Technology,* vol. 61, pp. 1221-1229, 2012.

[133] H. K. Dave, V. J. Mathai, K. P. Desai, and H. K. Raval, "Studies on quality of microholes generated on Al 1100 using micro-electro-discharge machining process," *The International Journal of Advanced Manufacturing Technology,* vol. 76, pp. 127-140, 2014.

[134] H.-S. Liu, B.-H. Yan, F.-Y. Huang, and K.-H. Qiu, "A study on the characterization of high nickel alloy micro-holes using micro-EDM and their applications," *Journal of Materials Processing Technology,* vol. 169, pp. 418-426, 2005.

[135] K. Mondol, M. S. Azad, and A. B. Puri, "Analysis of micro-electrical discharge drilling characteristics in a thin plate of Ti–6Al–4 V," *The International Journal of Advanced Manufacturing Technology,* vol. 76, pp. 141-150, 2013.

[136] H.-L. Yu, J.-J. Luan, J.-Z. Li, Y.-S. Zhang, Z.-Y. Yu, and D.-M. Guo, "A new electrode wear compensation method for improving performance in 3D micro

EDM milling," *Journal of Micromechanics and Microengineering,* vol. 20, p. 055011, 2010.

[137] Y.-Y. Tsai and T. Masuzawa, "An index to evaluate the wear resistance of the electrode in micro-EDM," *Journal of Materials Processing Technology,* vol. 149, pp. 304-309, 2004.

[138] O. Thao and S. S. Joshi, "Analysis of heat affected zone in the micro-electric discharge machining," *International Journal of Manufacturing Technology and Management,* vol. 13, p. 201, 2008.

Appendix A   Investigation   on   electro discharge diamond grinding of Inconel 718

The performance of electro discharge diamond surface grinding (EDDSG) on machining Inconel 718 has been investigated on MRR and average surface roughness. The EDDG setup as shown in Figure 3.4 has been used and experiments have been performed in surface grinding mode.

A.1 Control factors and their range

The wheel speed (W_S), current (C), POT (T_{on}), and duty factor (DF) were selected as control factors while MRR and R_a were chosen as performance measures. These control factors and their range were decided based on the literature, pilot experimentation, manufacturer's manual, and machine competence. The independent control factors and their levels in coded and actual values are shown in Table A.1.

Table A.1 Experimental control factors and their levels

Control factors (symbol)	Notation		Level				
	Unit		-2	-1	0	+1	+2
Wheel speed (A)	rpm	W_S	700	850	1000	1150	1300
Current (B)	A	C	2	4	6	8	10
Pulse-on-time (C)	µs	T_{on}	17	20	23	26	29
Duty factor (D)		DF	0.60	0.63	0.67	0.70	0.73

A.2 Experimental design

In this study, the experiments conducted based on the central composite design (CCD) of RSM. The experimental design matrix with a combination of control factors and corresponding performance measure values obtained from experimentation are listed in Table A.2.

Table A.2 Experimental matrix and observations during EDDG of Inconel 718

Std	Run	Control Factors				Performance Measures	
		Wheel Speed	Current	Pulse-on-Time	Duty factor	Material removal rate	Average Surface Roughness
		W_S (rpm)	C (A)	T_{on} (µs)	DF	MRR (mm³/min)	R_a (µm)
3	1	700	6	20	0.63	6.129	4.872
8	2	1300	6	26	0.63	22.344	2.703
12	3	1300	6	20	0.70	12.168	2.228
7	4	700	6	26	0.63	5.267	6.575
23	5	1000	4	23	0.60	16.377	5.535
5	6	700	2	26	0.63	5.422	3.870
27	7	1000	4	23	0.67	6.004	3.484
14	8	1300	2	26	0.70	11.156	2.228
26	9	1000	4	23	0.67	6.004	2.284
22	10	1000	4	29	0.67	13.443	3.583
25	11	1000	4	23	0.67	6.004	2.492
21	12	1000	4	17	0.67	4.515	2.230
28	13	1000	4	23	0.67	6.004	2.612
6	14	1300	2	26	0.63	17.919	3.383
24	15	1000	4	23	0.73	7.571	2.228
30	16	1000	4	23	0.67	6.004	2.312
20	17	1000	8	23	0.67	15.353	3.730
18	18	1600	4	23	0.67	22.326	2.229
17	19	400	4	23	0.67	4.959	7.126

9	20	700	2	20	0.70	4.469	4.420
16	21	1300	6	26	0.70	21.827	2.232
15	22	700	6	26	0.70	7.356	8.755
19	23	1000	0	23	0.67	8.127	5.270
11	24	700	6	20	0.70	6.277	7.889
29	25	1000	4	23	0.67	6.004	1.892
1	26	700	2	20	0.63	6.335	2.246
13	27	700	2	26	0.70	5.286	4.228
10	28	1300	2	20	0.70	4.701	2.228
4	29	1300	6	20	0.63	22.280	2.341
2	30	1300	2	20	0.63	21.230	2.360

A.3 Empirical models for performance measures

Analysis of variance (ANOVA) was executed to statistically investigate the results of the selected model. Significant control factors were recognized and interaction effects of these control factors on performance measures were studied using response surface graphs.

A.3.1 ANOVA for material removal rate

The experimental results for MRR shown in Table A.2 were examined using Design-Expert software. The results of ANOVA after backward elimination are summarized in Table A.3. The model F-value of 28.09 with its Prob>F value less than 0.0001 directs that the model is significant for MRR as it validates that the terms in the model have a significant effect on the response. There is only a 0.01 % chance that such a large model F value could occur due to noise. The significant model terms for MRR along with their percentage contributions are shown in Table A.3. The determination coefficient for MRR is found to be 0.9520 which suggest that the established model is accomplished of explaining the variation on MRR up to 95.20 % and model is adequate in

demonstrating the process. The other R^2 statistics, the Pred R^2 (0.8354), is in good agreement with the Adj R^2 (0.9181). The smaller value confirms enhanced accuracy and consistency of the performed experiments. The Adeq Precision found for the model is 17.64, which is well more than desired value of 4 and thus specifies a sufficient signal for the model. Hence, this model may be used to navigate the design space and forecast the values of the MRR within the limits of the factors studied.

Table A.3 The ANOVA Table for MRR

Source	Sum of squares	df	Mean square	F value	p-Value Prob. > F		% contri.
Model	1126.77	12	93.90	28.09	< 0.0001	significant	
W_s	618.33	1	618.33	184.96	< 0.0001		54.88
C	72.04	1	72.04	21.55	0.0002		6.39
T_{on}	39.64	1	39.64	11.86	0.0031		3.52
DF	109.65	1	109.65	32.80	< 0.0001		9.73
$W_s \times C$	25.24	1	25.24	7.55	0.0137		2.24
$W_s \times T_{on}$	10.15	1	10.15	3.04	0.0994		0.90
$W_s \times DF$	72.91	1	72.91	21.81	0.0002		6.47
$C \times DF$	17.86	1	17.86	5.34	0.0336		1.59
$T_{on} \times DF$	33.15	1	33.15	9.92	0.0059		2.94
W_s ^2	76.53	1	76.53	22.89	0.0002		6.79
C^2	38.82	1	38.82	11.61	0.0034		3.45
DF^2	42.78	1	42.78	12.80	0.0023		3.80
Residual	56.83	17	3.34				
Lack of Fit	52.01	12	4.33	4.50	0.0541	not significant	
Pure Error	4.82	5	0.96				
Cor Total	1183.61	29					
Std. Dev.		1.83		R-Squared		0.9520	
Mean		10.39		Adj R-Squared		0.9181	
C.V. %		17.59		Pred R-Squared		0.8354	
PRESS		194.78		Adeq Precision		17.645	

Regression equation for MRR

The empirical relation between the MRR and control factors (actual terms) can be expressed by the following second-order polynomial Eq.(iv):

$$MRR = 630.15 + 0.0866 \times W_s - 13.618 \times C - 9.573 \times T_{on} - 1575.39 \times DF$$

$$+ (2.0933 \times 10^{-3}) \times WS \times C + (8.85 \times 10^{-4})W_s \times T_{on} - 0.20331$$

$$\times W_s \times DF + 15.0917 \times C \times DF + 13.71 \times T_{on} \times DF$$

$$+ (1.83 \times 10^{-5}) \times W_s^2 + 0.294 \times C^2 + 1008.98 \times DF^2 \quad \dots\dots(iv)$$

A.3.2 ANOVA for surface roughness

The experimental results listed in Table A.2 were analyzed for ANOVA of average surface roughness. The results of ANOVA after backward elimination are summarized in Table A.4.

Table A.4 The ANOVA Table for Ra

Source	Sum of squares	df	Mean square	F value	p-Value Prob. > F		% contri.
Model	77.68	7	11.10	9.65	< 0.0001	significant	
W_s	45.23	1	45.23	39.35	< 0.0001		58.23
C	3.80	1	3.80	3.31	0.0827		4.89
DF	0.024	1	0.024	0.021	0.8867		0.03
$W_s \times C$	12.29	1	12.29	10.69	0.0035		15.82
$W_s \times DF$	5.76	1	5.76	5.01	0.0357		7.42
W_s ^2	6.44	1	6.44	5.60	0.0271		8.29
C^2	5.30	1	5.30	4.61	0.0431		6.82
Residual	25.29	22	1.15				
Lack of Fit	23.86	17	1.40	0.90	0.837	non significant	
Pure Error	1.43	5	0.29				
Cor Total	102.97	29					
Std. Dev.		1.07		R-Squared	0.8120		
Mean		3.65		Adj R-Squared	0.7274		
C.V. %		21.59		Pred R-Squared	0.6916		
PRESS		70.64		Adeq Precision	11.242		

Model F-value of 9.65 indicates that the model is significant. There is only a 0.01 % chance that a model F value this large could occur due to noise. Values of Prob>F less than 0.0500 indicate that the model terms are significant. The significant model terms along with their percentage contribution are listed in **Error! Reference source not ound.**. The other model statistics are also representing good model fit. Therefore, this quadratic model can be used to navigate the design space and considered substantial for fitting and predicting the experimental results.

Regression equation for average surface roughness

The empirical relation between the R_a and control factors (actual terms) expressed by the following second-order polynomial.

$$R_a = +83.75096 + 0.0277 \times W_s + 0.71 \times C + 0.11245 \times T_{on} - 291.2314 \times DF$$
$$- (1.46 \times 10^{-3}) \times W_s \times C - 0.05714 \times WS \times DF$$
$$+ (5.767 \times 10^{-6}) \times W_s{}^2 + 261.255 \times DF^2 \qquad \dots\dots(v)$$

A.4 Results and discussion

Perturbation plot and three-dimensional (3D) response curves have been used to discuss the effects of individual control factors as well as their interactions on the performance measures.

A.4.1 Influence of control factors on material removal rate

The comparative effects of significant control factors on MRR of Inconel 718 by EDDSG were shown in Perturbation plot (Figure A.1). A sharp slope for wheel speed and current directs that the MRR is highly sensitive to these factors while a relatively flat line for POT and duty factor directs towards comparatively less sensitivity of MRR towards them. The reasons for above results have been discussed in successive paragraphs while explaining the interaction effects.

Interactive effects of control factors on material removal rate

It is observed from the Table A.3 that the interactions which significantly contributes to the model are those between the wheel speed and current '$Ws{\times}C$', wheel speed and pulse-on-time '$W_s{\times}T_{on}$', wheel speed and duty factor '$W_s{\times}DF$', current and duty factor '$C{\times}DF$', and pulse-on-time and duty factor '$T_{on}{\times}DF$' and the interaction plots corresponding to these interaction terms are shown in Figure A.2 (a), (b), (c), (d), and (e) respectively.
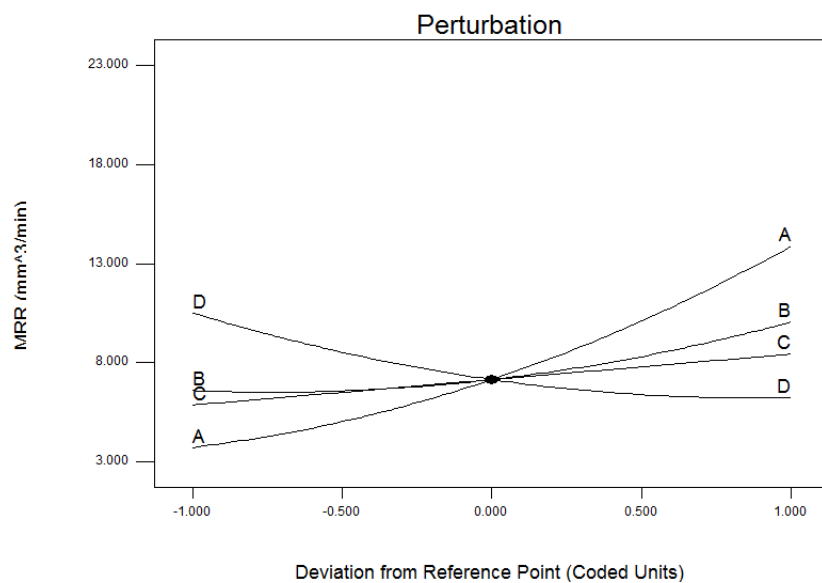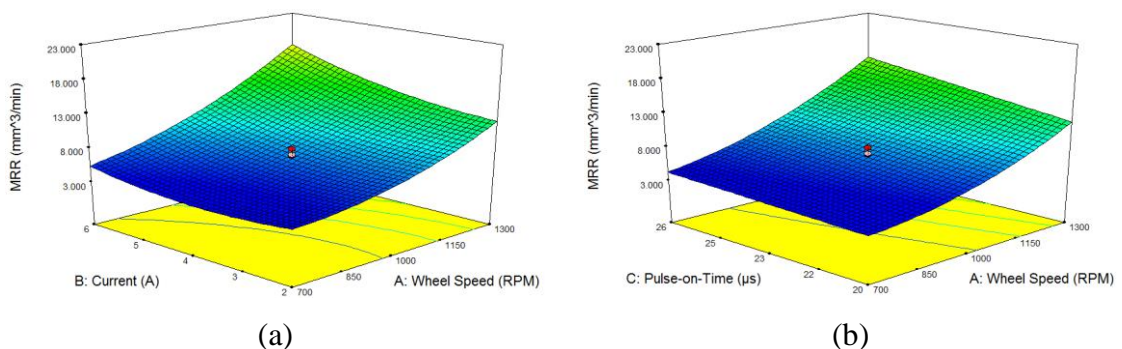

Figure A.1 Perturbation plot for MRR

It is seen that the MRR increases with increase in wheel speed, current, and pulse-on-time. The reasons behind the increase of MRR with an increase in wheel speed, current, and pulse-on-time are already discussed in section 0.
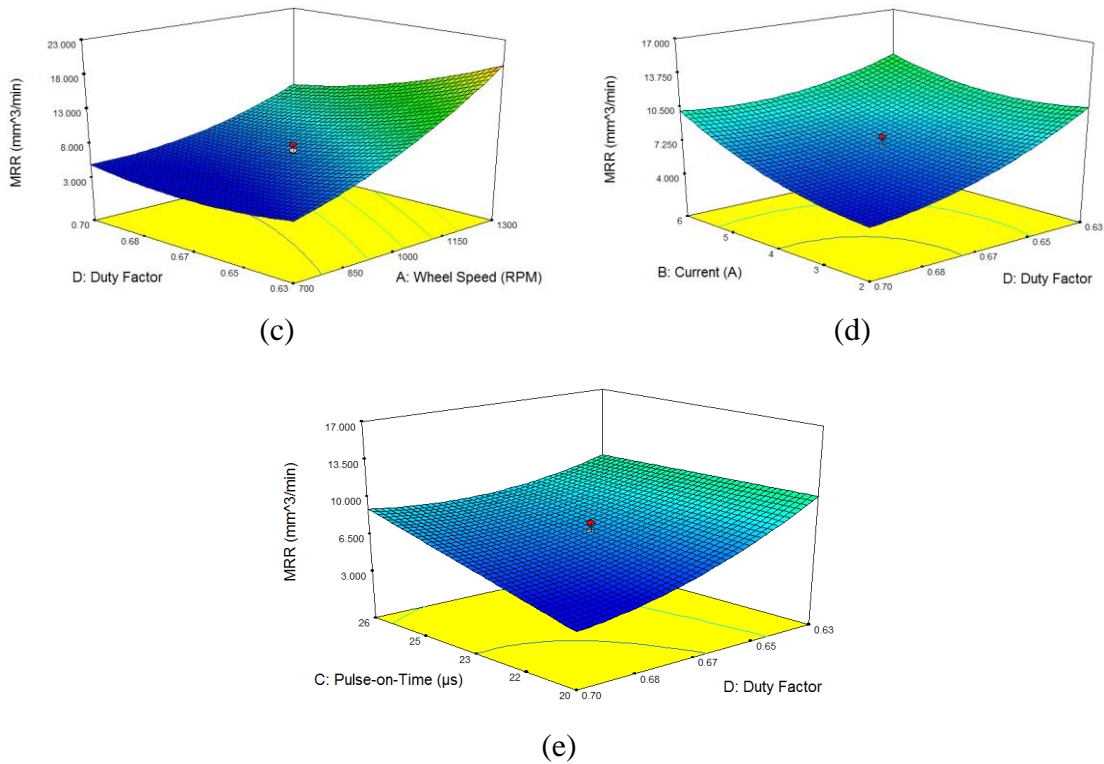

(a)

(b)

171

(c)

(d)

(e)

Figure A.2 (a), (b), (c), (d), and (e) shows the response graph of MRR

A.4.2 Influence of control factors on average surface roughness

The Perturbation plot for average surface roughness is shown in Figure A.3. A steep slope for wheel speed shows that the surface roughness is very sensitive to this factor.
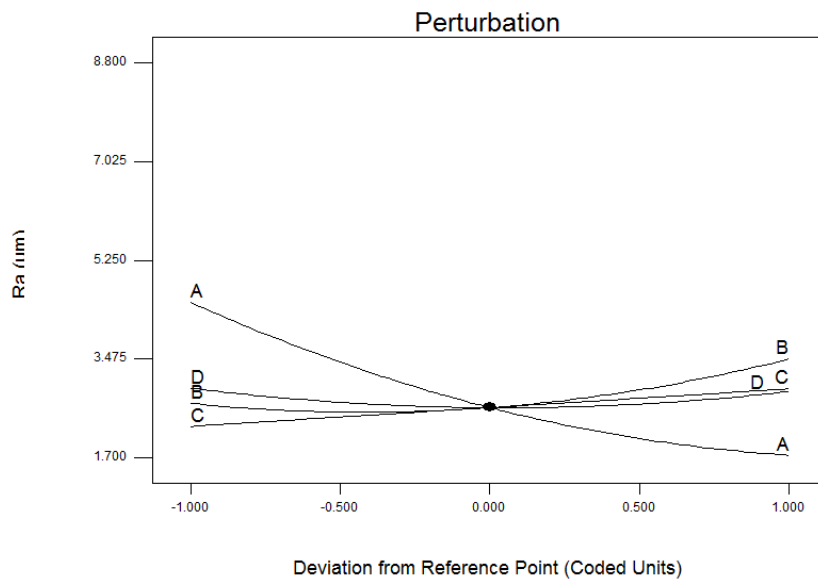

Figure A.3 Perturbation plots for Ra

Interactive Effects of Control Factors on Average Surface Roughness

The ANOVA results (Table A.4) shows that the interactions contributing significantly to the model are those between wheel speed and current '$Ws \times C$', wheel speed and duty factor '$Ws \times DF$'. It was observed that with an increase in wheel speed the surface roughness decreases. However, with an increase in current, pulse-on-time and duty factor, the surface roughness increases.
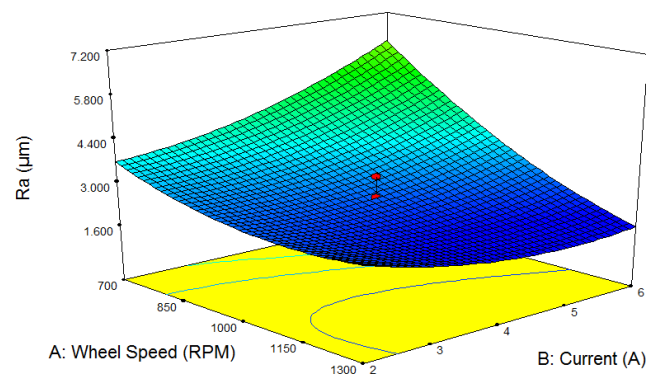
(a)
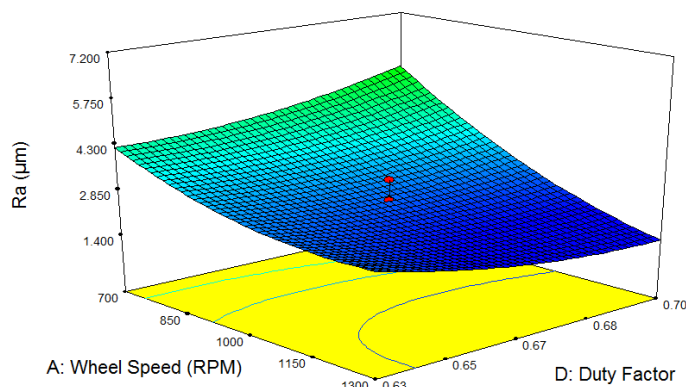
(b)

Figure A.4 (a), (b), and (c) shows the response graph of Ra

A.5 Summary

An experimental investigation has been performed to investigate the performance of EDDSG on machining of Inconel 718. The effects of the wheel speed (W_S), current (C), POT (T_{on}), and duty factor (DF) were examined on MRR and R_a. The wheel speed was observed to most significant control factor for both MRR and R_a. It was noted that with

an increase in wheel speed the MRR increase while the surface roughness decreases. Thus, the results of hybridizing EDM and surface grinding seen to positive enhancing the machining performance and the hybrid EDDSG found to be useful in fabricating the good surface finished components at high machining rate.

Appendix B   Investigations of different electrode materials in μ-ED drilling of Inconel-718

A study was carried out to identify the suitable electrode material for μ-ED drilling of Inconel 718 by investigating the influence of electrode material on process performance and geometrical accuracy of fabricated micro-holes. The copper, tungsten-copper and tungsten electrodes were chosen on the basis of their dissimilar electrical and thermal properties.

B.1 Control factors and their range

The tool wear is considered as a very critical factor in μ-ED drilling as wear of tool lead to reduced dimensional accuracy, shape and size of fabricated micro-features [95]. To offer solutions to minimize the tool wear researchers proposed different methods like uniform wear method, a model for volumetric wear ratio estimations, on-machine measurements, and reshaping of tool etc. [43]. However, the choice of electrode material has a vital impact on accuracy and shape of the final micro-feature produced in micro-EDM based operation. Therefore, three different electrode materials viz. copper, copper-tungsten, tungsten were chosen for comparison purpose. The properties of electrode material are shown in Table B.1. The experimental conditions are shown in Table B.2.

Table B.1 Properties of different electrode materials

Electrode material	Cooper (Cu)	Copper-tungsten (Cu-W)	Tungsten (W)
Composition (%)	99.9% Cu	40%Cu-60%W	99.9%W
Density (g.cm3)	8.92	12.6	19.3
Thermal conductivity (W/mK)	401	160	129
Electrical Conductivity (% I.A.C.S)	100	33	30

Table B.2 Experimental conditions

|	
Workpiece material	Inconel 718
Electrode materials	Cu, Cu-W, W
Dielectric fluid	Total EDM3 oil
Voltage (V)	80,90,100,110,120
Capacitance (µF)	0.001, 0.01,0.1,0.4

B.2 Results and discussion:

The effect of gap voltage and capacitance on MRR, EWR, overcut and taper angle with different electrode materials on the performance of µ-ED drilling of Inconel 718 are shown in Figure B.1, Figure B.2, Figure B.3 and Figure B.4, respectively. It was observed that the MRR increases with increase in both gap voltage as well as capacitance. The higher is gap voltage and capacitance then higher is discharge energy which will act on the workpiece increasing the MRR. The higher amount of spark discharge energy results in rapid melting and evaporation of workpiece material and thus increases MRR.

It was noticed that the electrode material plays a significant role in deciding the MRR. The dielectric breakdown in EDM action is dependent on both workpieces as well as an electrode material. The electrode material has a more noticeable effect on the breakdown of dielectric since it plays the first role in the breakdown on dielectric when

bare to pulse voltage or short term DC and AC voltages. Also, the electrical and thermal properties of electrode material are off important consideration as the dielectric breakdown also shows the dependency on these parameters. Being an electro-thermal process, the electrical and thermal conductivity and the melting points of both the electrode and workpiece material attributes major role in the EDM performance. It was observed that the copper electrodes results in highest MRR at all values of gap voltage and capacitance values, followed by copper-tungsten and tungsten electrodes.
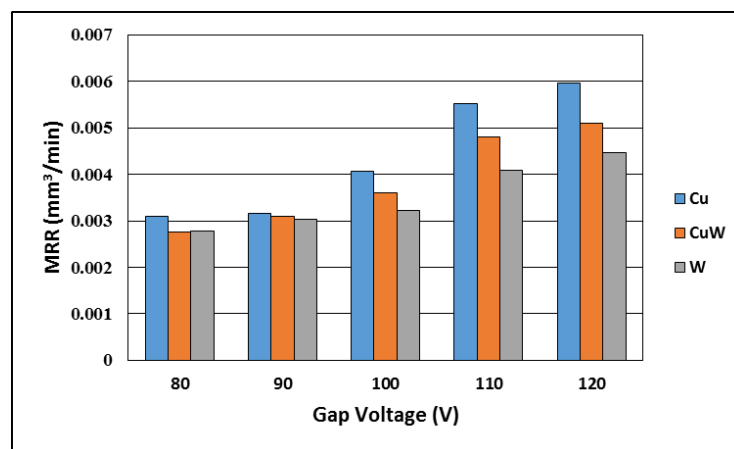
(a)
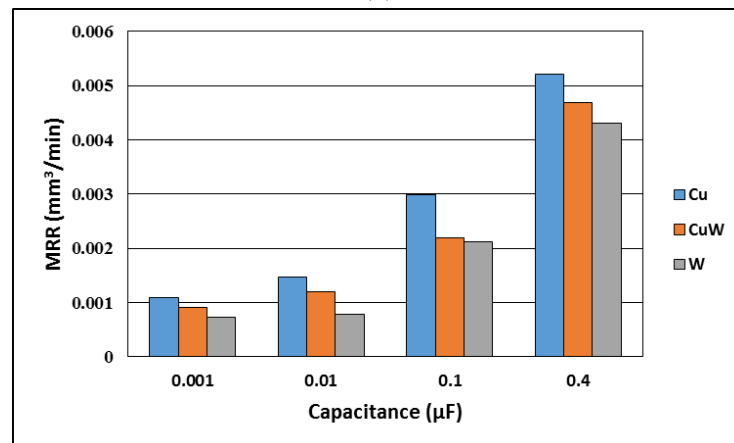
(b)

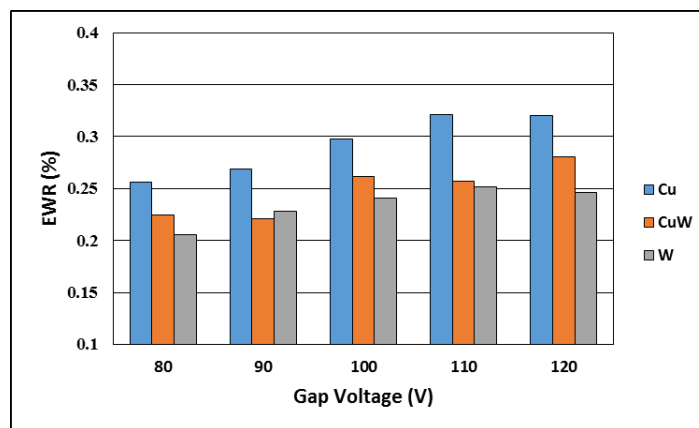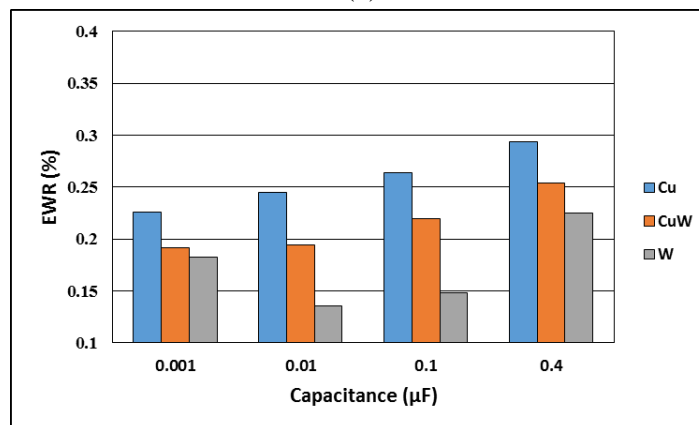*Figure B.1 Variation in MRR with (a) gap voltage and (b) capacitance*

As the high electrical and thermal conductivity of electrodes are more influencing factors on MRR, therefore the electrode material with higher electrical conductivity aids faster sparking process and improves the effectiveness of pulse resulting in higher MRR. The higher thermal conductivity is also significant to raise the temperature of the

workpiece above the melting point faster. The better performance of copper as compared to copper-tungsten and tungsten electrodes is resulted due to above reasons.

The comparison of electrode wear ratio (EWR) for different electrodes during micro-EDM drilling of Inconel 718 is represented in Figure B.2. It was observed that EWR increases with increase in both gap voltage and capacitance. At higher values of gap voltage and capacitance, a higher amount of discharge energy acts on electrodes also, thereby evaporating more electrode material. Further, the different properties viz. evaporation point, melting point, thermal conductivity, and thermal diffusivity are the important properties that influence the electrode wear of an electrode [137]. Higher melting and evaporation point is of critical requirement for electrode materials for having efficient EWR.


(a)

(b)

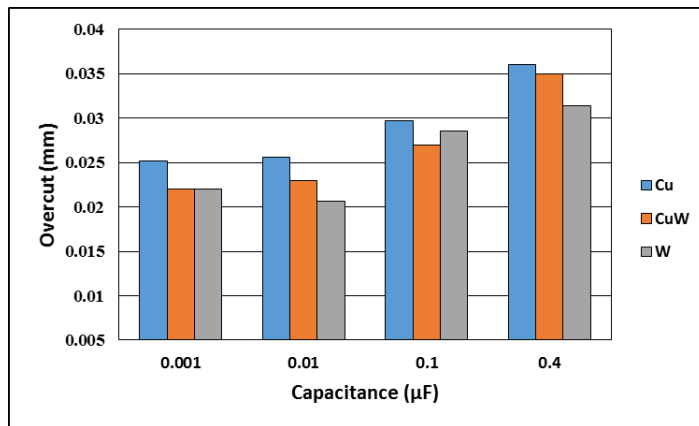*Figure B.2 Variation in EWR with (a) gap voltage and (b) capacitance*

It was found that the wear of tungsten electrode was lowest for all settings of voltage and capacitance as compared to copper-tungsten and copper electrodes. The EWR is nearly inversely proportional to the melting point of the electrode material. The copper-tungsten electrodes show moderate wear as compared to both copper and tungsten electrodes. While the copper electrode wears faster in spite of higher thermal and electrical conductivity.

The comparison of overcut and taper angle resulted by different electrodes during micro-EDM drilling of Inconel 718 is shown in Figure B.3 and Figure B.4. It was noted that capacitance and voltage have a considerable effect on overcut and the lower values of both voltage and capacitance are more appropriate to yield lower overcut. At lower voltage and capacitance values, the DE will be lower and hence lower workpiece volume will be ejected per discharge generating narrower crates and thus, resulting in lower overcut. The dimensional accuracy of micro-holes with tungsten electrodes was observed to be the best as compared to that with copper-tungsten and copper electrodes. As tungsten electrode possess higher melting and evaporation point that copper-tungsten and copper electrodes, it has less wear.
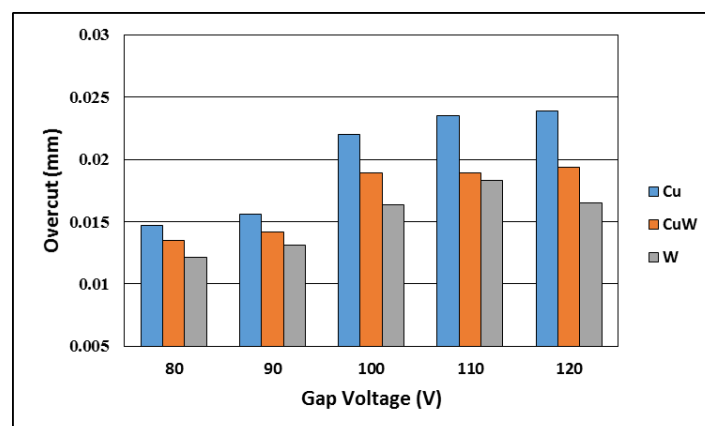
(a)

(b)

Figure B.3 Variation in overcut with (a) gap voltage and (b) capacitance
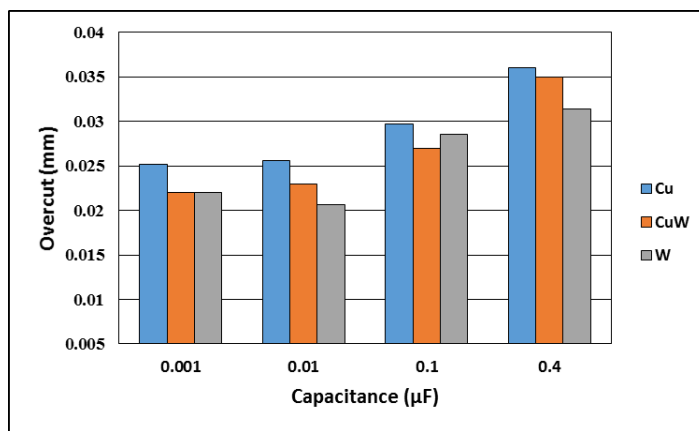
(a)
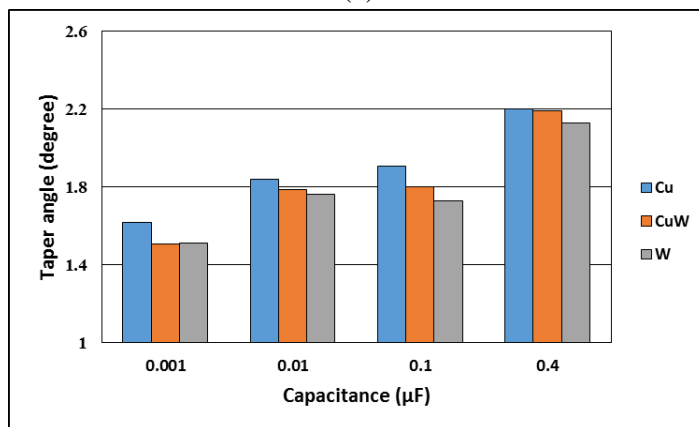
(b)

Figure B.4 Variation in taper angle with (a) gap voltage and (b) capacitance

The tungsten electrodes due to their larger thermal capability have excellent wear resistance and therefore results in an accurate geometric accuracy of fabricated micro-holes. Therefore, for achieving better geometric dimensions tungsten is recommended for the electrode material.

B.3 Summary:

The present study investigated the feasibility of machining micro-holes in Inconel 718 using the μ-ED drilling. Three different electrode materials viz. Copper, Copper-Tungsten and Tungsten have been elected as tool materials. The micro-EDM drilling performance of these three electrodess on Inconel 718 has been assessed based on the MRR, EWR, overcut and taper angle. Based on results obtained from the study, Tungsten material found to be suitable for achieving the dimensionally accurate micro-holes.

Appendix C Investigation on low-frequency vibration assisted μ-WEDM of Inconel 718

The micro wire electrical discharge machining (μ-WEDM), a variant of μ-EDM, is also one of the important and widely used nontraditional process owing to its capability to machine intricate and free forms with very thin wires. This process is used for fabrication of micro-features, however, only $2\,{}^1/_2$D can be fabricated. Therefore, the fabrication of straight micro-channels using μ-WEDM has been presented in this chapter. The assistance of low-frequency vibration in μ-ED drilling as well as in μ-ED milling found to be effective in enhancing the performance of these processes. Hence, it is also considered to investigate effects of low-frequency vibration in μ-WEDM while fabricating high-aspect-ratio straight micro-channels.

C.1 Experimental procedure:

The μ-WEDM setup on the DT-110 machine was used to fabricate the micro-channels. The photograph of the experimental setup is shown in Figure C.1. The workpiece specimen of size 27mm X 10mm X 2.5mm is prepared out of commercially available Inconel 718. The positive workpiece polarity was chosen as it leads to more material removal from the workpiece as compared to negative polarity electrode. The workpiece fixture was mounted on vibration device, and vibration device was clamped inside the main EDM tank. A cylindrical zinc coated brass wire (diameter 70μm) was used as a tool electrode. The commercial "TOTAL DIEL7500IN" dielectric fluid was used as dielectric oil due to its high flash point, and high dielectric strength.

The MRR was computed using following equation:

$$MRR_{\mu WEDM} = \frac{\nabla M_{wp}}{t} \qquad \left(\frac{mg}{min}\right) \qquad\qquad (C.1)$$

The kerf width was measured using AxioCam software and the Digital Microscope (Zeiss AxioCam AX10). The kerf width measured at five location along the length of the micro-channel (as shown in Figure C.2) and then average of these measurements was considered for result analysis.
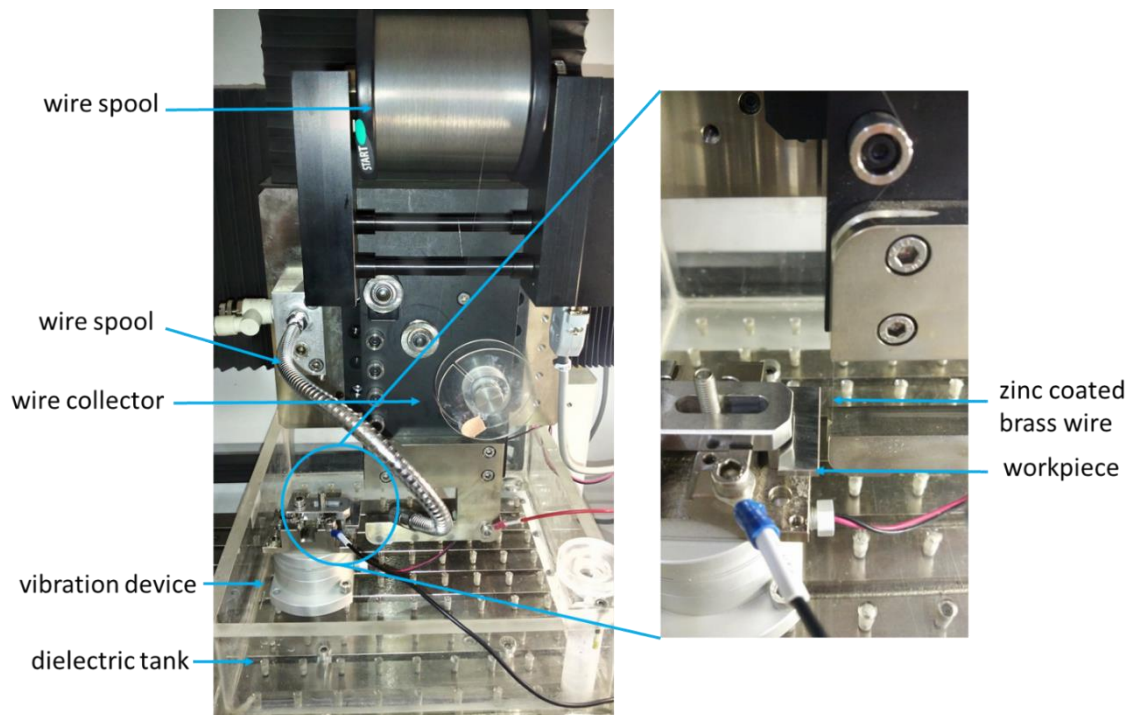
Figure C.1 Experimental setup of vibration-assisted µ-WEDM

C.2 Control factors and their range

The Box–Behnken design was utilized to plan the experiments and total 29 runs corresponding to 24 runs for side points, and five runs replicating the center position. The gap voltage (V_g), capacitance (Cp), feed rate (FR), and vibrational frequency (F) were designated as control factors while MRR and kerf width were chosen as performance measures. The control factors and their range, shown in **Error! Reference ource not found.**, were decided based on the literature, trial experiments, and machine

tools constraints. The experimental plan showing a set of the control factors and resultant performance measures acquired after conducting tests are given in Table C.1.
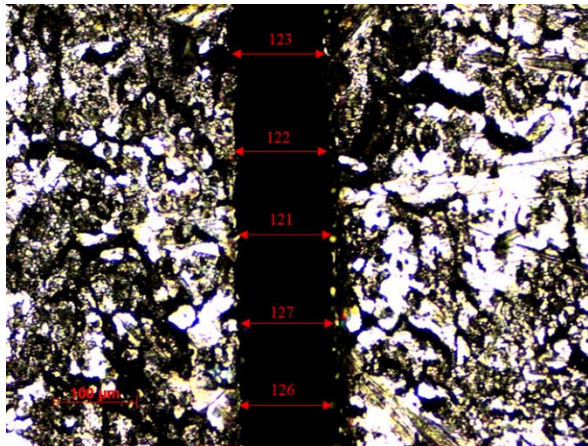
Figure C.2 Measurement of kerf width using optical microscope

Table C.1 Control factors and their levels

Control factors			Level		
	Unit	Notation	-1	0	1
Gap voltage	V	V_g	80	105	130
Capacitance	μF	Cp	0.01	0.1	0.4
Feed rate	mm/min	FR	0.1	0.25	0.4
Vibrational frequency	Hz	F	0	40	80

Table C.2 Experimental design matrix and observed performance measures in low-frequency assisted μ-WEDM of Inconel 718

Run order	Control factors (actual value)				Performance measures	
	Voltage (V)	Capacitance (μF)	Feed rate (mm/min)	Vibrational frequency (Hz)	MRR (mg/min)	Kerf width (μm)
1	105	0.1	0.25	40	0.001842	124
2	105	0.1	0.25	40	0.001614	122
3	80	0.1	0.25	0	0.003422	111
4	80	0.1	0.1	40	0.003982	109
5	105	0.1	0.25	40	0.001718	122
6	105	0.1	0.4	80	0.005795	121

7	130	0.1	0.4	40	0.003814	128
8	105	0.01	0.4	40	0.004416	97
9	130	0.4	0.25	40	0.001960	153
10	130	0.01	0.25	40	0.001419	98
11	80	0.1	0.25	80	0.005777	113
12	105	0.01	0.25	80	0.003069	98
13	130	0.1	0.1	40	0.000968	135
14	105	0.1	0.1	0	0.001171	123
15	105	0.01	0.1	40	0.000973	98
16	80	0.01	0.25	40	0.004381	95
17	105	0.1	0.25	40	0.001496	118
18	105	0.4	0.1	40	0.003045	147
19	130	0.1	0.25	0	0.001226	128
20	105	0.1	0.25	40	0.001212	120
21	105	0.1	0.1	80	0.001835	129
22	130	0.1	0.25	80	0.001945	134
23	80	0.4	0.25	40	0.006094	145
24	105	0.4	0.25	0	0.003611	155
25	105	0.01	0.25	0	0.001641	101
26	80	0.1	0.4	40	0.006040	109
27	105	0.4	0.4	40	0.006180	151
28	105	0.4	0.25	80	0.006065	153
29	105	0.1	0.4	0	0.003665	129

C.3 Results and discussion

C.3.1 Empirical models for performance measures

Mathematical relationships among the control factors and performance measures are established by developing multivariable regression models. The statistical significance of developed models was examined using analysis of variance (ANOVA) test. The

models were improved through backward elimination method. The results of ANOVA

for MRR and kerf width are summarized in Table C.3 and Table C.4, respectively.

Table C.3 The ANOVA table for MRR

Source	Sum of Square	df	Mean Square	F Value	p-value Prob>F	
Model	8.452E-005	8	1.056E-005	23.80	< 0.0001	significant
V_g	2.286E-006	1	2.286E-006	5.15	0.0345	
Cp	2.227E-005	1	2.227E-005	50.17	< 0.0001	
FR	2.064E-005	1	2.064E-005	46.48	< 0.0001	
F	9.187E-006	1	9.187E-006	20.69	0.0002	
$V_g \times FR$	3.042E-006	1	3.042E-006	6.85	0.0165	
$FR \times F$	3.004E-006	1	3.004E-006	6.77	0.0171	
$V_g{}^2$	1.885E-005	1	1.885E-005	42.45	< 0.0001	
$FR{}^2$	1.561E-006	1	1.561E-006	3.52	0.0754	
Residual	8.880E-006	20	4.440E-007			
Lack of Fit	8.412E-006	16	5.258E-007	3.50	0.0780	not significant
Pure Error	4.675E-007	4	1.169E-007			
Cor Total	9.340E-005	28				
	Std. Dev.		6.663E-004	R-Squared		0.9049
	Mean :		2.849E-003	Adj R-Squared		0.8669
	C.V. %		23.39	Pred R-Squared		0.7243
	PRESS		2.575E-005	Adeq Precision		18.046

V_g -Gap Voltage, Cp -Capacitance, FR -Feed rate, F-Vibrational Frequency

Figure C.3 shows the normal probability plot of the residuals which indicate that

residual fall in a straight line signifying that errors are normally distributed [2]. It can

also be seen that the actual response values are in good agreement with predicted values

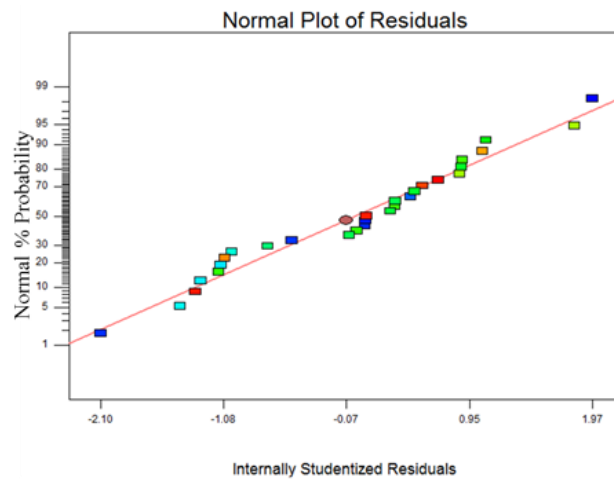by the models (Figure C.4).

Table C.4 ANOVA table for Kerf width

Source	Sum of Square	df	Mean Square	F Value	p-value Prob>F	
Model	9296.91	7	1328.13	95.69	< 0.0001	significant
V_g	747.59	1	747.59	53.86	< 0.0001	
Cp	8395.23	1	8395.23	604.85	< 0.0001	
FR	3.08	1	3.08	0.22	0.6422	
F	0.16	1	0.16	0.012	0.9146	
$FR \times F$	49.00	1	49.00	3.53	0.0742	

Cp ^2	786.10	1	786.10	56.64	< 0.0001	
F ^2	64.82	1	64.82	4.67	0.0424	
Residual	291.48	21	13.88			
Lack of Fit	268.94	17	15.82	2.81	0.1638	not significant
Pure Error	22.54	4	5.63			
Cor Total	9588.38	28				
Std. Dev.			3.73	R-Squared		0.9696
Mean :			122.94	Adj R-Squared		0.9595
C.V. %			3.03	Pred R-Squared		0.9423
PRESS			553.66	Adeq Precision		35.102

V_g -Gap Voltage, *Cp* -Capacitance, *FR* -Feed rate, *F*-Vibrational Frequency
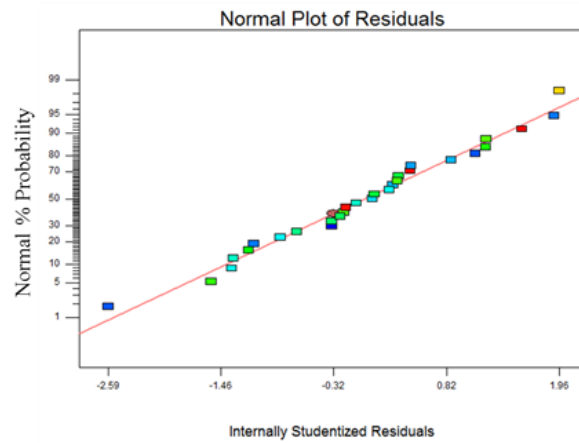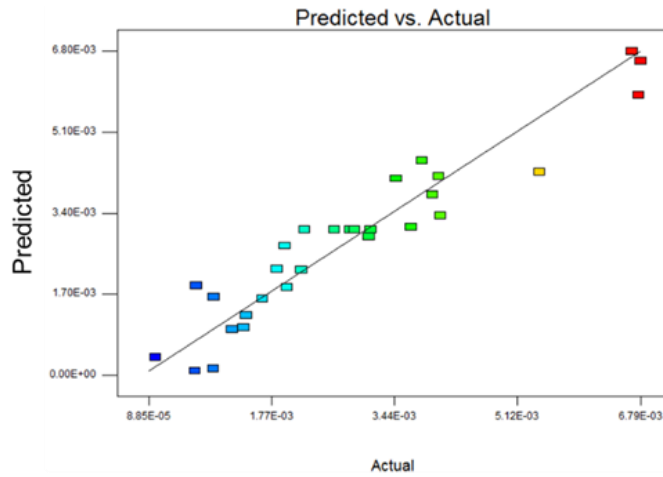

(a) For MRR

(a) For kerf

Figure C.3 Normal probability plot of residuals

The model F values of 23.80$_{MRR}$, 95.69$_{kerf}$ for MRR and kerf width respectively, with its Prob>F value less than 0.0001 directs that the models are significant. There is only a 0.01 % chance that such a large model F values could occur due to noise. The values of Prob>F less than 0.05 indicates the significance of model terms [2,12]. For MRR, the significant model are V_g, Cp, FR, F, $V_g \times FR$, $FR \times F$, and $V_g{}^2$ are terms contributing 2.70%, 26.38%, 24.45%, 10.88%, 3.60%, 3.55%, and 22.33%, respectively. While, V_g, Cp, Cp^2, and F^2 are significant model terms for kerf width contributing 7.78%, 87.47%, 8.19%, and 0.67%, respectively. The lack-of-fit values point out its significance or non-significance related to the pure error. When lack-of-fit values are non-significant, it shows that the model fits well with the experimental data. The lack-of-fit values for were found to be 0.078 and 0.1638 for MRR, and kerf width, respectively, indicating that developed models for MRR and kerf width are adequate and satisfactory.

The adequacy of model fit can be described with a determination coefficient (R^2). The R^2 values for MRR and kerf width are found to be 0.9049, and 0.9696, respectively suggesting that developed models are adequate in representing the process. The other R^2 statistics, the Pred R^2 values (0.7243$_{MRR}$, 0.9423$_{Kerf}$) are in agreement with the Adj R^2 (0.8669$_{MRR}$, 0.9595$_{Kerf}$). The C.V. values (23.39$_{MRR}$, 3.03kerf) directs higher accuracy and consistency of the performed experiments [28]. The Adeq Precision values, which signifies that signal-to-noise ratio, found to be 18.046$_{MRR}$ and 35.102$_{kerf}$ which are more than desired value of 4 and thus specifies a sufficient signal for the model. Therefore, developed models can be used to navigate within the design space.

(a) for MRR
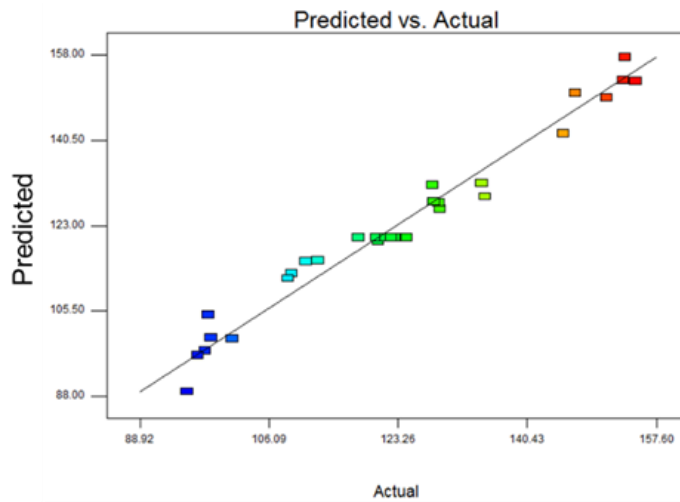
(b) for kerf

Figure C.4 Plot of predicted vs. actual response

The regression models for performance measures MRR and Kerf width are given by following second order polynomial equations:

$$MRR = -0.22818 + (5.15586 \times 10^{-4})V_g + (6.4794 \times 10^{-3})Cp$$

$$- (0.032039)FR - (1.42332 \times 10^{-5})F$$

$$+ (2.32532 \times 10^{-4})V_g \times F + (1.44429 \times 10^{-4})FR \qquad (7.2)$$

$$\times F - 2.6488\ Cp^2 + 0.021177\ FR^2$$

$$Kerf\ width = +58.55654 + 0.31572\ V_g + \ 310.69223\ Cp$$

$$+ 19.95333\ FR - (-4.47727 \times 10^{-3})F$$

$$- 0.58333\ FR \times F - 426.95416\ Cp^2 \tag{7.3}$$

$$+ (1.91534 \times 10^{-3})F^2$$

C.3.2   Analysis for MRR

The Perturbation plot showing effects of control factors on MRR in µ-WEDM of Inconel 718 is shown in Figure C.5. A sharp slope for gap voltage (V_g), capacitance (Cp), feed rate (FR), and vibrational frequency (F) directs that the MRR is highly sensitive to these factors. It is evident from the **Error! Reference source not found.** hat the interactions which significantly contributes to the MRR are those between the voltage and feed rate '$V_g \times FR$', and feed rate and vibrational frequency '$FR \times F$'. It is observed that MRR increases with increases linearly with increase in capacitance, feed rate, and vibrational frequency values. However, MRR increases initially with an increase in gap voltage up to an optimum value of 105V and then decreases with further increase in gap voltage (see, Figure C.6). The discharge energy (DE) engendered in RC pulse circuit is a multiplication of capacitance and voltage ($DE = 0.5CV^2$). When the voltage values reaches the breakdown voltage value, the DE stored by capacitor is released. The capacitance regulates the amount of the energy deposited and consequently, with increase in capacitance, the amount of DE, pulse current and pulse interval also increases boosting the MRR [30]. Therefore, the MRR increases prominently at high values of capacitance. The similar observation regarding increase of MRR with increase in DE also reported by [2,12]. The increase of MRR with increase in vibrational frequency (**Error! Reference source not found.**) values can be xplained with considering adhesion effect. In micro-EDM, the adhesion between electrode and workpiece plays important role on machining performance. Frequent

shorts circuits occurs due to adhesion and when short circuit occurs, machine pullbacks the electrode opposite to feed direction to maintain the spark gap [35]. Due to vibrational frequency, the workpiece vibrates and the adhesion between electrode and workpiece recovered effectively. Moreover, the vibrational movement of workpiece leads to effective evacuation of debris and molten metal from machining zone due to turbulent flow of dielectric in machining zone.
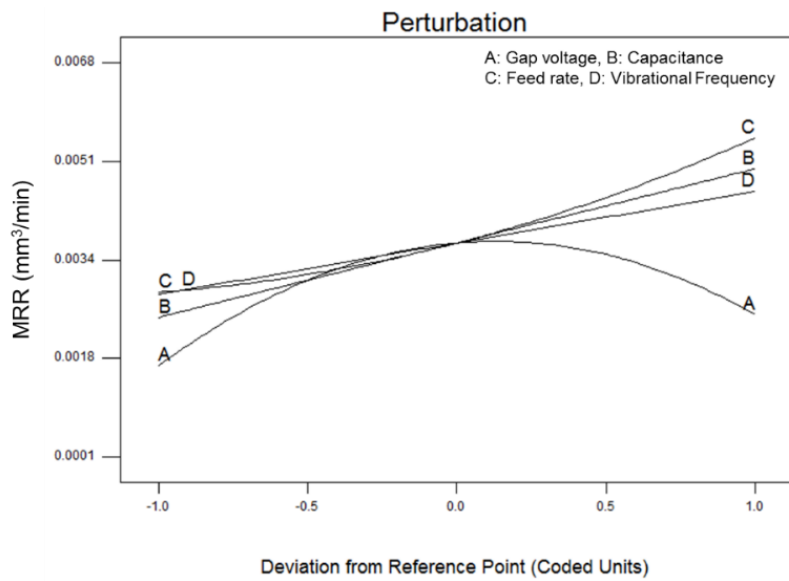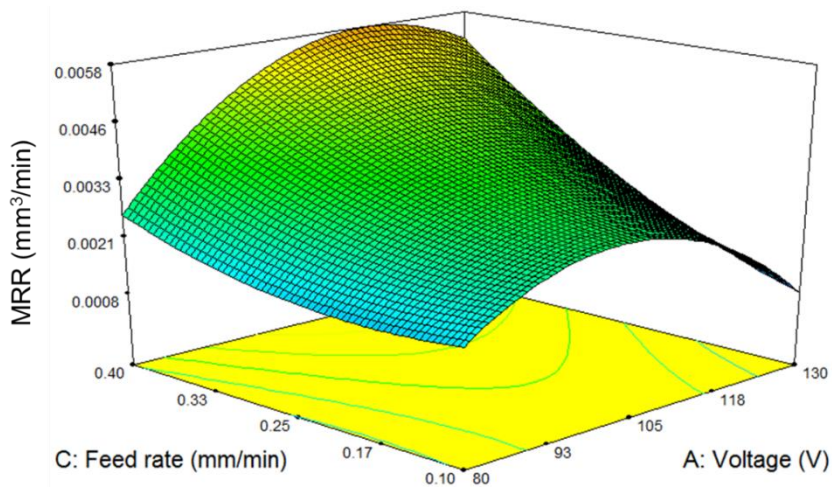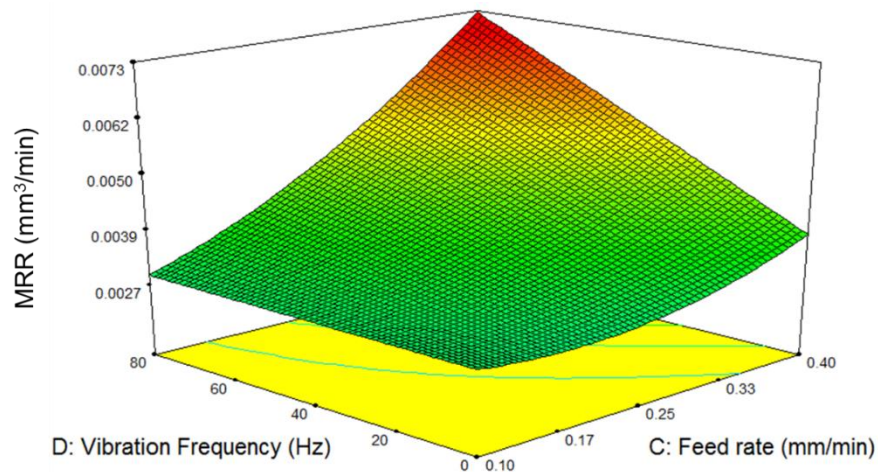

Figure C.5 Perturbation plot for MRR

(a)

(b)

Figure C.6 (a) and (b) Response surface for MRR

C.3.3 Analysis of kerf

Error! Reference source not found. shows the Perturbation plot for kerf width. The erf width is observed to be more sensitive to capacitance followed by gap voltage as compared feed rate and vibrational frequency. The capacitance and gap voltage lines are steep than the flat lines for feed rate and vibrational frequency. The kerf width increases with an increase in both gap voltage as well as capacitance values. The similar observation also reported by [11,12,35]. For achieving, lower kerf width, the low discharge energy values (i.e. low gap voltage and low capacitance) are suitable. The kerf width increases at high discharge energy due to the quantum electrons released from negative wire electrode striking with neutral particles in the dielectric fluids, which results in larger ionization effect. The kerf width will increase when a large amount of electrodes and ions strikes with the workpiece [11,35]. The machining at low discharge energy will enhance the dimensional accuracy and reduction of radius while cutting a corner in micro-machined components.
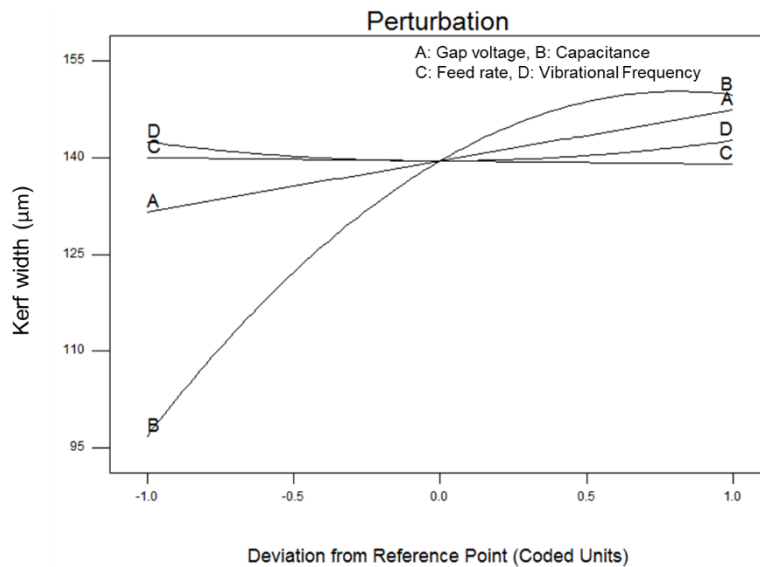
Figure C.7 Perturbation plot for kerf width

C.3.4 Microscopic investigation of surface topography of micro-channels

The surface topographical images of micro-channels fabricated by μ-WEDM in Inconel 718 are shown in **Error! Reference source not found.**. The effects different energy ettings viz. 320μJ and 2205μJ on channel surface are shown in in **Error! Reference source not found.** (a) and (b), respectively. It is observed that in μ-WEDM, the surface morphology depends on the applied discharge energy while machining. At low discharge energy setting, the machined surface observed to be very smooth. However, at high discharge energy settings, the spherical debris/globules and larger resolidified layer is observed on the machined surface. The formation of spherical debris/globules occurs rapid cooling and quenching of vaporized metal or splashed molten metal. At low discharge energy, the shape of the micro-channel is observed to be more accurate as compared to micro-channel at high discharge energy. **Error! Reference source not ound.** shows high-aspect-ratio (25: width 100 μm & length 2.5 mm) micro-channels 500 μm deep have been generated in Inconel 718 using μ-WEDM process.
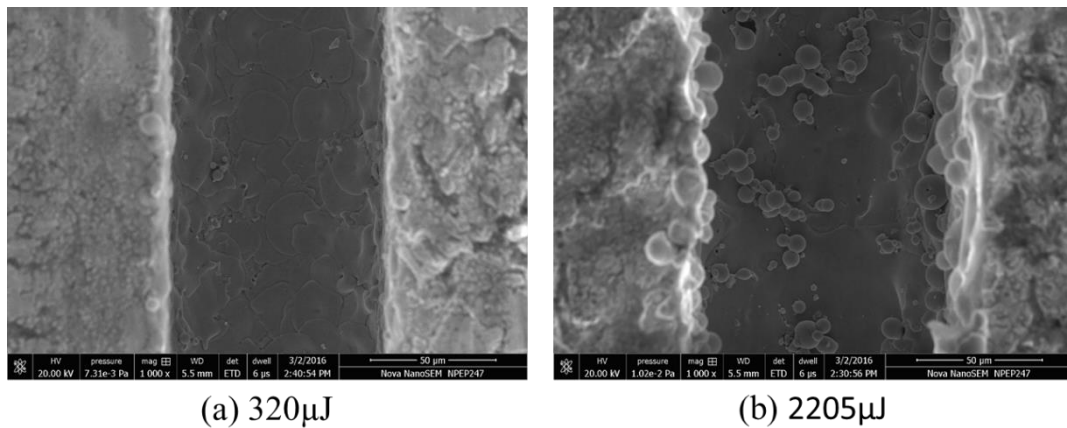
(a) 320μJ   (b) 2205μJ

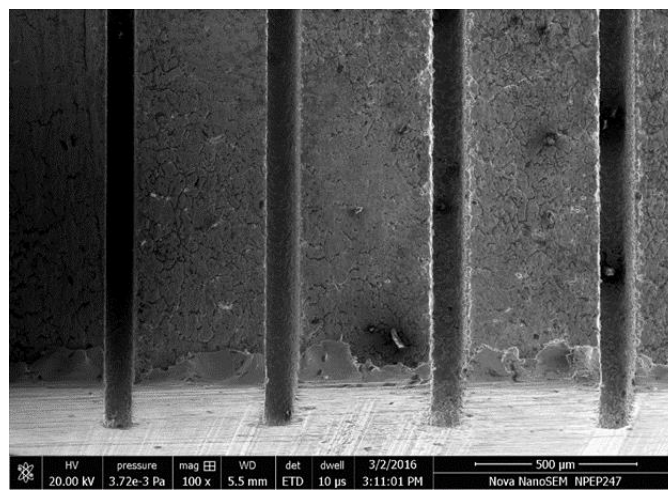*Figure C.8 Scanning electron microscope images of micro-channels at different energy settings*

Figure C.9 Micro-channels fabricated using μ-WEDM in Inconel 718

C.4 Summary

In this study was to complement and verify the feasibility of low-frequency vibration assistance in μ-WEDM. The gap voltage, capacitance, feed rate and vibrational frequency were chosen as control factors, whereas, the material removal rate (MRR) and kerf width were selected as performance measures while fabricating micro-channels in Inconel 718. It was observed that in μ-WEDM, the capacitance is the most significant factor affecting both MRR and kerf width. It was perceived that the low-frequency workpiece vibration improves the performance of μ-WEDM by improving the MRR due to enhanced flushing conditions and reduced electrode-workpiece adhesion.

Appendix D   Analysis of heat affected zone using microhardness measurement

Usually, in μ-EDM, the first layer on the machined surface is called the recast layer and below appears the HAZ, whose thickness could be between 5 and 200 μm. Therefore, in this analysis, measurement of microhardness was done at a distance of 30, 60, 100 and 180 μm from the wall of a hole as shown in Figure D.1. The microhardness measurements were done using micro Vickers hardness tester (Walter UHL), which allows loading in the range 10–1000 g. After the initial trials and calculation of the corresponding indentation size, a load of 50 g was chosen for this measurement. The microholes were fabricated at different discharge energy setting viz. 50 μJ, 500μJ and 2000 μJ without vibration and with vibration (30 Hz). The microhardness of the bulk material was also measured and was found to be around 592 Hv with a standard deviation of 12 Hv.

The results of microhardness measurement are shown in Figure D.2. It is observed from the figure that there is a definite reduction in the hardness of the material just outside the hole for all energy settings. The microhardness of the bulk material increases with increase in the distance from the edge of the hole. The microhardness at a distance of 180 μm from the edge of the hole appears to be closer in magnitude to the bulk microhardness.
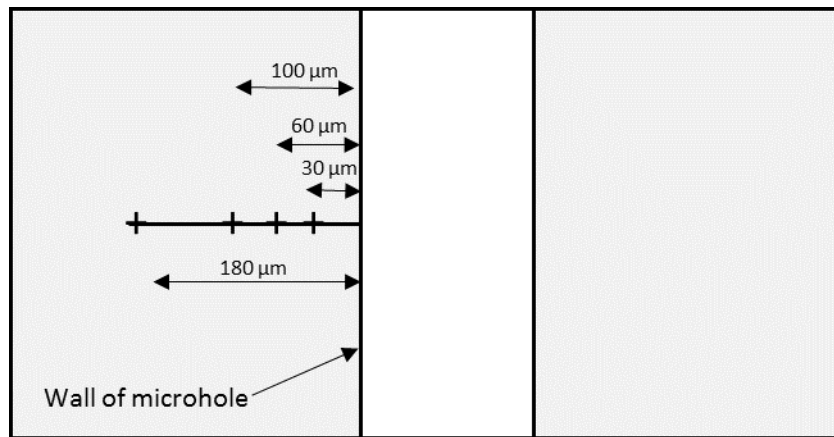
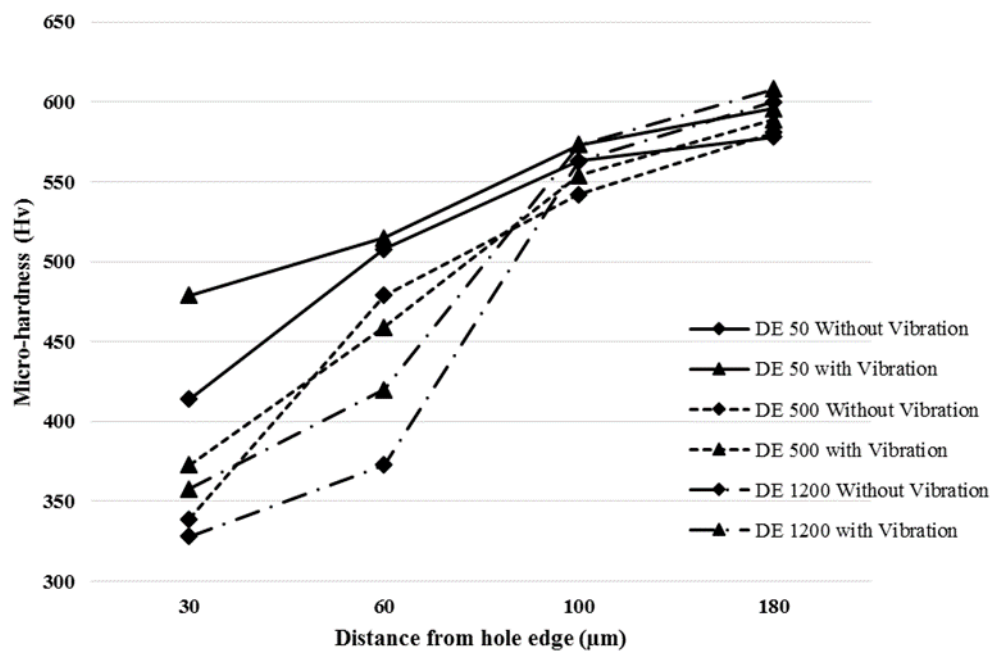*Figure D.1 Scheme of microhardness measurement*

Figure D.2 Microhardness variation away from the edge of fabrication micro-holes at various experimental settings

The reduction in the microhardness near to the edge of the hole could be due to a higher impact of spark heat flux. Since the micro-EDM spark is comparatively smaller in diameter and contains low energy [138], the melting and evaporation could get limited to the surface but heat might travel along the hole-wall into the bulk material. With the increase in the discharge energy, the microhardness value appeared to be reducing as the more heat energy will be acting on to the workpiece.

198

It is observed that with the application of the workpiece vibration at the same energy setting, there is a considerable reduction in the microhardness value as compared to that of without vibration assistance. This result can be explained by considering machining process efficiency which depends on the debris flushing dependent erosion rate.

With the increase in the depth of micro-holes, the debris removal becomes difficult and as a consequence of increased depth of hole cause secondary sparking. The machining process in this section of the hole continues in the lateral direction prominently than in the vertical direction due to debris accumulation. With the application of the workpiece vibration, the small working gap is subjected to periodical changes due to workpiece vibration, which helps in flushing out of debris effectively and therefore machining takes place effectively in the vertical direction. Overall, it can be interpreted that the workpiece vibration reduces the HAZ during μ-ED drilling owing to enhance debris removal and better dielectric flushing.

Appendix E   Publications

International Journals

1. D.R. Unune and H.S. Mali (2014) "Current status and applications of hybrid-micro-machining processes: A review", Proceedings of the Institution of Mechanical Engineers, Part B: Journal of Engineering Manufacture, 229 (10), 1680-1693. *SAGE*. doi.10.1177/0954405414546141. (Science Citation Indexed (SCI))

2. D.R. Unune and H.S. Mali (2015), "A study of multiobjective parametric optimization of electric discharge diamond grinding of Inconel 718" International Journal of Abrasive Technology, Vol.7, No.3, pp.187-199 *INDERSCIENCE*.

3. D.R. Unune and H.S. Mali (2015) "Artificial neural network–based and response surface methodology–based predictive models for material removal rate and surface roughness during electro-discharge diamond grinding of Inconel 718", Proceedings of the Institution of Mechanical Engineers, Part B: Journal of Engineering Manufacture, *SAGE*, doi: 10.1177/0954405415619347. (SCI)

4. D.R. Unune and H.S. Mali (2016) "Experimental investigation into low-frequency vibration assisted micro-WEDM of Inconel 718" Engineering Science and Technology, an International Journal. *ELSEVIER*. doi: 10.1016/j.jestch.2016.06.010.

5. D.R. Unune, V.P. Singh, and H.S. Mali (2015) "Experimental Investigations of Abrasive Mixed Electro Discharge Diamond Grinding of Nimonic 80A", Materials and Manufacturing Processes, Vol.31, pp.1718-1723. Taylor and Francis, doi:10.1080/10426914.2015.1090598 (SCI)

6. D.R. Unune and H.S. Mali (2015) "Study on material removal rate and average surface roughness measurement during additive mixed surface electro discharge diamond grinding of Inconel 718 by using response surface methodology",

International Journal of Advanced Manufacturing Technology, *SPRINGER*, ***In-review***. (SCI)

7. D.R. Unune and H.S. Mali (2015) "Parametric modeling and optimization of a low-frequency vibration assisted micro electro discharge drilling of Inconel 718" International Journal of Advanced Manufacturing Technology, *SPRINGER*. ***In-review***. (SCI)

8. D.R. Unune and H.S. Mali (2016) "Performance Investigations of a low-frequency vibration assisted µEDM milling of Inconel 718" Proceedings of the Institution of Mechanical Engineers, Part B: Journal of Engineering Manufacture, *SAGE*. ***In-review***. (SCI)

9. D.R. Unune and H.S. Mali (2016) "Microscopic investigations on effects of low-frequency workpiece vibration assisted micro-electro-discharge milling on quality of fabricated micro-channels", Journal of Mechanical Science and Technology, *SPRINGER*. ***In-review***. (SCI)

International Conferences

1. Mali H.S., D.R. Unune and S. Tiwari (2014) "Modelling and prediction of material removal rate in electrical discharge diamond surface grinding process of Inconel-718" Proceedings of 5th International and 26th All India Manufacturing Technology, Design and Research Conference (AIMTDR-2014), **IIT Guwahati**, 2014, p. 822:1-882:8.

2. D.R. Unune and H.S. Mali (2015) "Analysis on performance of micro-EDM drilled holes in Inconel-718 using different electrode materials" Proceedings of International Conference on Precision, Meso, Micro and Nano Engineering (COPEN-9), **IIT Bombay**. 10th-12th Dec. 2015. Mumbai.

3. D.R. Unune and H.S. Mali (2016), "Experimental investigations on low-frequency workpiece vibration in micro electro discharge drilling of Inconel 718", Proceedings of 6th International and 27th All India Manufacturing Technology, Design and Research Conference (AIMTDR-2016), **College of Engineering, Pune**, 2016. (**Accepted**)

Appendix F   Brief bio-data of the author

Mr. Deepak Rajendra Unune was born on 15th July 1986 in Vita, Dist. Sangli, Maharashtra, India. He completed bachelor's degree in Mechanical Engineering with first class with distinction from Rajarambapu Institute of Technology, Sakhrale, Sangli, Maharashtra, India and post graduate degree in Mechanical Engineering with first class from Government College of Engineering, Karad, Maharashtra, India. He worked in Bharat Forge Ltd. India which is a top leading forging company in the world for one-year industrial experience from July 2007 to July 2008 an Engineer in Die shop. During this industrial experience, he gained knowledge in conventional and non-conventional machining processes. He has academic experience as an Assistant Professor for 3 years in the various institutes from August 2010 to July 2013.

Since July 2013, he has been engaged in his doctoral research in the area of advanced manufacturing processes at Advanced Manufacturing and Mechatronics Lab in Mechanical Engineering Department, Malaviya National Institute of Technology Jaipur, Rajasthan, India under the Institute Research Fellowship scheme by Ministry of Human Resource Development, Government of India. He has published four research papers in Science Citation Indexed (SCI) journals and presented three research papers in International Conferences in reputed institutes during his Ph.D. tenure. Till today, he has published total 11 Journal papers and 11 conference papers. Currently, he is working as an Assistant Professor in Department of Mechanical-Mechatronics Engineering in The LNM Institute of Technology, Jaipur since July 2016.

Deepak Rajedra Unune (Email ID: deepunune@gmail.com)